The Role of N^6-methyladenosine RNA Methylation in the Regulation of Hematopoietic Stem Cells

Heather M. Lee

Submitted in partial fulfillment of the
requirements for the degree of
Doctor of Philosophy
under the Executive Committee
of the Graduate School of Arts and Sciences

COLUMBIA UNIVERSITY

2020

ABSTRACT

The Role of N^6-methyladenosine RNA Methylation in the Regulation of Hematopoietic Stem Cells

Heather M. Lee

Hematopoietic stem cells (HSCs) give rise to all blood cells and are characterized by their ability for life-long self-renewal and multilineage differentiation. HSC function is regulated by complex cell-intrinsic and -extrinsic pathways, but these regulatory mechanisms are not completely understood. Recent work has demonstrated that the epitranscriptional modification N^6-methyladenosine (m^6A) has important roles in the regulation of many physiologic and pathologic processes in various cell types, but it was previously unknown if and how m^6A may regulate adult HSC function. In this work, I uncover the role for m^6A in HSC regulation, both cell-intrinsically in regulating HSC differentiation and cell–extrinsically by regulating the formation the HSC bone marrow niche.

TABLE OF CONTENTS

LIST OF TABLES AND FIGURES

ACKNOWLEDGEMENTS

Completing this doctoral work has been an incredible privilege. Though my name is on the cover, this work was only possible because of the many people who helped me along the way.

First and foremost, I must thank my mentor Dr. Lei Ding for his guidance in this project and support whenever things have gone wrong. He has taught me not only how to conduct rigorous research, but how to ask the research questions that matter. Joining his lab was one of the best decisions I have ever made. I would also like to thank Dr. Steve Reiner, Dr. Hans Snoeck, and Dr. Uttiya Basu for serving on my thesis committee and guiding me throughout this process. I am a better scientist because of it.

Thank you to all of my collaborators, but particularly Dr. Chaolin Zhang, Suying Bao, and Yingzhi Qian, who were so generous with their time and energy in working on this project. Much of the work in this thesis was only possible with the technical support of CSCI Flow Cytometry core (particularly Mike Kissner) and HICCC Molecular Biology and Microscopy cores.

I am also so grateful to Columbia's MD/PhD program directors Dr. Patrice Spitalnik, Dr. Ron Liem, and Dr. Steve Reiner, for supporting me from the very first day.

Thank you to the people who inspired me to pursue research in the first place, Dr. Michael Brown, Dr. Lou Hammarskjöld, and Dr. David Rekosh, whose advice and wisdom I cherish.

I am lucky to have completed this work in the presence of wonderful colleagues in the Ding lab and CSCI. I especially want to thank Yeojin, Matt, Juliana, and Josh. It has been a great pleasure to spend each day in the lab beside them.

I am so thankful for all of my friends at Columbia and beyond, my loving family, and most of all, my best friend in the world, Sean. Their kindness, understanding and encouragement has been the greatest gift of my life.

CHAPTER 1

The Intersection of Hematopoietic Stem Cell Regulation and m^6A Epitranscriptional Modification.

Sections of this chapter are modified from the published article:

Yeojin Lee*, Matthew Decker*, Heather Lee*, and Lei Ding (2017)

Extrinsic regulation of hematopoietic stem cells in in development, homeostasis, and diseases

WIRES Dev Bio 6, e279

*Equal author contributions

INTRODUCTION

Multicellular organisms evolved tissue-specific stem cells to generate, sustain, and repair diverse tissue and organ types. Stem cells are constantly balancing two seemingly opposed functions: maintaining their undifferentiated stem cell state through self-renewal divisions and differentiating into downstream cells of multiple lineages. Much of what is known about how stem cells balance these states has been learned from hematopoietic stem cells (HSCs). HSCs have served as a paradigm tissue stem cell, having defined the rigorous standards of self-renewal and multi-lineage potential that characterize all tissue stem cells. HSCs give rise to all blood and immune cells in the hematopoietic system throughout life. These hematopoietic cells include myeloid cells, lymphoid cells, erythroid cells, and megakaryocytes generated from a series of restricted progenitors downstream of HSCs (Weissman and Shizuru, 2008).

Adult HSCs reside in the bone marrow and are primarily quiescent, but can be activated in response to physiological needs. This is best demonstrated in their function after transplantation. A single HSC can reconstitute the entire hematopoietic system of a mouse after irradiation, demonstrating the potency of these stem cells (Osawa et al., 1996). This ability to regenerate the hematopoietic system makes HSC transplantation a powerful treatment for a number of hematologic and autoimmune diseases. Thus, better understanding HSC biology can lead to improvements in current therapies for these diseases, as well as offering broader scientific implications for general stem cell biology.

HSC function is regulated by complex cell-intrinsic and -extrinsic pathways, but these regulatory mechanisms are not completely understood. Recent work has demonstrated that the epitranscriptional modification N^6-methyladenosine (m^6A) has important roles in the regulation of mRNA biology that can impact fundamental cellular processes. These roles for m^6A have been demonstrated in the context of specific cell types, including several types of stem cells and

hematopoietic cells, raising the question of if and how m^6A may regulate adult HSC function. In this chapter, I will summarize the current understanding of HSC-intrinsic and -extrinsic regulation and explore how m^6A regulates fundamental biology.

HEMATOPOIETIC STEM CELL REGULATION

In normal hematopoiesis, HSCs balance three states: i) division and differentiation to create mature hematopoietic cells, ii) division and self-renewal to populate the HSC pool, iii) quiescence to maintain a reservoir of HSCs for future needs (**Figure 1.1a**). These different states are controlled by a complex system of HSC-intrinsic and -extrinsic pathways that when disrupted can lead to hematopoietic perturbation, bone marrow failure or malignancy.

Cell-intrinsic regulation: cell fate decisions

As a model tissue stem cell, HSCs have been extensively studied. Through genetic mouse models, over 150 different genes have been shown to influence HSC biology (reviewed in Rossi et al., 2012). These genes belong to a large array of functional categories, including cell cycle programs, metabolic processes and specific signaling cascades. The full scope of this work has been extensively reviewed elsewhere, but of particular interest are programs that influence HSC fate, as the largely quiescent state and choice to self-renew versus differentiate distinguishes HSCs from downstream progenitor cells (Rossi et al., 2012; Eaves, 2015; Laurenti and Gottgens, 2018). HSC fate programs are coordinated through master regulators, often transcription factors or epigenetic regulators. Loss of quiescence regulators, such as *Pbx1*, *Gfi1*, *Irgm1*, *Prdm16*, *p57* and *p27* result in increased HSC proliferation and loss of the HSC pool and reconstitution capacity, suggesting excessive cycling exhausts their functional potential (Ficara et al., 2008; Hock et al., 2001; Feng et al., 2008; Aguilo et al., 2011; Zou et al., 2011). Once cycling, HSCs must then progress through fate determination programs to self-renew or

differentiate. *Myc* is known to be required specifically for HSC differentiation, but not self-renewal or survival (Wilson et al., 2004), while other factors like *FoxO3a* and *Bmi1* seem to be specifically required for self-renewal (Miyamoto et al., 2007; Iwama et al., 2004).

HSCs fate pathways are known to be highly regulated by epigenetic modifiers. Examples include *Bmi1*, a polycomb group gene involved in chromatin remodeling (Iwama et al., 2004), as well as DNA methyltransferases. DNA methyltransferase DNMT1, which is thought to maintain pre-existing methylation patterns, is essential for HSC survival, as loss of *Dnmt1* leads to complete loss of HSCs by apoptosis and death from bone marrow insufficiency (Broske et al., 2009). DNMT1 is particularly required for HSC self-renewal and lymphocyte differentiation, as *Dnmt1* hypomorph HSCs default to myeloerythroid differentiation (Broske et al., 2009). Consistent with this, DNA methylome maps demonstrate that lymphocyte lineage versus myeloid lineage commitment requires specific DNA methylation patterns (Ji et al., 2010; Farlik et al., 2016). On the other hand, loss of *de novo* DNA methyltransferase DNMT3a from HSCs leads to hypomethylation of downstream HSC progeny cells and increased multipotency gene expression, increasing self-renewal over differentiation (Challen et al., 2012). DNA demethylation also influences HSC function, as loss of Tet methylcytosine dioxygenase 2 (TET2) also promotes HSC self-renewal and myeloproliferation (Moran-Crusio et al., 2011; Li et al., 2011). DNA methylation patterns not only correlate with patterns of gene expression, but also correlate with histone modifications and chromatin accessibility, thus providing a mechanism to coordinate cell fate decisions in HSCs (Farlik et al., 2016). Whether there are additional intrinsic molecular mechanisms that may coordinate HSC fate programs in concert are still emerging.

Figure 1.1 Hematopoietic stem cell regulation.

(**a**) The majority of adult bone marrow hematopoietic stem cells (HSCs) are quiescent, but HSCs can be reversibly activated into the cell cycle to self-renew and replenish the HSC pool or differentiate to downstream progenitors.

(**b**) The adult HSC bone marrow niche is composed of many different cellular components, including perivascular mesenchymal stromal cells (MSCs) that express *Lepr* and *Prx1*, endothelial cells, sympathetic nerves, and adipocytes. Mesenchymal tissue in the limb marrow is derived from embryonic *Prx1*$^{+}$ MSCs. HSCs are also regulated by systemic circulating factors such as thrombopoietin (TPO), erythropoietin (EPO) and estrogen.

a

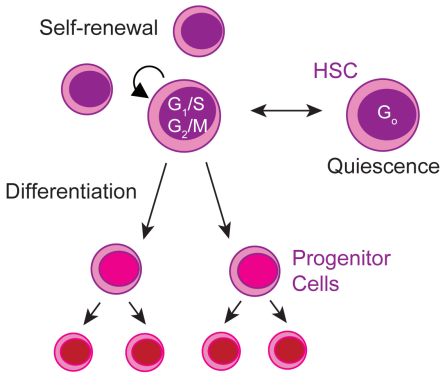

b

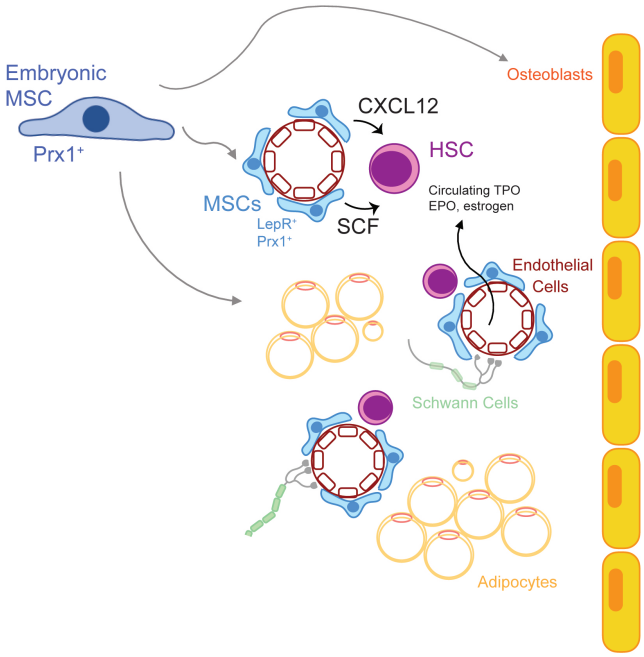

Figure 1.1

Cell-extrinsic regulation: the HSC niche

HSCs are also regulated by extrinsic signals that connect their function to physiologic needs. These extrinsic signals include long-range, systemically circulating cues such as estrogen, erythropoietin and thrombopoietin that can influence HSC proliferation, differentiation and maintenance, respectively (Nakada et al., 2014; Grover et al., 2014; Decker et al., 2018). However, much of what is known about HSC-extrinsic regulation comes from studies of their local microenvironment, or niche. HSCs move through niches in different organ sites several times throughout life to meet distinct physiological demands. Hematopoiesis begins in the yolk sac blood islands and aorta-gonad-mesonephros with the emergence of hematopoietic progenitors and pre-HSCs with limited transplantation potential (Matsubara et al., 2005). These pre-HSCs migrate to the fetal liver, where they mature and expand, generating an HSC pool with abundant self-renewal and multi-lineage potential (Morrison et al., 1995; Rebel et al., 1996). HSCs then start to migrate to the bone marrow, the predominant site of hematopoiesis in adults, around E17.5 (Christensen et al., 2004). This process depends on the expression of bone marrow C-X-C Motif Chemokine Ligand 12 (*Cxcl12*, also known as stromal cell-derived factor 1 or *Sdf-1*), as mice with loss of *Cxcl12* do not establish hematopoiesis in the bone marrow and instead have increased HSCs circulating in the peripheral blood (Nagasawa et al., 1996; Ara et al., 2003).

The adult bone marrow niche is the predominant site of adult hematopoiesis. It is composed of many different cellular components, including perivascular mesenchymal stromal cells (MSCs), endothelial cells, sympathetic nerves, megakaryocytes and adipocytes (reviewed in Lee et al., 2017) (**Figure 1.1b**). Although early studies suggested osteoblasts were the key component of the HSC niche, accumulating evidence suggests that they are not as critical as initially thought (Morrison and Scadden, 2014). MSCs are a key component of the niche and can be identified by a number of markers, including paired related homeobox 1 (*Prx1*), leptin receptor (*Lepr*), and platelet-derived growth factor receptor (PDGFR) (Morikawa et al., 2009;

Ding et al., 2012; Ding and Morrison, 2013; Zhou et al., 2014,). Imaging studies of the bone marrow niche consistently demonstrate that HSCs preferentially reside in close proximity to sinusoids surrounded by MSCs (Kiel et al., 2005; Sugiyama et al., 2006; Nombela-Arrieta et al., 2013; Acar et al., 2015; Chen et al., 2016). MSCs have higher expression of key HSC-supporting cytokines stem cell factor (*Scf*) and *Cxcl12* compared to other cell types in the bone marrow, supporting the idea that MSCs are important sources for HSC regulation (Ding et al., 2012; Ding and Morrison, 2013). Furthermore, conditional deletion of *Scf* or *Cxcl12* from MSCs using *Lepr-cre* or *Prx1-cre* causes a dramatic loss of HSCs from the bone marrow (Ding et al., 2012; Ding and Morrison, 2013; Greenbaum et al., 2013). In contrast, conditional deletion of *Scf* and *Cxcl12* from osteoblasts did not cause HSC defects (Ding and Morrison, 2013). Thus, MSCs are considered a critical component of the HSC bone marrow niche.

Although much progress has been made regarding the cellular components of the adult HSC niche, how the niche is established and regulated in the bone marrow is not completely understood. The limb bone marrow environment is largely derived from embryonic undifferentiated $Prx1^{+}$ progenitor cells. These cells give rise to all of the mesenchymal tissue of the limb, including bone, fat, cartilage, tendons, synovial cells and MSCs (Akiyama et al., 2005; Kawanami et al., 2009; Sanchez-Gurmaches et al., 2015). Transplantation of developing progenitor MSCs at E14.5 into recipient kidney capsules results in the formation of ectopic bone marrow with recipient HSCs, demonstrating that these cells are capable of generating all necessary mesenchymal components of the HSC niche (Chan et al., 2009). In adulthood, $LepR^{+}$ MSCs are largely quiescent, but can differentiate to osteoblasts and adipocytes to regenerate the niche during aging and after fracture or irradiation (Zhou et al., 2014). This population, which can also be identified by expression of PDGFRα, includes the vast majority of cells in the bone marrow that have characteristics of mesenchymal stem/progenitor cells (Morikawa et al., 2009). Interestingly, deletion of transcription factor *Foxc1* from MSCs using *Prx1-cre* shifted the balance of MSC differentiation towards greater adipogenesis and caused a dramatic loss of

bone marrow cellularity and HSCs (Omatsu et al., 2014). In contrast, loss of *Ebf3* from MSCs using *Prx1-cre* caused the opposite effect, inducing increased osteogenesis over adipogenesis (Seike et al., 2018). This led to osteosclerosis, loss of the bone marrow cavity, and loss of HSCs (Seike et al., 2018). In both cases, balanced regulation of MSC differentiation is required for maintaining functional HSCs. However, there is still little known about the underlying mechanisms regulating niche formation and maintenance.

From intrinsic cellular programs to environmental cues, the mechanisms controlling when and how HSCs are activated to differentiation and self-renewal from quiescence are not fully understood. It is likely that additional novel regulation also influences HSC function.

EPITRANSCRIPTIONAL REGULATION BY N^6-METHYLADENOSINE

m^6A is a modified adenosine found in RNA and is one of the most abundant mRNA modifications in eukaryotic cells (Meyer and Jaffrey, 2014). While discovered in 1974 (Desrosiers, Friderici and Rottman, 1974; Perry and Kelley, 1974), m^6A has only recently been appreciated to have important roles in target mRNA regulation and gene expression. m^6A RNA methylation is controlled by a dynamic system involving a methyltransferase complex that adds m^6A to target transcripts, demethylases that remove m^6A modification, and m^6A-binding proteins that regulate target RNA metabolism. Through its effects on target transcripts, m^6A has been shown to regular fundamental cellular processes and the study of m^6A has opened up a new field of understanding gene expression regulation by post-transcriptional RNA modifications, or “epitranscriptional” regulation (Meyer et al., 2012).

The m^6A methyltransferase complex is composed of several known proteins: methyltransferase-like 3 (METTL3), methyltransferase-like 14 (METTL14), Wilms-tumor associated protein (WTAP), RNA binding motif protein 15 (RBM15), and several other accessory proteins. METTL3 is thought to be the only catalytically active component of the

complex, as *Mettl3* knock-out cells display near complete loss of m^6A (Geula et al., 2015). METTL14 was initially thought to be a methyltransferase, but was later shown to have no enzymatic activity (Sledz and Jinek, 2016). METTL14 is now recognized to have a crucial non-catalytic role forming a heterodimer with METTL3, which stabilizes and increases METTL3's activity (Liu et al., 2014; Wang et al., 2016). WTAP also binds to METTL3 and METTL14 and is crucial in their localization to nuclear speckles enriched in pre-mRNA machinery (Ping et al., 2014). Localization to specific RNA targets is thought to be partially mediated through RBM15, which directly binds to METTL3 (Patil et al., 2016). There are also other recently identified m^6A methyltransferases, including methyltransferase-like 16 (METTL16) and ZCCHC4, that are capable of writing m^6A on small nuclear RNAs, ribosomal RNAs, and specific subsets of mRNAs, but their contribution to the m^6A epitranscriptome is thought to be minor (Pendelton et al., 2017; Ma et al., 2019).

Several groups have identified m^6A modified mRNA targets transcriptome-wide in different cell types by using m^6A-specific antibodies to immunoprecipitate (IP) and sequence m^6A-modified RNA (Dominissini et al., 2013; Meyer et al., 2012). Through such studies, an m^6A consensus sequence has been identified: DRACH, where D=A, G or U and H=A, C or U. However, the presence of a consensus sequence does not ensure that a given adenosine will be methylated. Sequencing studies have shown that m^6A is found predominantly near stop codons, long internal exons, and 3' untranslated regions (Dominissini et al., 2013; Meyer et al., 2012). Exactly how these sites are determined is still unknown.

m^6A modification has been shown to affect many aspects of target mRNA metabolism including alternative splicing, transcript stability, nuclear export, translation efficiency, and secondary RNA structure (Meyer and Jaffrey, 2014). These effects are thought to be mediated through m^6A-binding or "reader" proteins. These include the YTH (YT521-B homology) domain family and domain containing proteins YTHDF1-3 and YTHDC1-2, insulin- like growth factor 2 mRNA-binding proteins IGF2BP1–3, and heterogeneous nuclear ribonucleoproteins HRNPC,

HRNPG, and HRNPA2B1 (reviewed in Shi et al., 2019). Different readers have been associated with different effects on target RNA processing, including often conflicting functions. For example, IGF2BP proteins and YTHDC2 are thought to stabilize m^6A targets, increasing their gene expression (Huang et al., 2018; Hsu et al., 2017). In contrast, YTHDF2 is thought to decrease m^6A target expression by localizing targets to RNA decay processing bodies, promoting their degradation (Wang et al., 2014). Other studies suggest that m^6A targets are regulated not at the mRNA level, but at the protein level through effects on translation efficiency by YTHDF1 or m^6A-independent functions of METTL3 itself (Wang et al., 2015; Lin et al., 2016). These discrepancies may be due to differences in the studied cell types or environments and illustrate that m^6A regulation may have different functions depending upon the biologic context, such as variations in m^6A-binding proteins or m^6A targets within a cell. This notion of context-dependent roles for m^6A is consistent with m^6A profiling of 21 different human fetal tissues (including brain, heart kidney, lung, and liver) that demonstrated that while the majority of m^6A targets are conserved, there are also tissue-specific m^6A targets (Xiao et al., 2019). Tissue and cell type-specific methylation patterns may also suggest the possibility that m^6A can regulate cell type-specific processes.

Through effects on target RNA metabolism, m^6A-mediated regulation has proven to be critical to fundamental cellular processes such as DNA damage repair (Xiang et al., 2017), meiosis (Agarwala et al., 2012), circadian periods (Fustin et al., 2013), and cell fate (Aguilo et al., 2015; Batista et al., 2014; Chen et al., 2015; Guela et al., 2015; Wang, et al., 2014). Induced pluripotent stem cells, embryonic stem cells, and neural stem cells all have m^6A modified transcripts of genes implicated in controlling cell fate, suggesting that m^6A regulates cell fate determination (Batista et al., 2014; Wang, et al., 2014; Aguilo et al., 2015; Chen et al., 2015; Guela et al., 2015). Consistent with this notion, loss of *Mettl3* prevents embryonic stem cell transition from self-renewal to differentiation (Batista et al., 2014, Geula et al., 2015). Similarly, deletion of *Mettl14* in embryonic neural progenitors using *Nestin-cre* causes differentiation

defects (Wang et al., 2018). These results demonstrate that METTL3 and m^6A modification regulate differentiation processes in different types of stem cells, and raises the possibility that m^6A might also regulate cell fate in HSCs.

N^6-METHYLADENOSINE IN HEMATOPOIESIS

The role of m^6A in hematopoiesis has only begun to be explored. The first direct connection between m^6A and hematopoiesis came from investigations of hematopoietic development. *Mettl3*-deficient morphant zebrafish embryos have defects in endothelial-to-hematopoietic transition (EHT), the process for emergence of early hematopoietic stem/progenitor cells (HSPCs) from the hemogenic endothelium during development (Zhang et al., 2017). Consequently, the *Mettl3*-deficient embryos retain endothelial identity markers in the hemogenic endothelium and have reduced HSPCs (Zhang et al., 2017). This reduction in HSPC emergence was also recapitulated in *Vecadherin-cre; Mettl3*$^{fl/fl}$ mouse embryos, in which *Mettl3* deleted from endothelial cells of the aorta-gonad-mesonephros (Lv et al., 2018). While these early developmental HSPCs do not have reconstitution potential in transplantation, a requirement for definitive HSCs, this work demonstrates that m^6A impacts HSC emergence.

The role for m^6A has also been investigated in more mature hematopoietic cells. Human $CD34^+$ cord-blood cells, a mixed hematopoietic stem and progenitor population, transduced with *Mettl3* shRNA have reduced colony forming capacity and increased myeloid differentiation in culture (Vu et al., 2017). Conditional deletion of *Mettl3* from naïve T cells using *Cd4-cre* prevents proliferation and differentiation of naïve T cells, largely attributed to inhibition of T cell activation from loss of m^6A-mediated decay of SOCS genes (Li et al., 2017).

There is also evidence that m^6A plays a role in hematopoietic diseases. Multiple members of the m^6A pathway, including *Mettl3*, *Mettl14*, *Wtap* and *Rbm15*, are highly expressed in myeloid leukemia compared to other types of cancers (Vu et al., 2017; Jaffery and Kharas,

2017). *Mettl3* knock-down by shRNA or CRISPR-Cas9 in acute myeloid leukemia cell lines caused higher expression of differentiation markers, reduced proliferation and reduced colony formation in culture (Barbieri et al., 2017; Vu et al., 2017). Furthermore, immunodeficient mice transplanted with *Mettl3*-depleted leukemic cells showed delayed leukemia development and better survival, suggesting that m^6A is involved in myeloid leukemia progression and differentiation (Barbieri et al., 2017; Vu et al., 2017). *Myc* was found to be a highly methylated m^6A target in leukemia cells in multiple studies (Weng et al., 2017; Vu et al., 2017; Su et al., 2018). After *Mettl3* depletion, leukemia cells display reduced MYC protein levels that are thought to partially explain their altered cell fate (Barbieri et al., 2017; Vu et al., 2017; Su et al., 2018). As MYC is known to be a master regulator of differentiation in cancer and in normal HSCs, it is possible that *Myc* regulation by m^6A may also influence HSC function.

A common theme has emerged from these studies: METTL3 and m^6A are required in cell fate transition, and specifically differentiation rather than self-renewal, in multiple hematopoietic cell types, normal or pathologic. However, whether this influences adult HSC regulation was unknown. It is possible that m^6A modification influences HSC self-renewal, differentiation, quiescence, and/or survival. m^6A might also play a role in the regulation of MSC cell fate, thus impacting extrinsic regulation of HSCs in the bone marrow niche. Within the following chapters, I explore these ideas, looking at m^6A within HSCs in Chapter 2 and within MSCs in Chapter 3. Determining how RNA epitranscription impacts HSCs, both cell-intrinsically and –extrinsically, provides a new angle for understanding HSC function and may provide a new approach for developing tools to manipulate HSC function and new therapies for bone marrow transplant patients.

CHAPTER 2

The Requirement for *Mettl3*-dependent m^{6}A mRNA Methylation During Hematopoietic Stem Cell Differentiation

The work described in this chapter is published:

Heather Lee, Suying Bao, Yingzhi Qian, Shay Geula, Juliana Leslie, Chaolin Zhang, Jacob H. Hanna & Lei Ding (2019)

Stage-specific requirement for Mettl3-dependent m^{6}A mRNA methylation during hematopoietic stem cell differentiation

Nature Cell Biology, Vol 21, p700-709

H.L., J.L. and L.D. performed all of the experiments. S.B., Y.Q. and C.Z. performed the bioinformatics analysis on all sequencing data. S.G. and J.H.H. generated and validated the Mettl3fl strain and assisted with gene expression analysis and the development of the project. H.L. and L.D. designed the experiments, interpreted the results and wrote the manuscript with input from J.H.H. and C.Z. L.D. supervised the project.

SUMMARY

Hematopoietic stem cells (HSCs) maintain balanced self-renewal and differentiation, but how these functions are precisely regulated is not fully understood. N^6-methyladenosine (m^6A) mRNA methylation has emerged as an important mode of epitranscriptional gene expression regulation affecting many biological processes. We show that deleting the m^6A methyltransferase, *Mettl3*, from the adult hematopoietic system led to an accumulation of HSCs in the bone marrow and marked reduction of reconstitution potential due to a blockage of HSC differentiation. Interestingly, deleting *Mettl3* from myeloid cells using *Lysm-cre* did not impact myeloid cell number or function. m^6A sequencing revealed 2,073 genes with significant m^6A modification in HSCs. *Myc* was identified as a direct target of m^6A in HSCs. *Mettl3*-deficient HSCs failed to up-regulate MYC expression upon stimulation to differentiate and enforced expression of *Myc* rescued differentiation defects of *Mettl3*-deficient HSCs. Our results revealed a key role of m^6A in governing HSC differentiation.

INTRODUCTION

HSCs give rise to all blood cells, and are characterized by their ability for life-long self-renewal and multi-lineage differentiation. HSC function is regulated by complex cell-intrinsic and -extrinsic pathways (reviewed in Rossi et al., 2012; Morrison and Scadden, 2014), but the mechanisms that control balanced self-renewal and differentiation are poorly understood. Transcriptional, translational and epigenetic regulators have been shown to critically regulate HSC function (reviewed in Rossi et al., 2012). Whether other molecular mechanisms also regulate HSCs is unclear.

m^6A is a modified base found in eukaryotic mRNAs (Desrosiers, Friderici and Rottman, 1974). This modification of adenosine is abundant and functions as an epitranscriptomic regulator of target mRNAs through multiple mechanisms, including stability and translation efficiency (reviewed in Meyer and Jaffrey, 2017). m^6A is deposited onto mRNAs by a methyltransferase complex, composed of methyl transferase-like 3 (METTL3), methyl transferase-like 14 (METTL14) and Wilms-tumor associated protein (WTAP) and other accessory proteins (reviewed in Meyer and Jaffrey, 2017). METTL3 is the essential catalytic component of the complex (Geula et al., 2015; Sledz et al., 2016; Wang, Doxtader and Nam, 2016; Wang et al., 2016). m^6A has been shown to impact fundamental cellular processes, including DNA damage repair (Xiang et al., 2017), meiosis (Agarwala et al., 2012), and circadian clock (Fustin et al., 2013). Transcriptome-wide mapping of m^6A modification has revealed cell type-specific methylation targets, suggesting that m^6A regulates cell type-specific processes (Chen et al., 2015).

Interestingly, m^6A has been shown to impact stem and progenitor cell fate. Disruption of the m^6A pathway blocks the decay of naïve embryonic stem cell program (Geula et al., 2015; Batista et al., 2014). m^6A also plays a critical role in embryonic neurogenesis by regulating fetal neural stem and progenitor cells (Yoon et al., 2017; Wang et al., 2018). The role of m^6A in the hematopoietic system is emerging. Using zebrafish as a model, it has been shown that m^6A is required for endothelial to hematopoietic transition and the emergence of hematopoietic stem and progenitor cells (Zhang et al., 2017). shRNA knockdown of *Mettl3* or *Mettl14* in human hematopoietic stem and progenitor cells leads to myeloid differentiation *in vitro* (Vu et al., 2017; Weng et al., 2017). These studies show that m^6A plays critical roles for HSC emergence and *in vitro* function, but its role in mammalian adult HSCs and hematopoiesis *in vivo* remained unclear.

RESULTS

Deletion of *Mettl3* disrupts hematopoiesis and leads to accumulation of HSCs

We performed quantitative real-time PCR (qPCR) analysis to assess the expression of *Mettl3* in the hematopoietic system. *Mettl3* transcripts were expressed at approximately 4.5-fold higher levels in $CD150^{+}CD48^{-}Lin^{-}Sca1^{+}cKit^{+}$ HSCs compared with whole bone marrow cells (**Figure 2.1a**), suggesting that METTL3-mediated m^6A may regulate the function of HSCs.

To test whether m^6A regulates HSCs and hematopoiesis *in vivo*, we generated and validated a floxed allele of *Mettl3* (**Figure 2.1b**), and crossed it with *Mx1-cre* (Kuhn et al., 1995) to generate *Mx1-cre; Mettl3*$^{fl/fl}$ mice. We conditionally deleted *Mettl3* from the adult hematopoietic cells by intraperitoneally injecting polyinosinic-polycytidylic acid (pIpC) into 6-8 week old *Mx1-cre; Mettl3*$^{fl/fl}$ mice (**Figure 2.1b**). Efficient deletion in HSCs was achieved by 10 days after the last pIpC injection (**Figure 2.1c-d**). Ten to 14 days (short term) after the last pIpC injection, complete blood count analyses revealed a significant decrease in platelet count, but not white or red blood cell counts, in *Mx1-cre; Mettl3*$^{fl/fl}$ mice compared with pIpC-treated controls (**Figure 2.2a-c**). Recent work in the field has proposed that platelets can be directly generated from HSCs (Rodriguez-Fraticelli et al., 2018; Carrelha et al., 2018). The platelet phenotype raises the possibility that m^6A may regulate HSCs. The same phenotype persisted 2-3 months after the last pIpC injection (**Figure 2.2a-c**). By 4 months, white blood cell counts were also significantly reduced, with an altered white blood cell distribution (**Figure 2.2a** and **Figure 2.3a**). These data suggest that m^6A is required for hematopoiesis.

Figure 2.1 *Mettl3* is efficiently deleted from HSCs in *Mx1-cre; Mettl3$^{fl/fl}$* mice after Cre induction.

(**a**) qPCR analysis of *Mettl3* mRNA expression in wild-type bone marrow populations. (n=7 for WBM, n=6 for LSK, n=10 for HSC, n=6 for MPP, n=6 for LMPP, n=6 for CLP, n=4 for MEP, n=4 for CMP, n=3 for GMP, n=10 for $Gr1^{+}Mac1^{+}$).

(**b**) Schematic of Cre-mediated recombination of *Mettl3^{fl}* allele (left) and *Mx1-cre; Mettl3$^{fl/fl}$* pIpC treatment schedule (right).

(**c**) Representative genotyping results of colonies formed by single sorted HSCs after pIpC treatment. The majority of colonies show complete deletion, with rare colonies showing deletion of only one *Mettl3* allele. Experiment was repeated with biologically independent samples three times with similar results.

(**d**) qPCR analysis of *Mettl3* mRNA expression in HSCs from pIpC-treated control and *Mx1-cre; Mettl3$^{fl/fl}$* mice (n=4 for control, n=5 for *Mx1-cre; Mettl3$^{fl/fl}$*).

All samples are from biologically independent animals. Values are shown as individual points with mean ± s.d. P values were determined by unpaired two-sided Student's t-test.

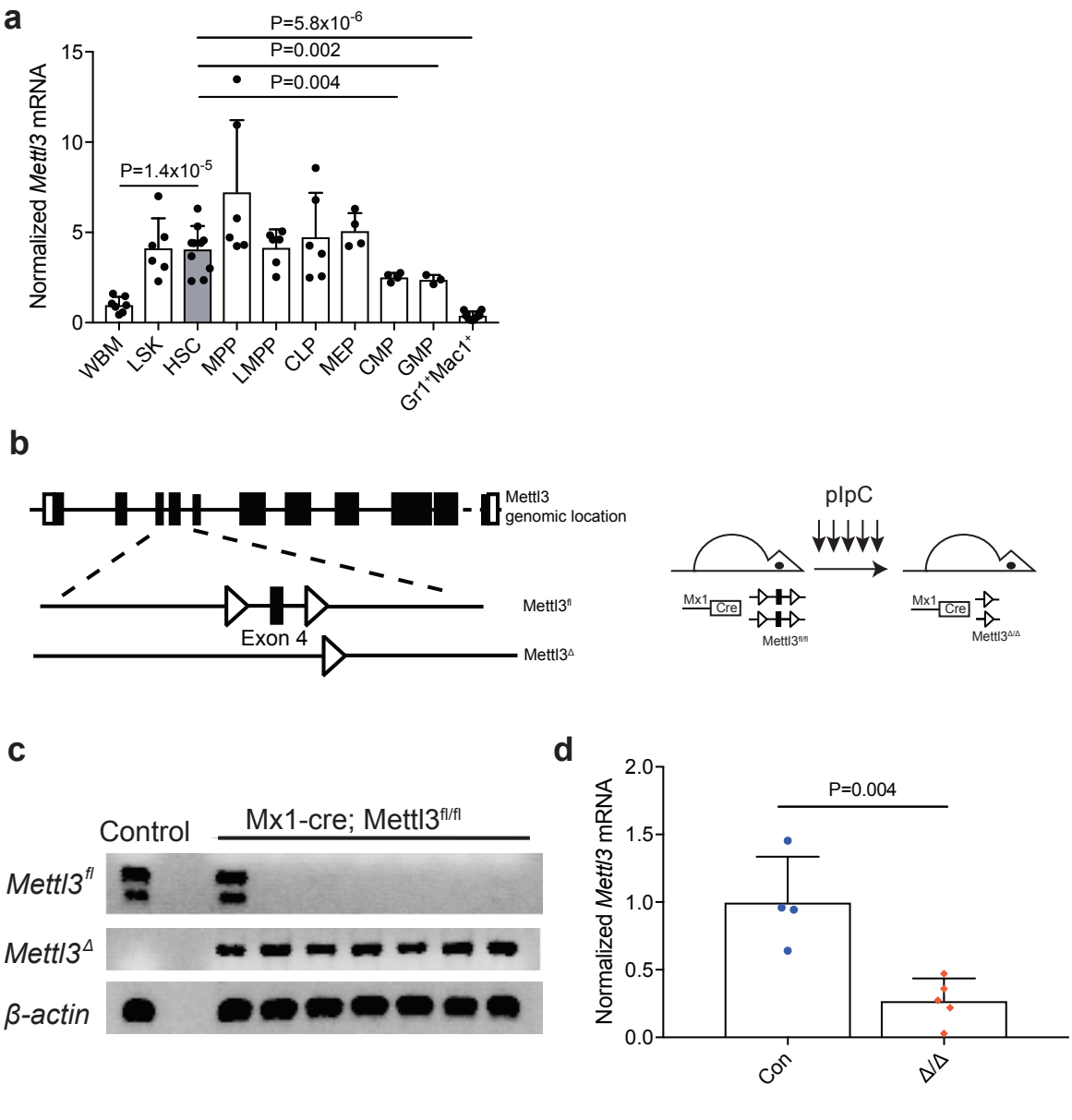
a
P=5.8x10-6
P=0.002
P=0.004
P=1.4x10-5
Normalized Mettl3 mRNA
15
10
5
0
WBM
LSK
HSC
MPP
LMPP
CLP
MEP
CMP
GMP
Gr1+Mac1+
b
Mettl3 genomic location
Mettl3fl
Exon 4
Mettl3Δ
pIpC
Mx1
Cre
Mettl3fl/fl
Mettl3Δ/Δ
c
Control
Mx1-cre; Mettl3fl/fl
Mettl3fl
Mettl3Δ
β-actin
d
P=0.004
Normalized Mettl3 mRNA
2.0
1.5
1.0
0.5
0.0
Con
Δ/Δ

Figure 2.1

Deletion of *Mettl3* led to a significant reduction in bone marrow cellularity (**Figure 2.2d**), but not spleen cellularity 10-14 days after the last pIpC injection (**Figure 2.3b**). However, by 2-4 months after the last pIpC injection, in addition to a significant bone marrow cellularity reduction, the spleen size and cellularity were significantly increased with a distortion of cell type distribution (**Figure 2.2e** and **Figure 2.3b-c**). The spleens contained more HSCs in *Mx1-cre; Mettl3$^{fl/fl}$* mice compared with controls (**Figure 2.2f**). These data are suggestive of extramedullary hematopoiesis after loss of m^{6}A.

In the bone marrow, Lin$^-$Sca1$^+$cKit$^+$ (LSK) hematopoietic progenitors (**Figure 2.2g**) and HSCs (**Figure 2.2h-j**) were significantly increased at all time points examined. The HSC pool uniquely expanded over time from 10-14 days to 4 months after the last pIpC injection: progressing from a 3-fold to a 17-fold increase in HSC frequency (**Figure 2.2h-j**). In contrast, CD150$^-$CD48$^-$LSK MPP frequency was not significantly increased while CD150$^-$CD48$^+$LSK progenitor frequency was only modestly increased (**Figure 2.2k** and **Figure 2.3e**). CD150$^+$CD48$^+$LSK megakaryocyte-skewed multipotent progenitor frequency was significantly increased (**Figure 2.3f**), suggesting that there is also an effect on the megakaryocyte lineage. Thus, at the top of the hematopoietic hierarchy, loss of m^{6}A preferentially leads to HSC accumulation.

We also examined other hematopoietic progenitors in the bone marrow. These included Lin$^-$Sca1^{low}cKit^{low}Flt3$^+$IL7Rα^+ common lymphoid progenitors (CLPs), CD34$^+$FcγR$^-$Lineage$^-$Sca1$^-$cKit$^+$ common myeloid progenitors (CMPs), CD34$^+$FcγR$^+$Lineage$^-$Sca1$^-$cKit$^+$ granulocyte/macrophage progenitors (GMPs), and CD34$^-$FcγR$^-$Lineage$^-$Sca1$^-$cKit$^+$ megakaryocytic/erythroid progenitors (MEPs). The frequencies of these hematopoietic progenitors were unchanged in *Mx1-cre; Mettl3$^{fl/fl}$* mice compared with controls until 4 months after the last pIpC treatment, when there was a modest decrease in GMP and a modest increase in MEP frequencies (**Figure 2.3g**). There was a significant increase in Lin$^-$Sca1$^-$

cKit^{+}CD150^{+}CD41^{+} megakaryocyte progenitors and CD41^{+} megakaryocytic cells in the bone marrow (**Figure 2.3h-i**), suggesting that the reduction in platelet counts (**Figure 2.2b**) is due to a differentiation defect in the megakaryocyte lineage. These data suggest that loss of *Mettl3* preferentially impacts HSCs, with effects on the megakaryocyte lineage.

Figure 2.2 Loss of *Mettl3* leads to accumulation of HSCs and perturbed hematopoiesis.

(**a - c**) White blood cell (**a**), platelet (**b**), and red blood cell counts (**c**) from pIpC-treated control and *Mx1-cre; Mettl3*$^{fl/fl}$ mice (n=7 for control (10-14d), n=7 for *Mx1-cre; Mettl3*$^{fl/fl}$ (10-14d), n=4 for control (2-3m), n=4 for *Mx1-cre; Mettl3*$^{fl/fl}$ (2-3m), n=3 for control (4m), n=4 for *Mx1-cre; Mettl3*$^{fl/fl}$ (4m)).

(**d**) Bone marrow cellularity per hindlimb (n=8 for control (10-14d), n=8 for *Mx1-cre; Mettl3*$^{fl/fl}$ (10-14d), n=5 for control (2-3m), n=6 for *Mx1-cre; Mettl3*$^{fl/fl}$ (2-3m), n=4 for control (4m), n=4 for *Mx1-cre; Mettl3*$^{fl/fl}$ (4m)).

(**e**) Representative images of the spleens from *Mx1-cre; Mettl3*$^{fl/fl}$ and control mice 10 days and 3 months after pIpC treatment, as indicated.

(**f**) Splenic HSC frequency (n=6 for control (10-14d), n=5 for *Mx1-cre; Mettl3*$^{fl/fl}$ (10-14d), n=6 for control (2-3m), n=6 for *Mx1-cre; Mettl3*$^{fl/fl}$ (2-3m), n=4 for control (4m), n=4 for *Mx1-cre; Mettl3*$^{fl/fl}$ (4m)).

(**g**) Frequencies of bone marrow Lin^{-}Sca-1^{+}c-Kit^{+} (LSK) progenitors (n=7 for control (10-14d), n=6 for *Mx1-cre; Mettl3*$^{fl/fl}$ (10-14d), n=6 for control (2-3m), n=7 for *Mx1-cre; Mettl3*$^{fl/fl}$ (2-3m), n=4 for control (4m), n=4 for *Mx1-cre; Mettl3*$^{fl/fl}$ (4m)).

(**h**) Frequency of bone marrow HSCs (n=7 for control (10-14d), n=6 for *Mx1-cre; Mettl3*$^{fl/fl}$ (10-14d), n=6 for control (2-3m), n=7 for *Mx1-cre; Mettl3*$^{fl/fl}$ (2-3m), n=4 for control (4m), n=4 for *Mx1-cre; Mettl3*$^{fl/fl}$ (4m)).

(**i**) Bone marrow HSCs per hindlimb (n=7 for control (10-14d), n=6 for *Mx1-cre; Mettl3*$^{fl/fl}$ (10-14d), n=5 for control (2-3m), n=6 for *Mx1-cre; Mettl3*$^{fl/fl}$ (2-3m), n=4 for control (4m), n=4 for *Mx1-cre; Mettl3*$^{fl/fl}$ (4m)).

(**j**) Fold increase in *Mx1-cre; Mettl3*$^{fl/fl}$ bone marrow HSC or MPP frequency compared to littermate control frequencies at indicated times after pIpC treatment (n=6 (10-14d), n=7 (2-3m), n=4 (4m)).

(**k**) Bone marrow $CD150^{-}CD48^{-}$LSK MPP frequencies (n=6 for control (10-14d), n=6 for *Mx1-cre; Mettl3*$^{fl/fl}$ (10-14d), n=6 for control (2-3m), n=7 for *Mx1-cre; Mettl3*$^{fl/fl}$ (2-3m), n=4 for control (4m), n=4 for *Mx1-cre; Mettl3*$^{fl/fl}$ (4m)).

All samples are from biologically independent mice. Values are shown as individual points with mean ± s.d. P values were determined by unpaired two-sided Student's t-test.

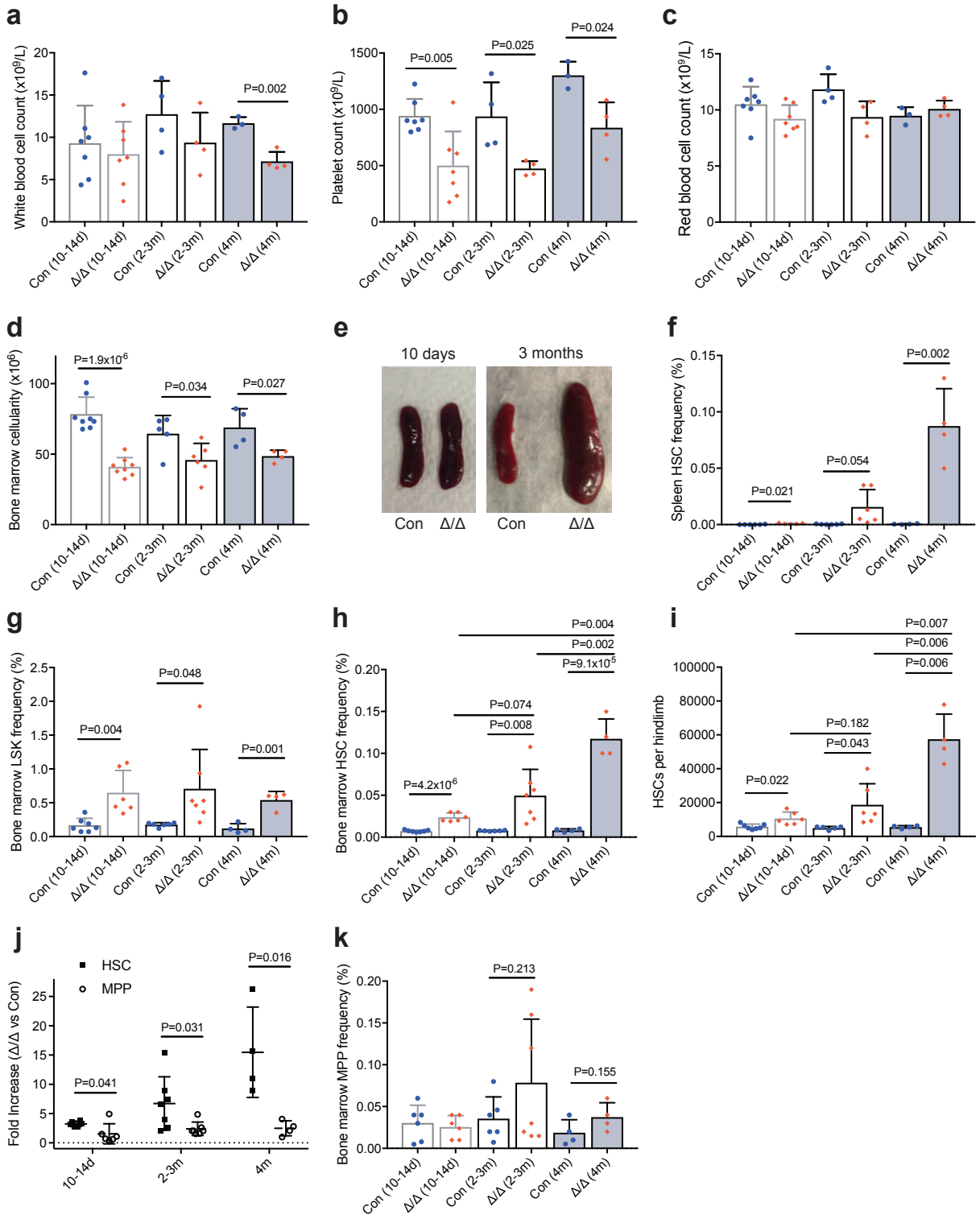
a
White blood cell count (x10⁹/L)
P=0.002
b
Platelet count (x10⁹/L)
P=0.005
P=0.025
P=0.024
c
Red blood cell count (x10⁹/L)
d
Bone marrow cellularity (x10⁶)
P=1.9x10⁶
P=0.034
P=0.027
e
10 days
3 months
Con
Δ/Δ
Con
Δ/Δ
f
Spleen HSC frequency (%)
P=0.021
P=0.054
P=0.002
g
Bone marrow LSK frequency (%)
P=0.004
P=0.048
P=0.001
h
Bone marrow HSC frequency (%)
P=4.2x10⁶
P=0.074
P=0.008
P=0.004
P=0.002
P=9.1x10⁵
i
HSCs per hindlimb
P=0.022
P=0.182
P=0.043
P=0.007
P=0.006
P=0.006
j
HSC
MPP
Fold Increase (Δ/Δ vs Con)
P=0.041
P=0.031
P=0.016
10-14d
2-3m
4m
k
Bone marrow MPP frequency (%)
P=0.213
P=0.155
Con (10-14d)
Δ/Δ (10-14d)
Con (2-3m)
Δ/Δ (2-3m)
Con (4m)
Δ/Δ (4m)

Figure 2.2

Figure 2.3 *Mx1-cre; Mettl3$^{fl/fl}$* mice have defective hematopoiesis.

(**a**) White blood cell count differential for control and *Mx1-cre; Mettl3$^{fl/fl}$* mice 4 months after pIpC treatment (n=3 for control, n=4 for *Mx1-cre; Mettl3$^{fl/fl}$*).

(**b**) Spleen cellularity (n=8 for control (10-14d), n=8 for *Mx1-cre; Mettl3$^{fl/fl}$* (10-14d), n=5 for control (2-3m), n=6 for *Mx1-cre; Mettl3$^{fl/fl}$* (2-3m), n=4 for control (4m), n=4 for *Mx1-cre; Mettl3$^{fl/fl}$* (4m)).

(**c**) Frequency of cell populations in the spleens of *Mx1-cre; Mettl3$^{fl/fl}$* mice at least 14 days after pIpC treatment with prominent splenomegaly compared to controls (n=5 for control, n=5 for *Mx1-cre; Mettl3$^{fl/fl,}$* , except LSK n=4 for control, n=4 for *Mx1-cre; Mettl3$^{fl/fl}$*).

(**d**) Representative flow cytometric plots of Lin$^-$ gated and LSK gated bone marrow cells stained for the indicated cell surface markers. Numbers represent the population frequencies among single live bone marrow cells.

(**e**) Bone marrow CD150$^-$CD48$^+$LSK progenitor frequencies (n=5 for control (10-14d), n=5 for *Mx1-cre; Mettl3$^{fl/fl}$* (10-14d), n=5 for control (2-3m), n=6 for *Mx1-cre; Mettl3$^{fl/fl}$* (2-3m), n=4 for control (4m), n=4 for *Mx1-cre; Mettl3$^{fl/fl}$* (4m)).

(**f**) Bone marrow CD150$^+$CD48$^+$LSK progenitor frequencies (n=5 for control (10-14d), n=5 for *Mx1-cre; Mettl3$^{fl/fl}$* (10-14d), n=5 for control (2-3m), n=6 for *Mx1-cre; Mettl3$^{fl/fl}$* (2-3m), n=4 for control (4m), n=4 for *Mx1-cre; Mettl3$^{fl/fl}$* (4m)).

(**g**) Frequencies of bone marrow progenitor populations. CLP, common lymphoid progenitor; CMP, common myeloid progenitors; GMP, granulocyte–monocyte progenitors; MEP, megakaryocyte–erythroid progenitors; LMPP, lymphoid-primed multipotent progenitors (n=4 for control (10-14d), n=4 for *Mx1-cre; Mettl3$^{fl/fl}$* (10-14d), n=5 for control (2-3m), n=6 for *Mx1-cre; Mettl3$^{fl/fl}$* (2-3m), n=4 for control (4m), n=4 for *Mx1-cre; Mettl3$^{fl/fl}$* (4m)).

(**h**) Frequency of megakaryocyte progenitors (Lineage$^-$Sca1$^-$cKit$^+$CD150$^+$CD41$^+$) cells in the bone marrow >10 days after pIpC treatment (n=5 for control, n=6 for *Mx1-cre; Mettl3$^{fl/fl}$*).

(**i**) Frequencies of mature cell populations in the bone marrow (n=4 for control (10-14d), n=4 for *Mx1-cre; Mettl3*$^{fl/fl}$ (10-14d), n=5 for control (2-3m), n=5 for *Mx1-cre; Mettl3*$^{fl/fl}$ (2-3m), n=4 for control (4m), n=4 for *Mx1-cre; Mettl3*$^{fl/fl}$ (4m)).

(**j**) 2'-7'-dichlorofluorescein diacetate (DCFDA) staining (ROS levels) by flow cytometry in HSCs 2-3 months after pIpC treatment (n=3 for control, n=3 for *Mx1-cre; Mettl3*$^{fl/fl}$).

(**k**) γH2AX staining by flow cytometry in HSCs 2-3 months after pIpC treatment (n=3 for control, n=3 for *Mx1-cre; Mettl3*$^{fl/fl}$).

All samples were from biologically independent animals. Values are shown as individual points with mean ± s.d. In (**h**) and (**i**), normalized geometric mean fluorescence intensity (MFI ± s.d.) values are shown. P values were determined by unpaired two-sided Student's t-test.

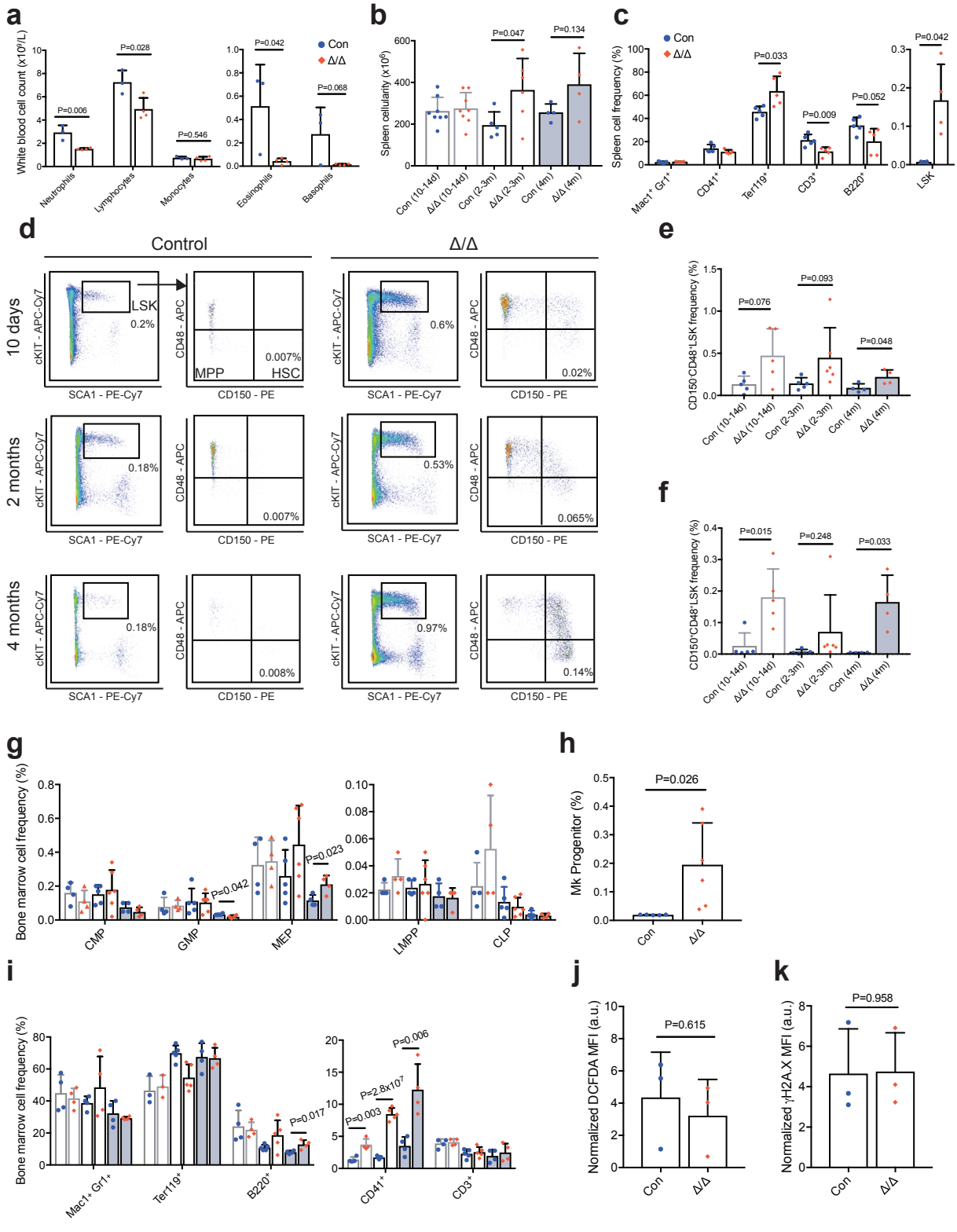
a
White blood cell count (x10⁹/L)
P=0.006
P=0.028
P=0.546
P=0.042
P=0.068
Con
Δ/Δ
Neutrophils
Lymphocytes
Monocytes
Eosinophils
Basophils
b
Spleen cellularity (x10⁶)
P=0.047
P=0.134
Con (10-14d)
Δ/Δ (10-14d)
Con (2-3m)
Δ/Δ (2-3m)
Con (4m)
Δ/Δ (4m)
c
Spleen cell frequency (%)
Con
Δ/Δ
P=0.033
P=0.009
P=0.052
P=0.042
Mac1+ Gr1+
CD41+
Ter119+
CD3+
B220+
LSK
d
Control
Δ/Δ
10 days
2 months
4 months
cKIT - APC-Cy7
SCA1 - PE-Cy7
CD48 - APC
CD150 - PE
LSK
0.2%
MPP
HSC
0.007%
0.6%
0.02%
0.18%
0.53%
0.065%
0.008%
0.97%
0.14%
e
CD150+CD48-LSK frequency (%)
P=0.076
P=0.093
P=0.048
f
CD150+CD48-LSK frequency (%)
P=0.015
P=0.248
P=0.033
g
Bone marrow cell frequency (%)
P=0.042
P=0.023
CMP
GMP
MEP
LMPP
CLP
h
Mk Progenitor (%)
P=0.026
Con
Δ/Δ
i
Bone marrow cell frequency (%)
P=0.017
P=0.006
P=2.8x10⁻⁷
P=0.003
Mac1+ Gr1+
Ter119+
B220+
CD41+
CD3+
j
Normalized DCFDA MFI (a.u.)
P=0.615
k
Normalized γH2A.X MFI (a.u.)
P=0.958

Figure 2.3

Deletion of *Mettl3* preferentially blocks HSC differentiation

HSCs from pIpC-injected *Mx1-cre; Mettl3*$^{fl/fl}$ mice did not incorporate more BrdU (**Figure 2.4a**), but underwent slightly more cell death (**Figure 2.4b**), suggesting that the accumulation of HSCs may be the result of blocked differentiation rather than enhanced self-renewal. The *Mettl3*-deficient HSCs did not have elevated levels of reactive oxygen species (ROS) or γH2Ax staining (**Figure 2.3h-i**). Consistent with an HSC differentiation defect, pIpC-injected *Mx1-cre; Mettl3*$^{fl/fl}$ mice had worse survival compared to controls when challenged with a myeloablative agent, 5-fluorouracil (5FU) (**Figure 2.4c**).

To directly assess the differentiation potential of *Mettl3*-deficient HSCs, we performed methylcellulose assays. Single HSCs from pIpC-treated *Mx1-cre; Mettl3*$^{fl/fl}$ or control mice were directly sorted into methylcellulose, which supports myelo-erythroid differentiation *in vitro* (Ding et al., 2012; Ding and Morrison, 2013). Significantly fewer *Mettl3*-deficient HSCs formed colonies compared with control HSCs, particularly multipotent granulocyte, erythrocyte, monocyte and megakaryocyte (GEMM) colonies (**Figure 2.4d**). The vast majority of the colonies formed by *Mettl3*-deficient HSCs were significantly smaller compared with those formed by control HSCs (**Figure 2.4e-f**). Flow cytometric analysis on cells from these colonies showed that *Mettl3*-deficient HSCs failed to differentiate while control HSCs readily differentiated into $Gr1^+$ and $Mac1^+$ myeloid cells (**Figure 2.4g-i**). A few colonies were formed at normal sizes by *Mettl3*-deficient HSCs and genotyping revealed that these colonies had escaped complete *Mettl3* deletion (**Figure 2.4j-k**). *Mettl3*-deficient HSCs in the spleens also failed to differentiate (**Figure 2.5a**).

In contrast, when *Mettl3*-deficient whole bone marrow cells were plated into methylcellulose, colonies formed at similar numbers, size and types compared with controls (**Figure 2.5b**). We further plated sorted *Mettl3*-deficient restricted progenitors (LSK, $CD150^-$ $CD48^+$LSK and $CD150^+CD48^+$LSK), into methylcellulose. They formed normal numbers of colonies, similar in size and type compared with controls (**Figure 2.5c**). Flow cytometry analysis

confirmed that these colonies contained normal numbers of differentiated cells (**Figure 2.5d**). Taken together, these data suggest that loss of *Mettl3* preferentially leads to a differentiation block in HSCs but not in restricted progenitors *in vitro*.

Figure 2.4 *Mettl3* is essential for adult HSC differentiation *in vitro*.

(**a**) Frequency of $BrdU^+$ HSCs 10-14 days after pIpC treatment (n=4 for control, n=4 for *Mx1-cre; Mettl3*$^{fl/fl}$).

(**b**) Frequency of $DAPI^-$ $AnnexinV^+$ HSC, MPP and LSK populations 10-14 days after pIpC (n=6 for control, n=6 for *Mx1-cre; Mettl3*$^{fl/fl}$).

(**c**) Kaplan-Meyer survival analysis of control and *Mx1-cre; Mettl3*$^{fl/fl}$ mice treated with weekly 5-FU injections 10 days after the last dose of pIpC. P value by log-rank test (n=4 for control, n=4 for *Mx1-cre; Mettl3*$^{fl/fl}$).

(**d**) Frequencies of colony formation from single sorted HSCs. Colony-forming units (CFU) scored as granulocyte, erythroid, macrophage, megakaryocyte (GEMM), granulocyte, macrophage (GM), megakaryocyte (Mk), or erythrocyte (E) colonies (n=7 for control, n=7 for *Mx1-cre; Mettl3*$^{fl/fl}$).

(**e**) Representative image of CFU-GM from single HSCs from control (left) and *Mettl3*-deleted (right) single HSCs, genotypes confirmed by PCR. Scale bars are 400um.

(**f**) The proportion of large colonies (estimated >5,000 cells) out of all colonies formed from HSCs (n=6 for control, n=6 for *Mx1-cre; Mettl3*$^{fl/fl}$) or LSK cells (n=6 for control, n=6 for *Mx1-cre; Mettl3*$^{fl/fl}$).

(**g**) Representative flow cytometric histograms of mature myeloid cell surface markers Gr-1 and Mac-1 on HSC-derived colony cells from pIpC-treated control and *Mx1-cre; Mettl3*$^{fl/fl}$ mice.

(**h-i**) Quantification of expression of Gr-1 (**h**) and Mac-1 (**i**) cell surface markers on HSC and LSK colony cells by flow cytometry (HSC n=8 for control, n=6 for *Mx1-cre; Mettl3*$^{fl/fl}$; LSK n=6 for control, n=6 for *Mx1-cre; Mettl3*$^{fl/fl}$).

(**j**) Representative images of colonies from control and *Mx1-cre; Mettl3*$^{fl/fl}$ LSK cells. Experiment was repeated four times from biologically independent animals with similar results. Scale bars are 400um.

(**k**) Representative genotyping image of colonies formed by single HSCs grouped by size. Experiment was repeated four times from biologically independent animals with similar results. All samples are from biologically independent animals. Values are shown as individual points with mean ± s.d. P values were determined by unpaired two-sided Student's t-test.

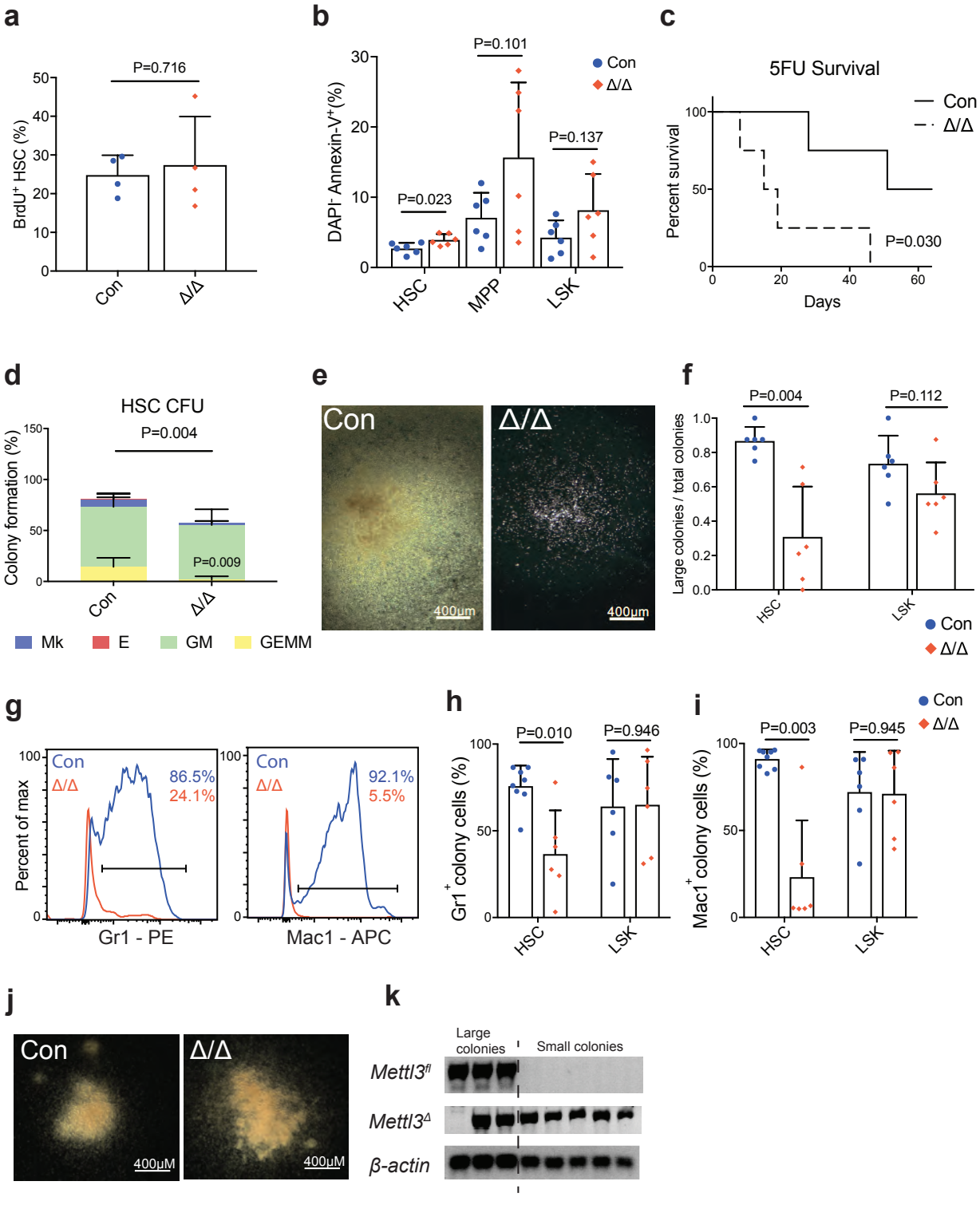
a
P=0.716
BrdU+ HSC (%)
Con
Δ/Δ
b
P=0.101
P=0.137
P=0.023
DAPI- Annexin-V+(%)
Con
Δ/Δ
HSC
MPP
LSK
c
5FU Survival
Con
Δ/Δ
Percent survival
P=0.030
Days
d
HSC CFU
P=0.004
P=0.009
Colony formation (%)
Con
Δ/Δ
Mk
E
GM
GEMM
e
Con
Δ/Δ
400μm
400μm
f
P=0.004
P=0.112
Large colonies / total colonies
HSC
LSK
Con
Δ/Δ
g
Con
Δ/Δ
86.5%
24.1%
92.1%
5.5%
Percent of max
Gr1 - PE
Mac1 - APC
h
P=0.010
P=0.946
Gr1+ colony cells (%)
HSC
LSK
i
Con
Δ/Δ
P=0.003
P=0.945
Mac1+ colony cells (%)
HSC
LSK
j
Con
Δ/Δ
400μM
400μM
k
Large colonies
Small colonies
Mettl3fl
Mettl3Δ
β-actin

Figure 2.4

Figure 2.5 HSCs preferentially require *Mettl3* compared to other hematopoietic progenitors for differentiation *in vitro*.

(**a**) Quantification of the frequency of $Gr1^+$ and $Mac1^+$ cells by flow cytometry on colony cells from splenic HSCs in *Mx1-cre; Mettl3*$^{fl/fl}$ mice at least 14 days after pIpC treatment with prominent splenomegaly compared to controls (n=5 for control, n=5 for *Mx1-cre; Mettl3*$^{fl/fl}$).

(**b**) Numbers of colonies formed from 10,000 bone marrow cells, scored as CFU-GEMM, CFU-GM, CFU-E, or CFU-MK (n=4 for control, n=4 for *Mx1-cre; Mettl3*$^{fl/fl}$).

(**c**) Number of colonies formed from control and *Mx1-cre; Mettl3*$^{fl/fl}$ cells of the indicated populations 10 days after pIpC treatment. 200 LSK cells, 50 MPP cells, 24 $CD150^-CD48^+$LSK and 24 $CD150^+CD48^+$LSK cells were plated per experiment. (For LSK and MPP: n=4 for control, n=4 for *Mx1-cre; Mettl3*$^{fl/fl}$; for $CD150^-CD48^+$LSK and $CD150^+CD48^+$LSK: n=3 for control, n=3 for *Mx1-cre; Mettl3*$^{fl/fl}$).

(**d**) Quantification of the frequency of $Gr1^+$ and $Mac1^+$ cells by flow cytometry on colony cells from the indicated cell populations from mice 10 days after pIpC treatment. (MPP: n=7 for control, n=7 for *Mx1-cre; Mettl3*$^{fl/fl}$; $CD150^-CD48^+$LSK: n=10 for control, n=8 for *Mx1-cre; Mettl3*$^{fl/fl}$; $CD150^+CD48^+$LSK: n=7 for control, n=6 for *Mx1-cre; Mettl3*$^{fl/fl}$;).

All samples are from biologically independent animals. Values are shown as individual points with mean ± s.d. P values were determined by unpaired two-sided Student's t-test.

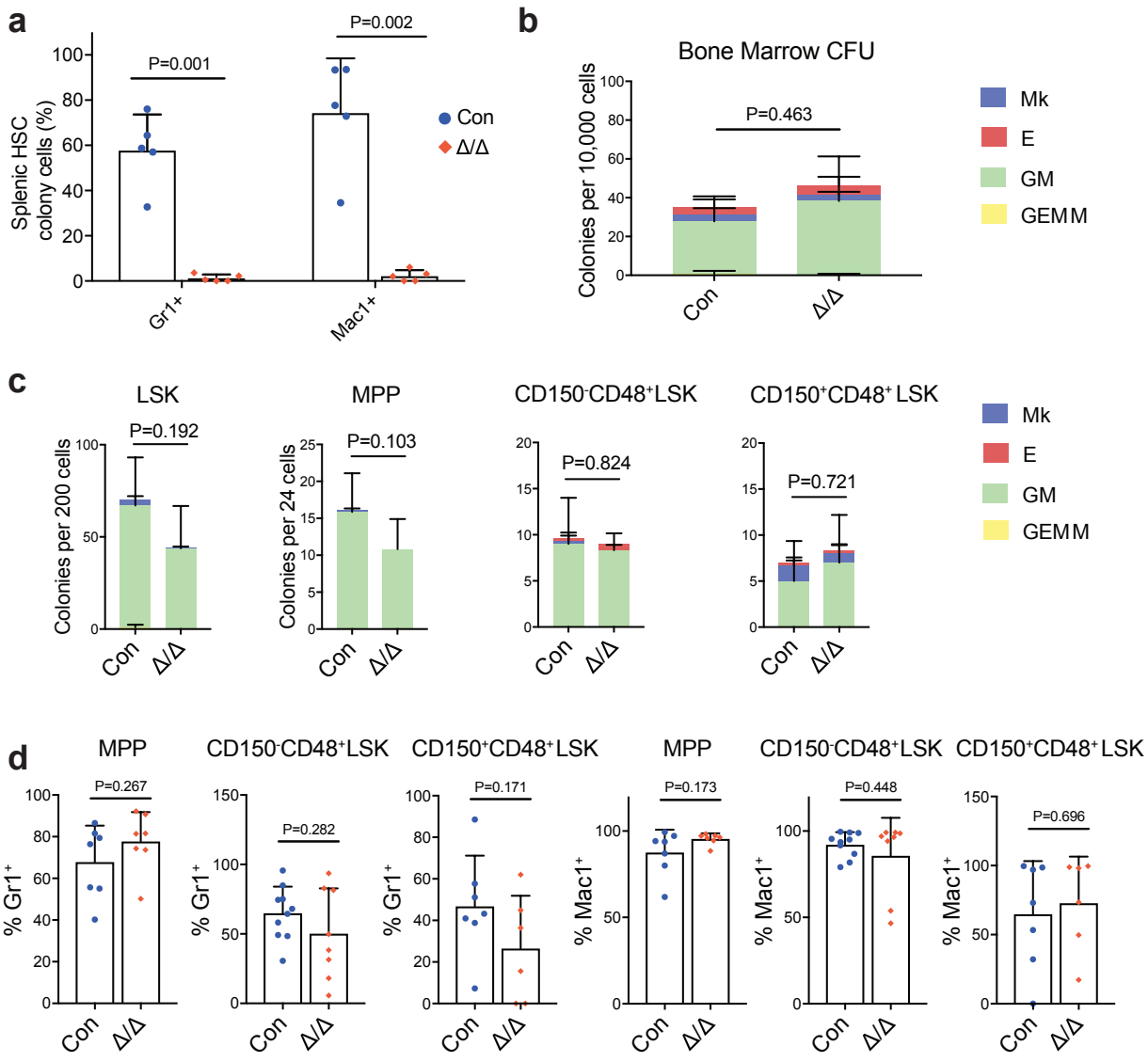
a
P=0.001
P=0.002
Splenic HSC colony cells (%)
Con
Δ/Δ
Gr1+
Mac1+
b
Bone Marrow CFU
P=0.463
Colonies per 10,000 cells
Mk
E
GM
GEMM
Con
Δ/Δ
c
LSK
MPP
CD150-CD48+LSK
CD150+CD48+ LSK
P=0.192
P=0.103
P=0.824
P=0.721
Colonies per 200 cells
Colonies per 24 cells
d
MPP
CD150-CD48+LSK
CD150+CD48+LSK
P=0.267
P=0.282
P=0.171
P=0.173
P=0.448
P=0.696
% Gr1+
% Mac1+

Figure 2.5

Deletion of *Mettl3* leads to cell-intrinsic HSC reconstitution and differentiation defects *in vivo*

To test whether loss of *Mettl3* leads to HSC defects *in vivo*, we performed competitive reconstitution assays by transplanting 500,000 bone marrow cells from *Mx1-cre; Mettl3*$^{fl/fl}$ or control mice 10 days after the last pIpC injection along with 500,000 wild-type competing bone marrow cells into lethally irradiated recipient mice. *Mettl3*-deficient bone marrow cells contributed significantly lower levels of overall, myeloid, B and T lineage cells in the peripheral blood and a trend towards lower levels of HSCs in the bone marrow compared with controls (**Figure 2.6a** and **Figure 2.7a**). Genotyping analysis on sorted residual donor-derived peripheral blood cells demonstrated that these residual cells escaped complete *Mettl3* deletion (**Figure 2.7b**). To specifically test whether HSCs were functionally defective, we sorted and transplanted *Mettl3*-deficient and control HSCs along with wild-type competing bone marrow cells into lethally irradiated mice. While control HSCs readily reconstituted the recipient mice in all major hematopoietic lineages, *Mettl3*-deficient HSCs failed to give any discernable reconstitution (**Figure 2.6b** and **Figure 2.7c**). These data suggest that *Mettl3*-deficient HSCs are defective in reconstituting recipient mice.

To determine whether *Mettl3* is required cell-intrinsically for HSC function, we transplanted *Mx1-cre; Mettl3*$^{fl/fl}$ or control bone marrow cells, without pIpC treatment, along with wild-type competitor bone marrow cells into irradiated recipient mice. We waited at least 8 weeks after transplantation for stable bone marrow chimerism to be established. *Mettl3* was then deleted by pIpC injection and donor-derived peripheral blood cells were monitored over time. Overall reconstitution by *Mettl3*-deficient bone marrow cells was significantly lower than controls (**Figure 2.6c**). The reconstitution defects were mainly in the myeloid and B lineages, but not in the T cell lineages (**Figure 2.6c**), consistent with the slow turnover kinetics of T cells in adults *in vivo*. After 16 weeks, the recipient mice were sacrificed and analyzed for the frequencies of donor-derived bone marrow HSCs and hematopoietic progenitors. *Mettl3*-

deficient HSCs were present at similar levels compared with control HSCs (**Figure 2.6d**), suggesting that HSC self-renewal is largely normal. However, these HSCs generated gradually less mature hematopoietic cells along the differentiation hierarchy (**Figure 2.6d**). Consistent with the depletion of donor-derived myeloid cells in the peripheral blood (**Figure 2.6c**), very little CMPs, GMPs and MEPs were derived from *Mettl3*-deficient HSCs (**Figure 2.6d**). Genotyping on sorted donor-derived cells in recipient mice showed that these residual cells escaped complete *Mettl3* deletion (**Figure 2.7d**). These data suggest that *Mettl3* is required for HSC differentiation *in vivo*.

We also conditionally deleted *Mettl3* from hematopoietic cells using *Rosa26-creER*[25]. We noncompetitively transplanted bone marrow cells from *Rosa26-creER; Mettl3*$^{fl/fl}$ mice into irradiated recipient mice and then deleted *Mettl3* by administering tamoxifen. Deletion of *Mettl3* led to a significantly higher frequency of HSCs in the recipient mice (**Figure 2.7e**), recapitulating the *Mx1-cre; Mettl3*$^{fl/fl}$ model (**Figure 2.2h**). We also competitively transplanted *Rosa26-creER; Mettl3*$^{fl/fl}$ bone marrow cells together with recipient-type bone marrow cells and waited at least 8 weeks after transplantation for stable bone marrow chimerism before administering tamoxifen. Tamoxifen-induced deletion of *Mettl3* also led to a significant reduction in reconstitution activity (**Figure 2.7f**), similar to *Mx1-cre; Mettl3*$^{fl/fl}$ mice (**Figure 2.6c**).

Figure 2.6 Loss of *Mettl3* disrupts HSC differentiation *in vivo*.

(**a**) Competitive transplantation of 500,000 donor whole bone marrow cells from pIpC-treated *Mx1-cre; Mettl3*$^{fl/fl}$ or *Mettl3*$^{fl/fl}$ controls with 500,000 competitor cells. Multi-lineage chimera levels in the peripheral blood were assessed up to 16 weeks after transplantation (n=7 for control, n=8 for *Mx1-cre; Mettl3*$^{fl/fl}$*;* samples were from independent recipients of two independent donor pairs from two experiments).

(**b**) Competitive transplantation of 50 sorted HSCs from pIpC-treated *Mx1-cre; Mettl3*$^{fl/fl}$ or controls with 300,000 competitor cells. Multi-lineage chimera levels in the peripheral blood were assessed up to 16 weeks after transplantation (n=9 for control, n=9 for *Mx1-cre; Mettl3*$^{fl/fl}$*;* samples were from independent recipients of two independent donor pairs from two experiments).

(**c**) 500,000 donor whole bone marrow cells from untreated *Mx1-cre; Mettl3*$^{fl/fl}$ or controls with 500,000 competitor cells were transplanted into lethally irradiated recipient mice. Recipients were treated with pIpC after stable peripheral blood chimerism was established. Multi-lineage peripheral blood chimera levels shown as the percentage of the original chimera level up to 16 weeks after pIpC treatment (n=11 for control, n=12 for *Mx1-cre; Mettl3*$^{fl/fl}$*;* samples were from independent recipients of three independent donor pairs from three experiments).

(**d**) Chimera levels of indicated bone marrow cell populations 20 weeks after pIpC treatment from (**c**) (n=9 for control, n=9 for *Mx1-cre; Mettl3*$^{fl/fl}$; samples were from independent recipients of three independent donor pairs from three experiments).

Values are shown as individual points with mean ± s.d. P values were determined by unpaired two-sided Student's t-test.

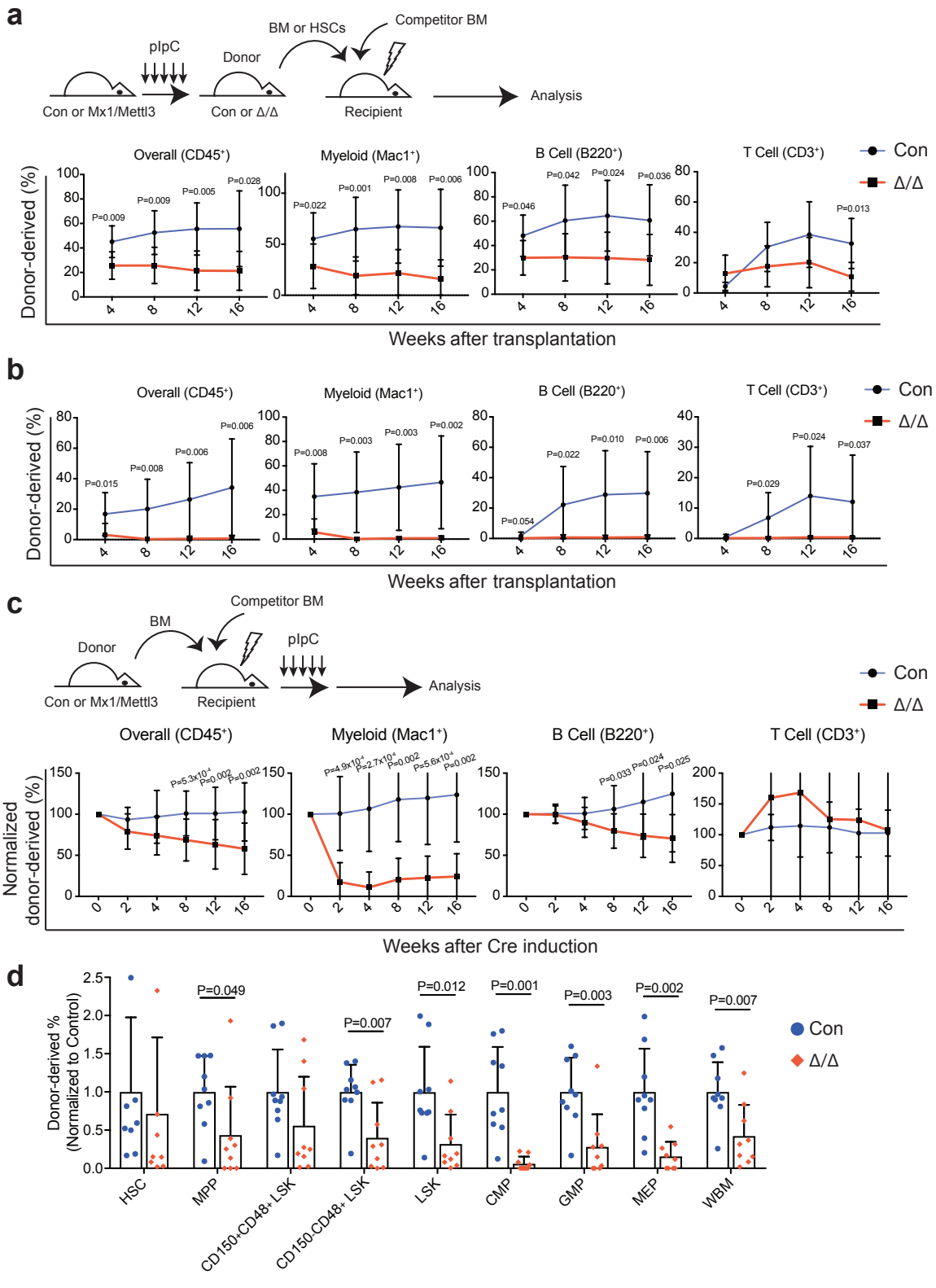
a
pIpC
BM or HSCs
Competitor BM
Donor
Con or Mx1/Mettl3
Con or Δ/Δ
Recipient
Analysis
Overall (CD45+)
Myeloid (Mac1+)
B Cell (B220+)
T Cell (CD3+)
Con
Δ/Δ
Donor-derived (%)
Weeks after transplantation
b
Overall (CD45+)
Myeloid (Mac1+)
B Cell (B220+)
T Cell (CD3+)
Con
Δ/Δ
Donor-derived (%)
Weeks after transplantation
c
Competitor BM
BM
Donor
pIpC
Con or Mx1/Mettl3
Recipient
Analysis
Con
Δ/Δ
Overall (CD45+)
Myeloid (Mac1+)
B Cell (B220+)
T Cell (CD3+)
Normalized donor-derived (%)
Weeks after Cre induction
d
Donor-derived % (Normalized to Control)
P=0.049
P=0.007
P=0.012
P=0.001
P=0.003
P=0.002
P=0.007
Con
Δ/Δ
HSC
MPP
CD150+CD48+ LSK
CD150-CD48+ LSK
LSK
CMP
GMP
MEP
WBM

Figure 2.6

***Mettl3* is not required for myelopoiesis**

To directly test whether the observed predominant myeloid lineage reconstitution defect (**Figure 2.6c**) was a consequence of loss of *Mettl3* in myeloid cells, we conditionally deleted *Mettl3* from myeloid cells by generating *Lysm-cre; Mettl3*$^{fl/fl}$ mice. Consistent with previous reports (Clausen et al., 1999), *Lysm-cre* efficiently recombined in bone marrow myeloid cells (**Figure 2.7g**). Six to 8-week old *Lysm-cre; Mettl3*$^{fl/fl}$ mice had normal peripheral blood counts (**Figure 2.7h** and **Figure 2.8a-b**), normal bone marrow and spleen cellularity (**Figure 2.7i** and **Figure 2.8c**), and normal frequencies of myeloid cells in the bone marrow and spleens (**Figure 2.8d**).

Mettl3-deficient bone marrow myeloid cells from *Lysm-cre; Mettl3*$^{fl/fl}$ mice formed macrophages with normal morphology (**Figure 2.7j**). When challenged with lipopolysaccharide (LPS), these macrophages showed normal up-regulation of inflammatory cytokines, *Tnfa*, *Il1b* and *Il6* (**Figure 2.8e**). *Mettl3*-deficient bone marrow-derived macrophages also displayed robust engulfing activity, similar to controls (**Figure 2.8f**). These data suggest that *Mettl3* is not required for the maintenance or function of mature myeloid cells and the observed reconstitution deficiencies (**Figure 2.6c**) are a consequence of HSC differentiation defects. Furthermore, these data provide conclusive evidence that there is a stage-specific dependence on *Mettl3* and m^{6}A during hematopoietic differentiation *in vivo*.

Figure 2.7 HSCs, but not mature myeloid cells, require *Mettl3* for function *in vivo*.

(**a**) Chimera levels of bone marrow HSCs 16 weeks after transplantation from Fig. 3a (n=7 for control, n=6 for *Mx1-cre; Mettl3$^{fl/fl}$;* samples were from independent recipients of two independent donor pairs from two experiments).

(**b**) Representative genotyping images of *Mx1-cre; Mettl3$^{fl/fl}$* donor-derived cells 20 weeks after transplantation from Fig. 3a showing incomplete deletion of *Mettl3*. Experiment was repeated twice with similar results.

(**c**) Chimera levels of bone marrow HSCs 16 weeks after transplantation from Fig. 3b (n=9 for control, n=9 for *Mx1-cre; Mettl3$^{fl/fl}$* ; samples were from independent recipients of two independent donor pairs from two experiments).

(**d**) Representative genotyping images of *Mx1-cre; Mettl3$^{fl/fl}$* donor-derived cells 12 weeks after pIpC treatment from Fig. 3c showing incomplete deletion of *Mettl3*. Experiment was repeated twice with similar results.

(**e**) 1 million donor whole bone marrow cells from untreated *Rosa26-CreER; Mettl3$^{fl/fl}$* or control mice were noncompetitively transplanted into lethally irradiated recipient mice. Recipients with peripheral blood chimerism of >90% were treated with tamoxifen (TAM) 6 weeks after the transplantation. The frequency of donor HSCs 8 weeks after TAM is shown (n=4 for control, n=3 for *Rosa26-CreER; Mettl3$^{fl/fl}$* ; samples were from independent recipients of two independent donor pairs from two experiments).

(**f**) Schematic of experimental design (top). 500,000 donor whole bone marrow cells from untreated *Rosa26-CreER; Mettl3$^{fl/fl}$* or control mice with 500,000 competitor cells were transplanted into lethally irradiated recipient mice. Recipients were treated with tamoxifen (TAM) 6 weeks after the transplantation. Multi-lineage peripheral blood chimera levels are shown as the percentage of original chimera levels up to 16 weeks after TAM treatment (n=12 for control, n=11 for *Rosa26-CreER; Mettl3$^{fl/fl}$* ; samples were from independent recipients of three independent donor pairs from three experiments).

(**g**) qPCR analysis of *Mettl3* mRNA expression in cultured bone marrow macrophages (n=3 for control, n=3 for *LysM-cre; Mettl3*$^{fl/fl}$).

(**h**) Red blood cell and platelet peripheral blood counts (n=6 for control, n=6 for *LysM-cre; Mettl3*$^{fl/fl}$).

(**i**) Spleen cellularity (n=5 for control, n=5 for *LysM-cre; Mettl3*$^{fl/fl}$).

(**j**) Representative images of macrophages derived from control or *LysM-cre; Mettl3*$^{fl/fl}$ bone marrow. Experiment was repeated three times with similar results. Scale bars are 100um.

All samples are from biologically independent animals. Values are shown as individual points with mean ± s.d. P values were determined by unpaired two-sided Student's t-test.

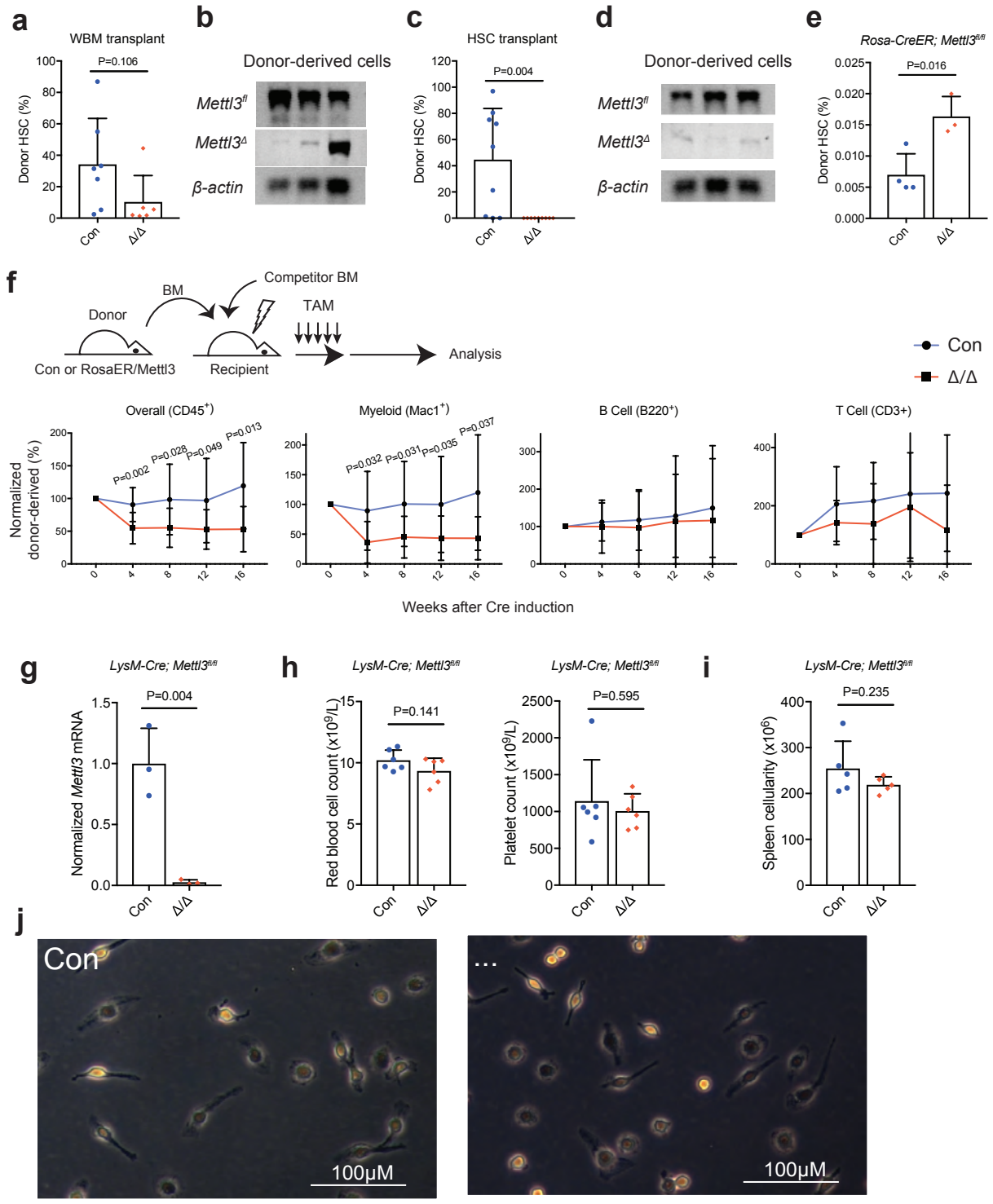
a
WBM transplant
P=0.106
Donor HSC (%)
Con
Δ/Δ
b
Donor-derived cells
Mettl3fl
Mettl3Δ
β-actin
c
HSC transplant
P=0.004
Donor HSC (%)
Con
Δ/Δ
d
Donor-derived cells
Mettl3fl
Mettl3Δ
β-actin
e
Rosa-CreER; Mettl3fl/fl
P=0.016
Donor HSC (%)
Con
Δ/Δ
f
BM
Competitor BM
Donor
TAM
Con or RosaER/Mettl3
Recipient
Analysis
Con
Δ/Δ
Overall (CD45+)
Myeloid (Mac1+)
B Cell (B220+)
T Cell (CD3+)
Normalized donor-derived (%)
P=0.002
P=0.028
P=0.049
P=0.013
P=0.032
P=0.031
P=0.035
P=0.037
Weeks after Cre induction
g
LysM-Cre; Mettl3fl/fl
P=0.004
Normalized Mettl3 mRNA
Con
Δ/Δ
h
LysM-Cre; Mettl3fl/fl
P=0.141
Red blood cell count (x10^9/L)
LysM-Cre; Mettl3fl/fl
P=0.595
Platelet count (x10^9/L)
Con
Δ/Δ
i
LysM-Cre; Mettl3fl/fl
P=0.235
Spleen cellularity (x10^6)
Con
Δ/Δ
j
Con
100μM
...
100μM

Figure 2.7

Figure 2.8 Loss of *Mettl3* has no impact on myeloid cell maintenance or function.

(**a**) White blood cell counts in *LysM-cre; Mettl3*$^{fl/fl}$ mice (n=6 for control, n=6 for *LysM-cre; Mettl3*$^{fl/fl}$).

(**b**) Frequencies of differential white blood cell counts in *LysM-cre; Mettl3*$^{fl/fl}$ mice (n=6 for control, n=6 for *LysM-cre; Mettl3*$^{fl/fl}$).

(**c**) Bone marrow cellularity (n=5 for control, n=5 for *LysM-cre; Mettl3*$^{fl/fl}$).

(**d**) Frequencies of bone marrow (left) and spleen (right) neutrophils (Mac1^{+}Gr1^{+}) and macrophages (Mac1^{+}F4/80^{+}) by flow cytometry (n=5 for control, n=5 for *LysM-cre; Mettl3*$^{fl/fl}$).

(**e**) qPCR analysis of cytokine expression by unstimulated and LPS-stimulated bone marrow macrophages (n=3 for control, n=3 for *LysM-cre; Mettl3*$^{fl/fl}$).

(**f**) Representative histogram (left) and quantification (right) of bone marrow macrophage phagocytosis of fluorescent-labeled beads (n=3 for control, n=3 for *LysM-cre; Mettl3*$^{fl/fl}$). Shaded area denotes background staining (4^{o}C incubation).

All samples were from biologically independent animals. Values are shown as individual points with mean ± s.d. P values were determined by unpaired two-sided Student's t-test.

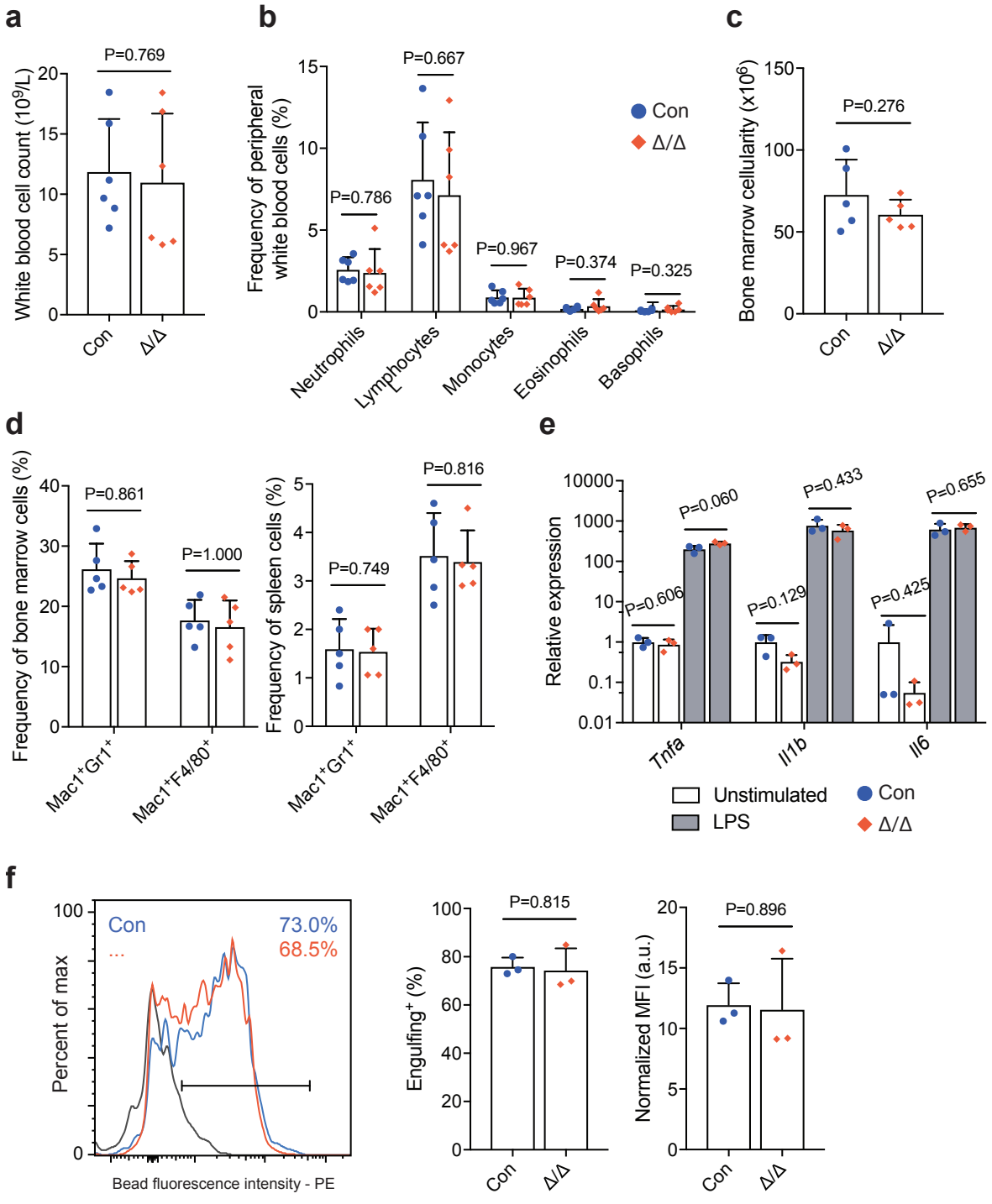
a
White blood cell count (10^9/L)
P=0.769
Con
Δ/Δ
b
Frequency of peripheral white blood cells (%)
P=0.786
P=0.667
P=0.967
P=0.374
P=0.325
Neutrophils
Lymphocytes
Monocytes
Eosinophils
Basophils
Con
Δ/Δ
c
Bone marrow cellularity (x10^6)
P=0.276
Con
Δ/Δ
d
Frequency of bone marrow cells (%)
P=0.861
P=1.000
Mac1+Gr1+
Mac1+F4/80+
Frequency of spleen cells (%)
P=0.749
P=0.816
Mac1+Gr1+
Mac1+F4/80+
e
Relative expression
P=0.606
P=0.060
P=0.129
P=0.433
P=0.425
P=0.655
Tnfa
Il1b
Il6
Unstimulated
LPS
Con
Δ/Δ
f
Percent of max
Con
73.0%
68.5%
Bead fluorescence intensity - PE
Engulfing+ (%)
P=0.815
Con
Δ/Δ
Normalized MFI (a.u.)
P=0.896
Con
Δ/Δ

Figure 2.8

Identification of m^{6}A targets in HSCs

To identify direct m^{6}A targets in rare HSCs, we developed an m^{6}A-tagged mRNA immunoprecipitation sequencing (meRIP-seq) method to analyze the m^{6}A methylome of 2,000 freshly sorted wild-type HSCs from 6-8 week old mice (**Figure 2.9a-b**). 2,073 transcripts (FDR<0.05 and fold>2) were significantly enriched in the m^{6}A antibody-bound fraction compared to the non-bound fraction and were defined as high-confidence m^{6}A targets (**Figure 2.9c-d**). This represented only ~9% of the genes expressed in the input mRNA fraction, suggesting that m^{6}A preferentially marks a subset of genes in HSCs. We also performed meRIP-seq on *Mettl3*-deficient HSCs from *Mx1-cre; Mettl3$^{fl/fl}$* mice 10 days after pIpC administration. The enrichment of 995 transcripts (~48% of the high-confidence m^{6}A targets) was significantly reduced ($p<0.05$) in *Mettl3*-deficient HSCs, suggesting that the m^{6}A modification of these targets depended acutely on METTL3 (**Figure 2.9e-f, Appendix B**). The lack of complete elimination of m^{6}A may be due to residue METTL3 protein, slow turnover of some target mRNAs or antibody detection of cap region m^{6}Am, which unlike m^{6}A, is known not to be regulated by *Mettl3* but is also detected by the anti-m^{6}A antibodies used (Mauer et al., 2017).

Gene ontology (GO) analysis of m^{6}A-tagged mRNAs demonstrated enrichment of genes related to nucleic acid metabolism, cell cycle regulation, transcription, RNA binding, and cellular stress responses, immune system development and hematopoiesis (**Figure 2.10a**). Supporting feed-forward regulation, several genes encoding components of the m^{6}A pathway, including WTAP and m^{6}A-reader proteins (reviewed in Meyer and Jaffrey, 2017), were also targets of m^{6}A (**Figure 2.10b**). Consistent with the differentiation defects observed in *Mettl3*-deficient HSCs (**Figures 2.1-2.8**), we observed significant enrichment of genes associated with hematopoietic differentiation (**Figure 2.10a**). These data suggest that m^{6}A regulates HSC differentiation by directly targeting hematopoietic differentiation pathways. Several known HSC regulators were identified as major targets of m^{6}A, including *Myc*, *Junb*, and *Tet2* (**Figure 2.10c**). More importantly, the enrichment of these genes in the m^{6}A-bound fraction was significantly

decreased when *Mettl3* was deleted from HSCs, suggesting the m^6A modification of these genes is dependent on METTL3 (**Figure 2.9e-f** and **Figure 2.10c**).

Figure 2.9 meRIP-seq analysis identifies direct mRNA targets of m^{6}A in HSCs.

(**a**) Schematic of meRIP-seq workflow for low numbers of cells (such as HSCs).

(**b**) Representative bioanalyzer graphs of meRIP-seq elution sample libraries after tagmentation generated using anti-m^{6}A-antibody and IgG for immunoprecipitation. Experiment was repeated three times with similar results.

(**c**) Heat map of transcript abundance between input, m^{6}A-tagged, and unbound fractions. A total of 5,676 genes with log2(RPKM) ≥5 in ≥4 samples and stdev[log2(RPKM)]≥0.6 are shown.

(**d**) Volcano plot of meRIP-seq transcript expression differences between m^{6}A-tagged and unbound fractions in HSCs. The x-axis specifies the log2 fold-changes (FC) and the y-axis specifies the $\log_{10}$ false discovery rate (FDR). Dashed vertical and horizontal lines indicate the filtering criteria (log2(FC)>1 and FDR<0.05). Orange dots represent 2,621 transcripts showing statistically significant differences between bound and non-bound factions, of which 2,073 are significantly enriched in the m^{6}A-tagged fraction.

(**e**) Volcano plot of meRIP-seq transcript expression differences between m^{6}A-tagged and unbound fractions in *Mx1-cre; Mettl3$^{fl/fl}$* (*Mettl3$^{\Delta/\Delta}$*) HSCs 10 days after Cre induction. The x-axis specifies the $\log_2$ fold-changes (FC) and the y-axis specifies the $\log_{10}$ false discovery rate (FDR). Dashed vertical and horizontal lines indicate the filtering criteria ($\log_2$(FC)>1 or <-1 and FDR<0.05). Orange dots represent transcripts showing statistically significant differences between m^{6}A-tagged and un-bound factions, with select genes labeled. Data were from three biologically independent animals. The statistics was controlled for multiple testing by false discovery rate.

(**f**) Comparison of m^{6}A enrichment in wild-type (WT) HSCs vs *Mettl3$^{\Delta/\Delta}$* HSCs. The x-axis specifies the $\log_2$ fold-change (FC) expression difference between m^{6}A-tagged and unbound fractions in WT HSCs. The y-axis specifies the $\log_2$FC expression difference between m^{6}A-tagged and unbound fractions in *Mx1-cre; Mettl3$^{fl/fl}$* (*Mettl3$^{\Delta/\Delta}$*) HSCs 10 days after Cre induction. In both axes, positive sums represent enrichment in the m^{6}A fraction. All dots shown are

transcripts found to be methylated in WT HSCs (log_2(FC)>1 and FDR<0.05). Blue dots and select labeled genes represent transcripts found to have significantly different m^6A enrichment in WT vs. *Mettl3*$^{\Delta/\Delta}$ ($p<0.05$). The dotted line represents equal m^6A enrichment in WT vs. *Mettl3*$^{\Delta/\Delta}$ - dots below this line have decreased m^6A enrichment in *Mettl3*$^{\Delta/\Delta}$ compared to WT HSCs. The statistics was controlled for multiple testing by false discovery rate.

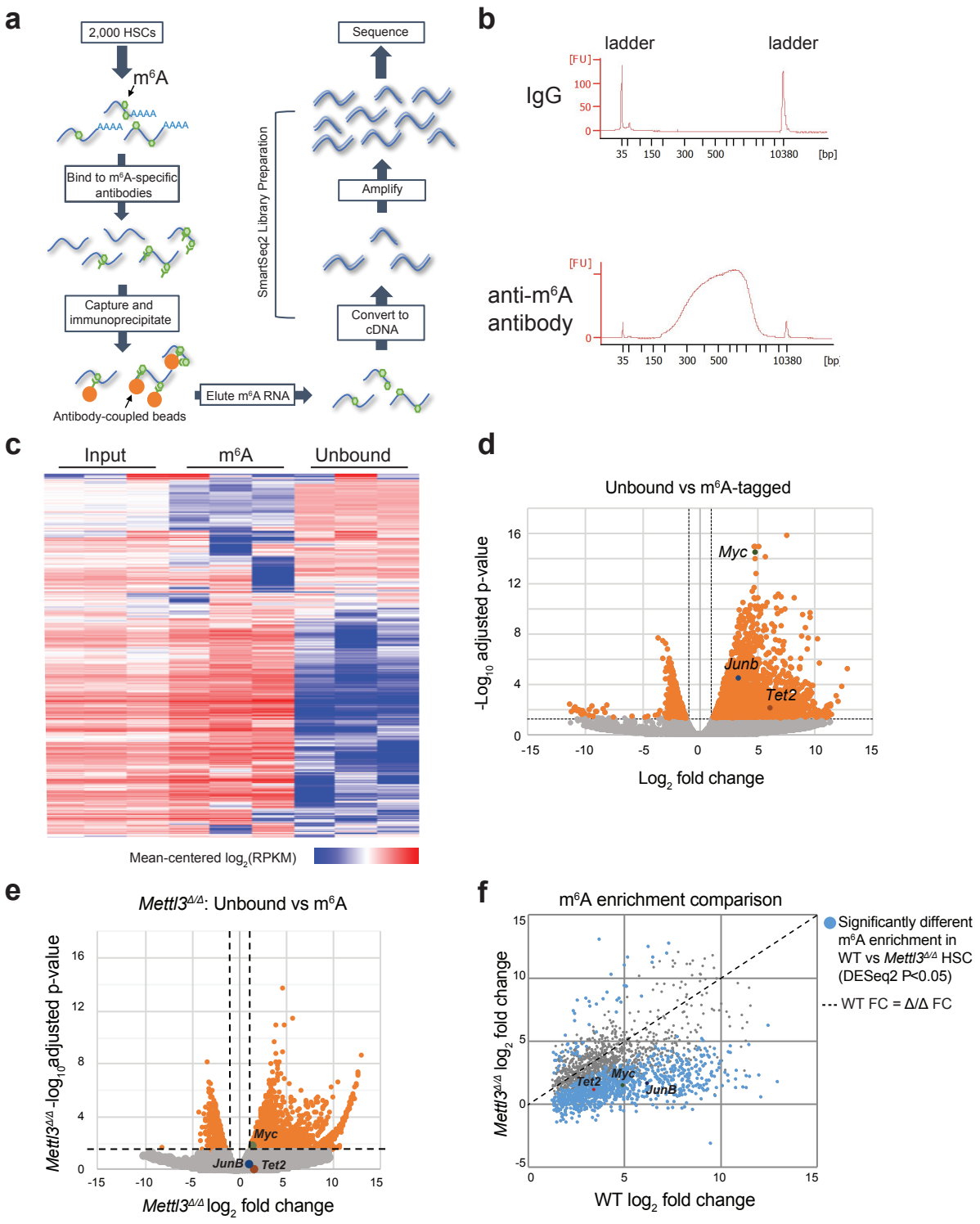
a
2,000 HSCs
m6A
Bind to m6A-specific antibodies
Capture and immunoprecipitate
Antibody-coupled beads
Elute m6A RNA
Convert to cDNA
Amplify
Sequence
SmartSeq2 Library Preparation
b
ladder
ladder
IgG
[FU]
100
50
0
35
150
300
500
10380
[bp]
anti-m6A antibody
c
Input
m6A
Unbound
Mean-centered log2(RPKM)
d
Unbound vs m6A-tagged
-Log10 adjusted p-value
Log2 fold change
Myc
Junb
Tet2
e
Mettl3Δ/Δ: Unbound vs m6A
Mettl3Δ/Δ -log10adjusted p-value
Mettl3Δ/Δ log2 fold change
Myc
JunB
Tet2
f
m6A enrichment comparison
Mettl3Δ/Δ log2 fold change
WT log2 fold change
Significantly different m6A enrichment in WT vs Mettl3Δ/Δ HSC (DESeq2 P<0.05)
WT FC = Δ/Δ FC
Tet2
Myc
JunB

Figure 2.9

Figure 2.10 Identification of HSC regulators as m^{6}A methylation targets.

(**a**) Gene ontology analysis of biological processes enriched in m^{6}A-tagged transcripts in WT HSCs.

(**b**) meRIP-seq data showing that many components of the m^{6}A pathway are targets of m^{6}A in HSCs and this methylation is largely eliminated in *Mx1-cre; Mettl3$^{fl/fl}$* (*Mettl3$^{\Delta/\Delta}$*) HSCs 10 days after Cre induction. Data were from n=3 biologically independent samples for control and *Mettl3$^{\Delta/\Delta}$*.

(**c**) meRIP-seq data showing that transcripts of some known HSC regulators are m^{6}A-tagged in wild-type HSCs, and this methylation is largely eliminated in *Mx1-cre; Mettl3$^{fl/fl}$* (*Mettl3$^{\Delta/\Delta}$*) HSCs 10 days after Cre induction. Data were from n=3 biologically independent samples for control and *Mettl3$^{\Delta/\Delta}$*.

(**d**) Gene set enrichment analysis plots showing that *Mettl3*-deficient HSCs lose HSC gene signature, as determined by RNA-seq profiling. Analysis completed on gene list ranked by $\log_{10}$ FDR and fold change sign, with enrichment determined after 1,000 permutations. Data were from n=3 biologically independent samples for control and *Mettl3$^{\Delta/\Delta}$*. The statistics was computed using GSEA, and controlled for multiple comparisons by false discovery rate.
All sequencing data were from n=3 biologically independent animals for control and *Mettl3$^{\Delta/\Delta}$*.

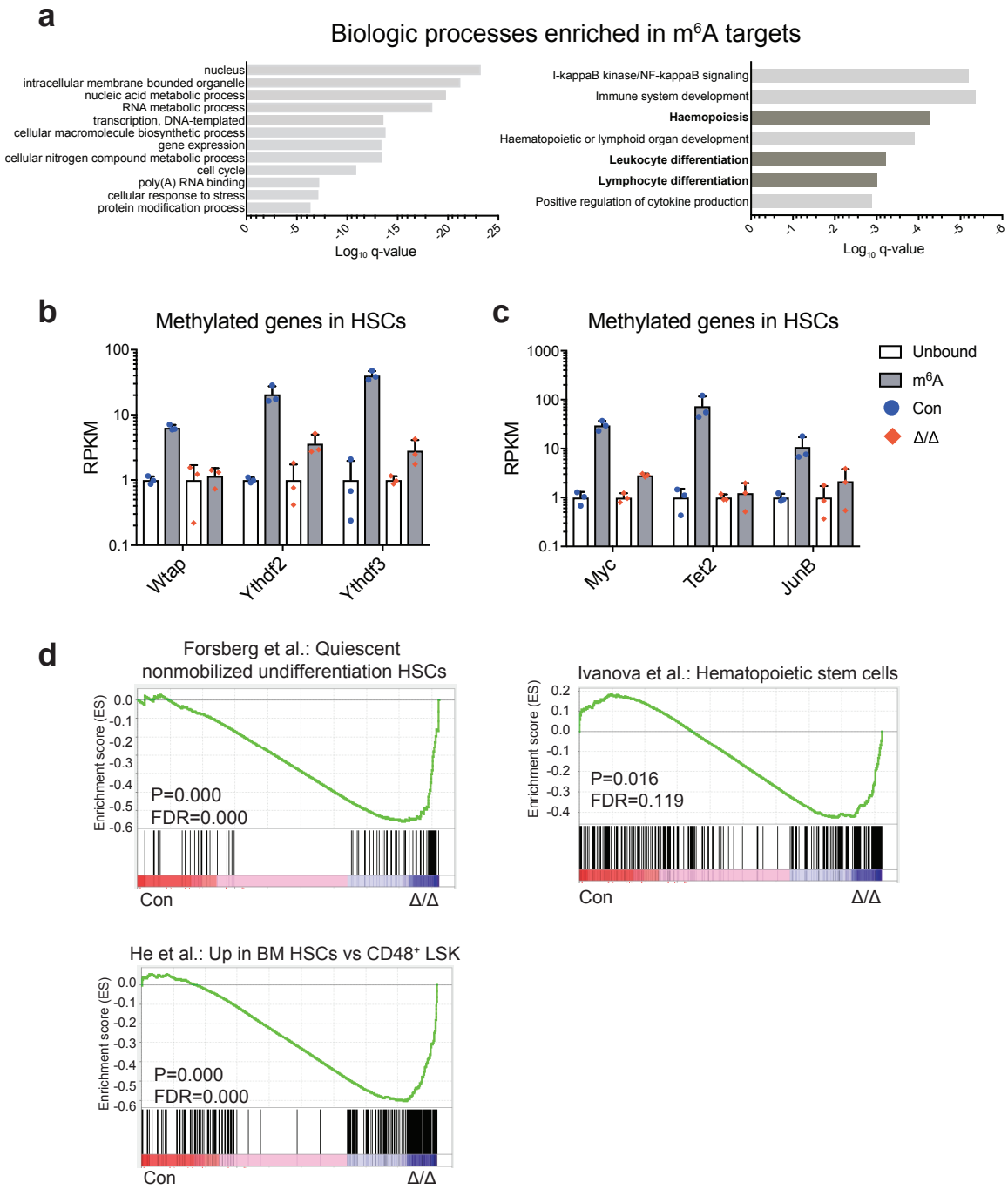
a
Biologic processes enriched in m6A targets
nucleus
intracellular membrane-bounded organelle
nucleic acid metabolic process
RNA metabolic process
transcription, DNA-templated
cellular macromolecule biosynthetic process
gene expression
cellular nitrogen compound metabolic process
cell cycle
poly(A) RNA binding
cellular response to stress
protein modification process
Log10 q-value
I-kappaB kinase/NF-kappaB signaling
Immune system development
Haemopoiesis
Haematopoietic or lymphoid organ development
Leukocyte differentiation
Lymphocyte differentiation
Positive regulation of cytokine production
Log10 q-value
b
Methylated genes in HSCs
RPKM
Wtap
Ythdf2
Ythdf3
c
Methylated genes in HSCs
RPKM
Myc
Tet2
JunB
Unbound
m6A
Con
Δ/Δ
d
Forsberg et al.: Quiescent nonmobilized undifferentiation HSCs
Enrichment score (ES)
P=0.000
FDR=0.000
Con
Δ/Δ
Ivanova et al.: Hematopoietic stem cells
Enrichment score (ES)
P=0.016
FDR=0.119
Con
Δ/Δ
He et al.: Up in BM HSCs vs CD48+ LSK
Enrichment score (ES)
P=0.000
FDR=0.000
Con
Δ/Δ

Figure 2.10

Deletion of *Mettl3* leads to a loss of HSC identity without drastic alterations of the transcriptome

To further understand the molecular mechanisms underpinning the functional defects of *Mettl3*-deficient HSCs, we performed RNA-seq analysis on *Mettl3*-deficient HSCs using Smart-seq2 (Picelli et al., 2014). 830 genes showed significant expression differences ($p<0.05$). After stringent analysis with multiple comparisons correction, only 7 genes showed significant expression differences (FDR<0.05) between *Mettl3*-deficient and control HSCs (**Figure 2.11a**). As expected, *Mettl3* was one of the most significantly down-regulated genes in *Mettl3*-deficient HSCs (**Figure 2.11a**). Gene set enrichment analysis (GSEA) (Subramanian et al., 2005) showed that *Mettl3* deficiency predominantly led to a loss of expression of HSC identity-associated genes defined by previous publications (Forsberg et al., 2010; He et al., 2011; Ivanova et al., 2002) (**Figure 2.10d**). These data suggest that METTL3-mediated m^6A modestly altered HSC identity without profoundly impacting global mRNA levels.

m^6A has been shown to negatively regulate target mRNA stability (reviewed in Meyer and Jaffrey, 2014). We thus assessed whether m^6A targets were up-regulated in *Mettl3*-deficient HSCs. 95 out of 384 up-regulated genes in *Mettl3*-defieient HSCs ($p<0.05$ and fold>1.2) were m^6A targets (**Figure 2.11b**). But none of the 7 high-confidence differentially expressed genes (FDR<0.05) (**Figure 2.11a**) were high-confidence m^6A targets. Compared to non-m^6A targets, transcripts of m^6A targets had slightly increased abundance in *Mettl3*-deficient HSCs (**Figure 2.11c**). Taken together, these data suggest that although m^6A may directly control the transcript levels of some genes, it predominantly regulates target mRNAs post-transcriptionally in HSCs.

Figure 2.11 Loss of *Mettl3* in HSCs does not cause major transcriptomic changes.

(**a**) List of differentially expressed genes in control and *Mx1-cre; Mettl3*$^{fl/fl}$ HSCs 10 days after Cre induction by RNA-seq analysis (FDR<0.05). The statistics was controlled for multiple testing by false discovery rate.

(**b**) Diagram of overlap between 384 up-regulated genes in *Mettl3*-deficient HSCs compared with controls (defined as p<0.05, fold>1.2) identified by RNA-seq and 2,073 methylated targets identified by meRIP-seq in wild-type HSCs. P value for enrichment was determined by hypergeometric probability test.

(**c**) Cumulative distribution of $\log_2$ (gene expression ratios, *Mettl3*-deficient/control). Genes were separated as m^{6}A and non-m^{6}A as assessed by meRIP-seq. Insert is the box plot of the $\log_2$ fold change in expression of non-m^{6}A and m^{6}A targets in HSCs. Plot displays the mean, standard deviation and interquartile range. P value was determined by two-sided Kolmogorov-Smirnov test.

(**d**) meRIP-qPCR data showing *Myc* enrichment in m^{6}A-bound fraction in control and *Mx1-cre; Mettl3*$^{fl/fl}$ HSCs 10 days after pIpC treatment (n=3 for control, n=4 for *Mx1-cre; Mettl3*$^{fl/fl}$). Data shown were normalized to the expression of *Rplp0*, a target found not to be methylated in HSCs by our meRIP-Seq analysis.

(**e**) qPCR analysis of *Myc* expression by control and *Mettl3*-deficient HSCs 10-14 days after pIpC treatment (n=5 for control, n=6 for *Mx1-cre; Mettl3*$^{fl/fl}$) and after overnight cytokine activation (right; n=5 for control, n=5 for *Mx1-cre; Mettl3*$^{fl/fl}$). All samples were from biologically independent animals. Values are shown as mean ± s.d. P values were determined by paired two-sided Student's t-test.

(**f**) Gene set enrichment analysis plots, as determined by HSC RNA-seq profiling of control and *Mx1-cre; Mettl3*$^{fl/fl}$ HSCs 10 days after pIpC treatment (n=3 for control and *Mettl3*$^{\Delta/\Delta}$). *Mettl3*-deficient HSCs significantly lose *Myc* target genes. Analyses were completed on gene list ranked by $\log_{10}$ FDR and fold-change sign. P values were determined by the GSEA algorithm

after 1,000 permutations. The statistics was computed using GSEA, and controlled for multiple comparisons by false discovery rate.

a

Gene	Log_2 FC in Δ/Δ	Adujusted p-value
Vps33a	2.477	0.005
Mettl3	-2.374	0.014
Alox5	8.744	0.014
Crybb1	-10.367	0.030
Selp	1.786	0.030
Rnf32	-10.315	0.030
Sult1a1	-2.799	0.033

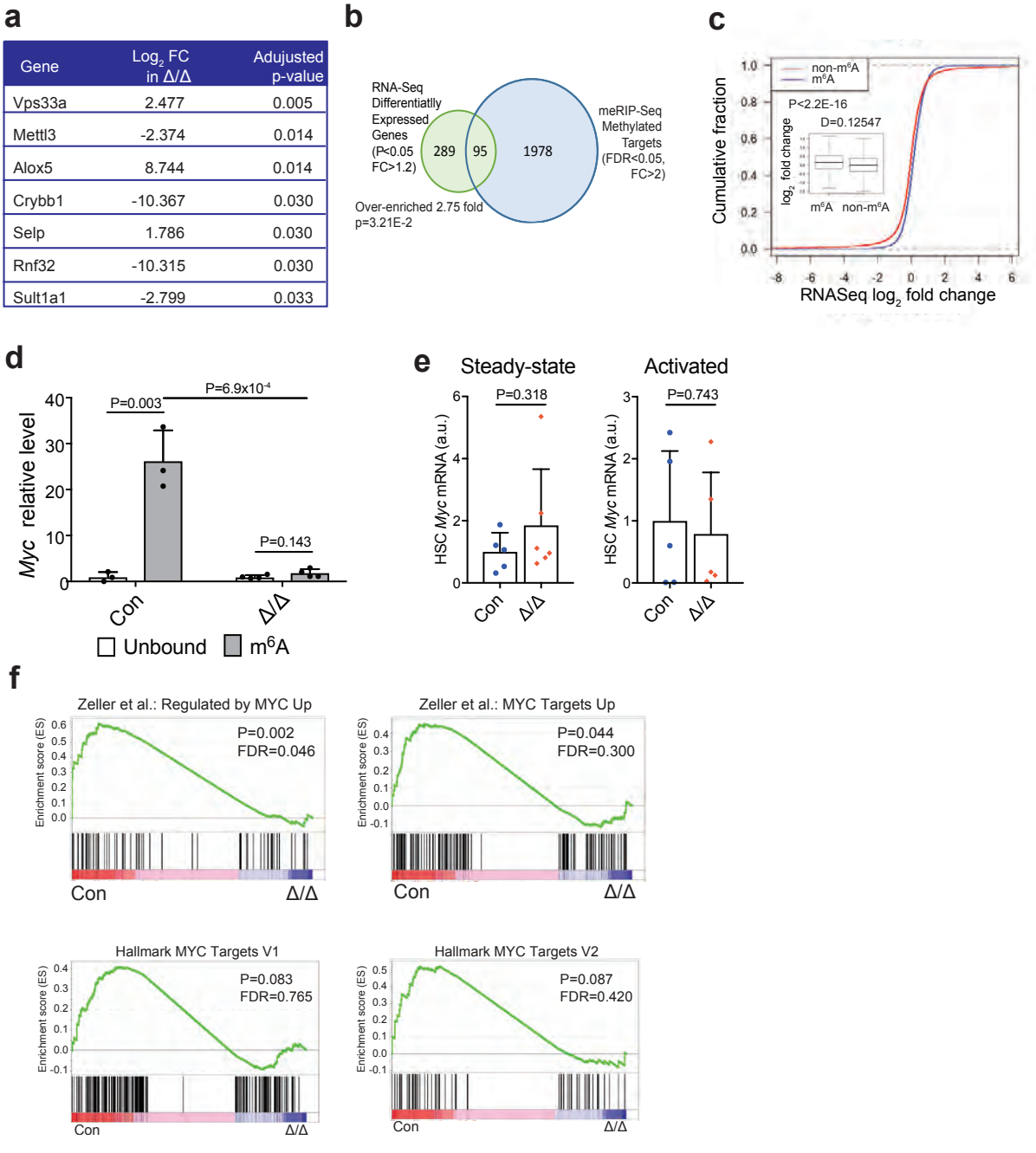

Figure 2.11

Myc is a direct target of m^{6}A in HSCs

It has been shown that the MYC protein level is very low in HSCs, and is up-regulated upon differentiation through post-transcriptional mechanisms (Reavie et al., 2010; Ehninger et al., 2014). Furthermore, deletion of *Myc* blocks HSC differentiation while accumulated higher levels of MYC protein promotes HSC differentiation (Reavie et al., 2010; Wilson et al., 2004). Prompted by the observations that *Myc* is a major determinant of HSC differentiation and the phenotypic similarity between *Myc* and *Mettl3* conditional knockout mice (accumulation of HSCs and blockage of differentiation), we investigated whether *Myc* is a direct target of m^{6}A in HSCs. Our meRIP-seq analyses revealed that *Myc* was one of the top candidates highly enriched in m^{6}A antibody-bound fraction compared with non-bound fraction (~30 fold enrichment; FDR=3.96x10^{-15}) (**Figure 2.9d** and **Figure 2.10c**), in a *Mettl3*-dependent manner (**Figure 2.9e-f** and **Figure 2.10c**). We confirmed these meRIP-seq data using qPCR on independent samples (**Figure 2.11d**). Interestingly, *Myc* transcript levels were not significantly changed in *Mettl3*-deficient HSCs compared with controls (**Figure 2.11e**). Using several previously published *Myc* target gene sets (Zeller et al., 2003; Liberzon et al., 2011), GSEA revealed a significant decrease in *Myc* target gene signatures in *Mettl3*-deficient HSCs (**Figure 2.11f**), suggesting that m^{6}A may primarily regulate *Myc* mRNA translation.

The *Myc* protein level can be directly measured by a knockin *Myc*-GFP translational reporter *in vivo*, where GFP is directly fused with MYC (Huang et al., 2008). To assess the impact of *Mettl3* deletion on the level of *Myc* protein in HSCs, we generated *Mx1-cre; Mettl3$^{fl/fl}$; Myc-GFP* mice. Consistent with prior publications (Reavie et al., 2010; Ehninger et al., 2014), HSCs express lower levels of MYC-GFP compared to hematopoietic progenitors at steady state (**Figure 2.12a**). Deletion of *Mettl3* led to a modest significant reduction of MYC-GFP in HSCs (**Figure 2.12b**). Remarkably, upon activation to differentiate, *Mettl3*-deficient HSCs failed to up-regulate MYC-GFP while control HSCs could readily do so (**Figure 2.12b**). *Mettl3* deletion did not lead to changes in HSC *Myc* transcript levels under the activation condition (**Figure 2.11e**).

Given that m^6A primarily regulates target mRNA stability and translation (Meyer and Jaffrey, 2017; Yue et al., 2015), these data suggest that m^6A is required for *Myc* mRNA translation in HSCs, particularly upon differentiation.

Figure 2.12 *Mettl3* regulates HSC function by targeting *Myc*.

(**a**) Quantification of the mean fluorescence intensity (MFI) of GFP expression in LSK subsets from *Mx1-cre; Mettl3$^{fl/fl}$; Myc-GFP* mice or *Myc-GFP* controls at least 10 days after pIpC treatment (n=4 for *Myc-GFP* controls, n=4 for *Mx1-cre; Mettl3$^{fl/fl}$; Myc-GFP)*. Values were normalized to GFP-negative control cells of the same population.

(**b**) Schematic of experimental design (top). Representative FACS plots of MYC-GFP expression in HSCs at steady-state (bottom left) and after cytokine activation (bottom right). Quantification of the mean fluorescence intensity (MFI) of GFP expression in HSCs after cytokine activation (n=7 for *MYC-GFP* controls, n=7 for *Mx1-cre; Mettl3$^{fl/fl}$; MYC-GFP)*. Values were normalized to GFP-negative control cells.

(**c**) Schematic of experimental design (top). Representative FACS plots (bottom left) showing gating strategy for analysis of virally transduced colony cells derived from sorted HSCs from *Mx1-cre; Mettl3$^{fl/fl}$* mice 10 days after pIpC treatment. Representative FACS plot (middle) and quantification (right) of the frequency of Mac-1^{+} cells in virally transduced colonies from sorted HSCs from *Mx1-cre; Mettl3$^{fl/fl}$* mice 10 days after pIpC treatment (n=3 for pMIG, n=3 for pMIG-*Myc*).

All samples were from biologically independent animals. Values are shown as individual points with mean ± s.d. P values were determined by paired two-sided Student's t-test.

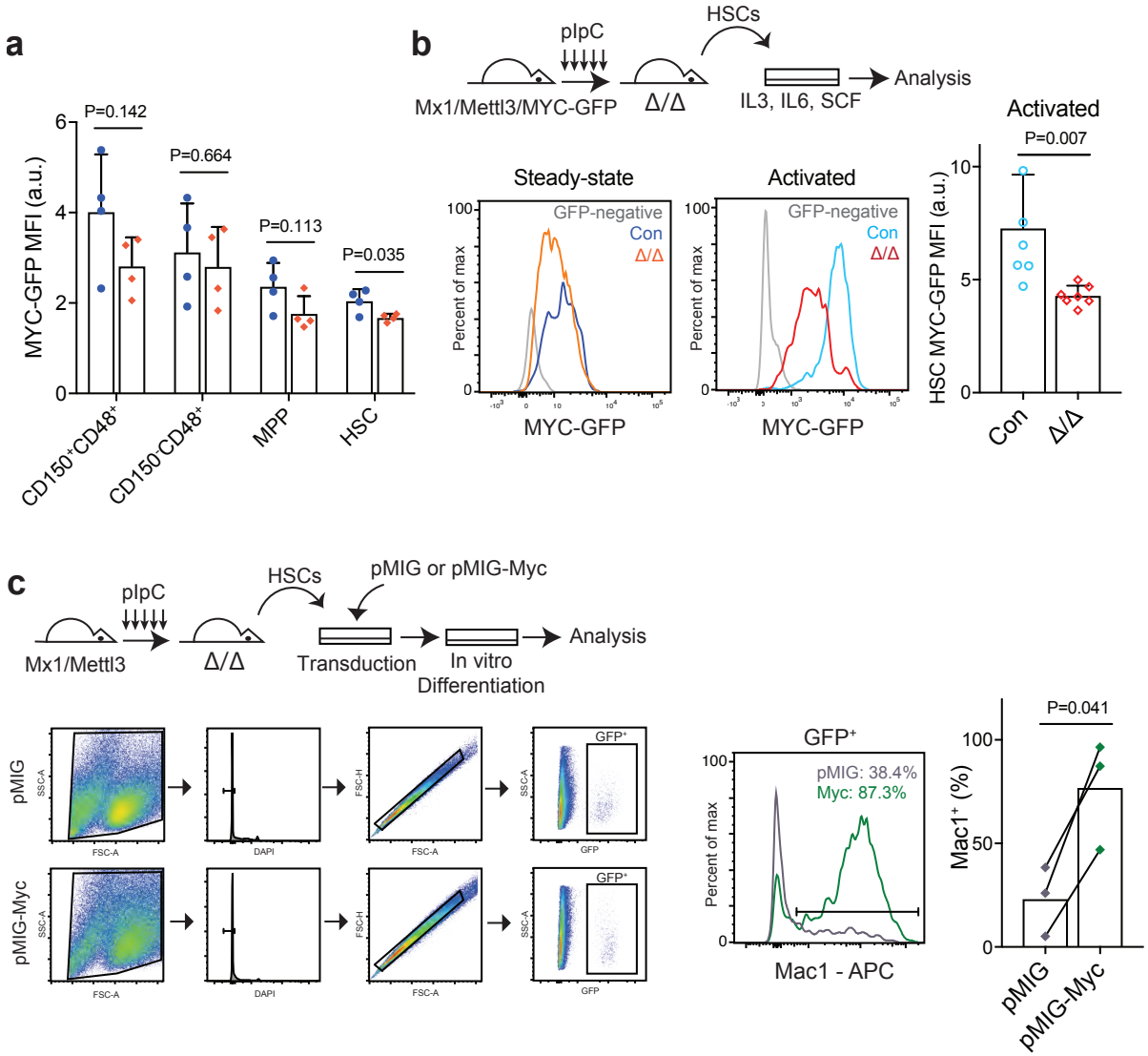
a
MYC-GFP MFI (a.u.)
P=0.142
P=0.664
P=0.113
P=0.035
CD150+CD48+
CD150-CD48+
MPP
HSC
b
pIpC
HSCs
Mx1/Mettl3/MYC-GFP
Δ/Δ
IL3, IL6, SCF
Analysis
Steady-state
Activated
GFP-negative
Con
Δ/Δ
Percent of max
MYC-GFP
Activated
P=0.007
HSC MYC-GFP MFI (a.u.)
Con
Δ/Δ
c
pIpC
HSCs
pMIG or pMIG-Myc
Mx1/Mettl3
Δ/Δ
Transduction
In vitro Differentiation
Analysis
pMIG
pMIG-Myc
FSC-A
SSC-A
DAPI
FSC-H
GFP
GFP+
GFP+
pMIG: 38.4%
Myc: 87.3%
Percent of max
Mac1 - APC
P=0.041
Mac1+ (%)
pMIG
pMIG-Myc

Figure 2.12

Forced expression of MYC can rescue *Mettl3*-depleted HSC differentiation defects

We tested whether forced expression of *Myc* can rescue the HSC differentiation defects caused by *Mettl3* deletion. We transduced *Mettl3*-defiecent HSCs with *Myc*-expressing or control retrovirus (**Figure 2.12c**) and assessed their differentiation potential *in vitro*. Forced expression of *Myc* significantly rescued the differentiation defect of *Mettl3*-deficient HSCs compared with controls (**Figure 2.12c**). To assess whether *Myc* expression rescues HSC differentiation defects *in vivo*, we generated *Mx1-cre; Mettl3$^{fl/fl}$; Rosa-loxpMyc* mice. The *Rosa-loxpMyc* mice express *Myc* in a Cre-dependent manner (Calado et al., 2012), allowing testing of the impact of *Myc* expression on *Mettl3*-deficient HSCs *in vivo*. We treated 6-8 weeks old *Mx1-cre; Mettl3$^{fl/fl}$; Rosa-loxpMyc* and control *Mx1-cre; Mettl3$^{fl/fl}$* mice with pIpC. However, *Mx1-cre* is known to be expressed in hepatocytes and consistent with previous reports of hepatocellular carcinoma development from liver *Myc* overexpression (Zheng et al., 2017), many *Mx1-cre; Mettl3$^{fl/fl}$; Rosa-loxpMyc* mice developed liver nodules resembling hepatocellular carcinomas after the pIpC administration (**Figure 2.13a**). Analysis up to 3 weeks after pIpC treatment revealed normal blood counts in *Mx1-cre; Mettl3$^{fl/fl}$; Rosa-loxpMyc* mice compared with control mice (**Figure 2.13b**), suggesting that the defects in the megakaryocyte lineage of *Mettl3* deletion are largely rescued by *Myc* expression. However, HSC frequency remained elevated in these mice compared to controls (**Figure 2.13c**), suggesting that the increase in HSC frequency may be related to perturbation of other m^{6}A targets in addition to *Myc*. To specifically assess the function of HSCs, we transplanted 50 HSCs from the bone marrow of *Mx1-cre; Mettl3$^{fl/fl}$; Rosa-loxpMyc*, *Mx1-cre; Mettl3$^{fl/fl}$*, and littermate control mice with competitor bone marrow cells. No reconstitution could be observed by HSCs from *Mx1-cre; Mettl3$^{fl/fl}$* mice (**Figure 2.13d-e**), consistent with our prior results (**Figure 2.6b**). In contrast, 6 out of 12 mice transplanted with HSCs from *Mx1-cre; Mettl3$^{fl/fl}$; Rosa-loxpMyc* mice were multi-lineage reconstituted four weeks after transplantation (**Figure 2.13d-e**). The recipients of *Mx1-cre; Mettl3$^{fl/fl}$; Rosa-loxpMyc* HSCs with the highest chimerism died prior to subsequent analysis time points, likely due to

hematopoietic disease. However, all together these data suggest that forced expression of *Myc* can partially rescue HSC differentiation defects, both *in vitro* and *in vivo* and confirm that *Myc* is a major functional target of m^6A in HSCs.

Figure 2.13 Forced *Myc* expression partially rescues *Mettl3*-depleted HSC differentiation defects *in vivo*.

(**a**) Representative images of control and *Mx1-cre; Mettl3$^{fl/fl}$; Rosa-loxpMyc* (Mx1/Mettl3/Myc) livers 3 weeks after pIpC treatment.

(**b**) White blood cell counts, red blood cell counts and platelet counts in control and *Mx1-cre; Mettl3$^{fl/fl}$; Rosa-loxpMyc* mice, as indicated (n=4 for control, n=4 for *Mx1-cre; Mettl3$^{fl/fl}$; Rosa-loxpMyc*).

(**c**) Frequencies of hematopoietic stem cells in control and *Mx1-cre; Mettl3$^{fl/fl}$; Rosa-loxpMyc* bone marrow (n=4 for control, n=4 for *Mx1-cre; Mettl3$^{fl/fl}$; Rosa-loxpMyc*).

(**d**) Frequencies of donor-derived CD45^{+}, Mac1^{+}, B220^{+}, or CD3^{+} cells as indicated in control, *Mx1-cre; Mettl3$^{fl/fl}$* and *Mx1-cre; Mettl3$^{fl/fl}$; Rosa-loxpMyc* HSC recipients 4 weeks after transplantation (n=11 for control, n=4 for *Mx1-cre; Mettl3$^{fl/fl}$;* n=12 for *Mx1-cre; Mettl3$^{fl/fl}$; Rosa-loxpMyc*).

(**e**) Numbers of total recipients and responders after transplantation of 50 HSCs from control, *Mx1-cre; Mettl3$^{fl/fl}$* or *Mx1-cre; Mettl3$^{fl/fl}$; Rosa-loxpMyc* donors as indicated with 300,000 competitor bone marrow cells. Recipients were judged as responders if they showed donor-derived myeloid, B and T cells in the peripheral blood 4 weeks after transplantation. Samples were from independent recipients of two independent donor pairs from two experiments. P value determined by Fisher's exact test.

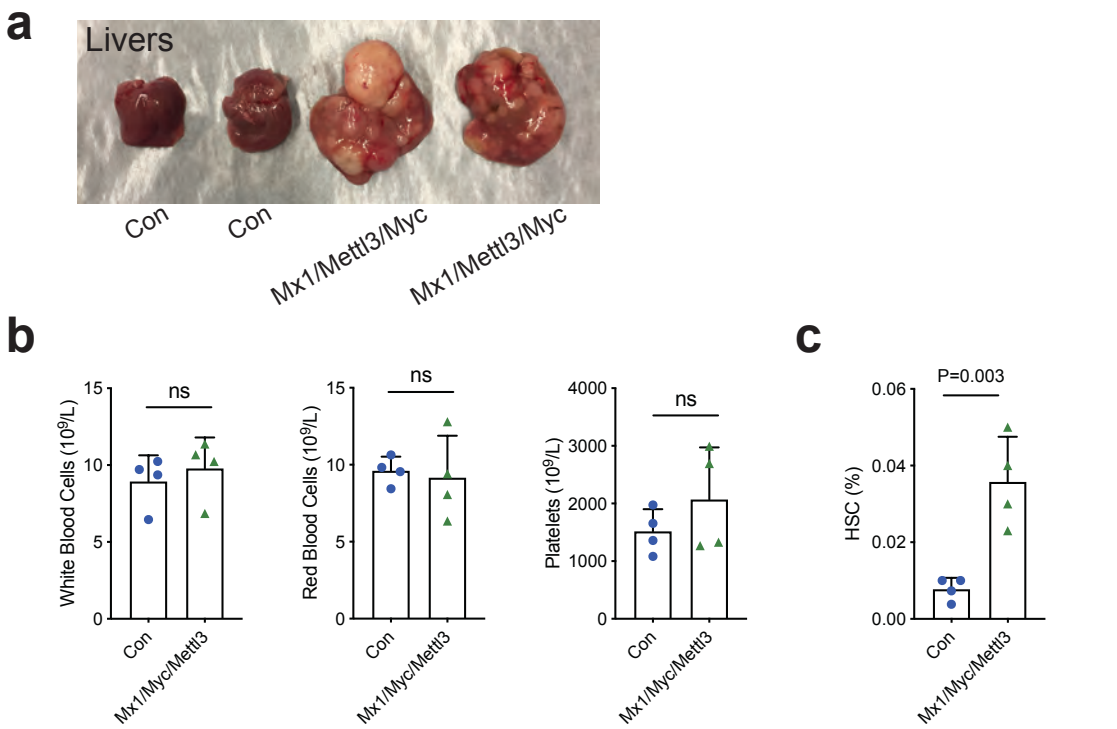

e

HSC Donor	Recipients	Responses
Control	11	10
Mettl3$^{\Delta/\Delta}$	13	0
Myc/Mettl3$^{\Delta/\Delta}$	12	6

P=0.005

Figure 2.13

DISCUSSION

We demonstrate that m^6A is preferentially required for adult HSC differentiation *in vivo* and *in vitro,* but not mature myeloid cell maintenance or function. These results demonstrate that m^6A is not a general cellular house-keeping mechanism, but rather a modification with specific roles in HSCs. Our results are in contrast to reports that show m^6A inhibits differentiation of $CD34^+$ human hematopoietic progenitor cells *in vitro* (Vu et al., 2017; Weng et al., 2017). Since those experiments were performed using shRNAs on cells of mixed populations of HSCs and progenitors *in vitro*, it is not clear what the effects on human HSCs are *in vivo*. Of note, we observed differences between HSCs and progenitors in their response to *Mettl3* deletion (**Figure 2.4** and **Figure 2.5**), suggesting that the roles of m^6A in HSCs and progenitors need to be assessed independently. Consistent with our data, two other recent publications also showed that conditional deletion of *Mettl3* led to accumulation of HSCs in the bone marrow (Yeo et al., 2018; Cheng et al., 2019). Cheng *et al* similarly demonstrated that loss of *Mettl3* reduces MYC expression and forced MYC expression can partially rescue HSC differentiation defects, consistent with our findings (Cheng et al., 2019).

In contrast to its role in enabling HSC differentiation, m^6A inhibits differentiation in AML leukemic cells (Vu et al., 2017; Weng et al., 2017; Barbieri et al., 2017). This surprising difference may reflect distinct mechanisms of action for m^6A in leukemic cells and HSCs, and suggests that it may be possible to develop m^6A-targeted therapies against leukemia cells without damaging HSC function. More work is needed to elucidate the differences in the role of m^6A between leukemic cells and HSCs.

We found that HSC self-renewal and quiescence is largely intact after *Mettl3* deletion (**Figure 2.1a** and **Figure 2.6d**). Thus, it appears that m^6A specifically regulates HSC differentiation. m^6A-mediated epitranscriptional regulation in HSCs may provide a fast and flexible mechanism to control mature blood cell output, allowing the organism to adapt to ever-

changing physiological demands. *Mettl3*-deficient HSCs failed to establish bone marrow chimera in transplantation (**Figure 2.7a-d**), suggesting that m^6A may regulate HSC homing and/or engraftment, which will be interesting to further investigate in the future.

ACKNOWLEDGEMENTS

L.D. was supported by the Rita Allen Foundation and the National Heart, Lung and Blood Institute (R01HL132074). H.L. was supported by the Columbia Medical Scientist Training Program and the National Heart, Lung and Blood Institute (F30HL142196-01). The work by S.B., Y.Q. and C.Z. is in part supported by grants from the National Institute of Health (R01NS89676, R01GM124486, and R03HG009528). S.B. is supported by a Columbia Precision Medicine Research Fellowship. J.H.H. is supported by a generous gift from Ilana and Pascal Mantoux, and research grants from the: European Research Council, Kimmel Stem Cell Research Center, Flight Attendant Medical Research Council (FAMRI), Israel Science Foundation (ISF), Israel Cancer Research Fund (ICRF), New York Stem Cell Foundation (NYSCF). J.H.H. is a New York Stem Cell Foundation (NYSCF)–Robertson Investigator. We thank M. Kissner at the Columbia Stem Cell Initiative, S. Ho at the Columbia Center for Translational Immunology and A. Figueroa at the Department of Microbiology and Immunology for flow cytometry assistance. We thank I. Ivanov at the Department of Microbiology and Immunology for sharing the Lysm-cre mice and H. Snoeck for sharing the Mx1-cre mice. We thank C. Schindler, S. Ghosh and A. Lepelley at the Department of Microbiology and Immunology for helping macrophage assays. This research was funded in part through the NIH/NCI Cancer Center Support Grant P30CA013696.

CHAPTER 3

The Requirement for *Mettl3*-dependent m^6A mRNA Methylation in the Hematopoietic Stem Cell Niche

SUMMARY

Hematopoietic stem cells (HSCs) reside in a bone marrow niche that supports them throughout life. Mesenchymal stromal cells (MSCs) are known to be a key component of the bone marrow niche, but how the niche and its HSC-supporting function are regulated is not fully understood. N^6-methyladenosine (m^6A) mRNA methylation has emerged as an important mode of epitranscriptional gene expression regulation affecting many biological processes. We show that deleting the m^6A methyltransferase, *Mettl3*, from embryonic *Prx1*$^+$ MSCs in the bone marrow niche of long bones causes a loss of normal bone marrow architecture and decreased bone marrow cellularity. Within the *Mettl3*-deficient bone marrow, HSCs were preferentially depleted, likely caused by the loss of a key HSC-supporting factor CXCL12 from the niche. Interestingly, deleting *Mettl3* from post-natal MSCs using *Lepr-cre* did not impact HSC numbers, suggesting the dependence on *Mettl3* is specific to the establishment of the niche, rather than its maintenance. Thus, our results revealed a key role for m^6A in the establishment of the bone marrow HSC niche.

INTRODUCTION

Throughout life, hematopoietic stem cells (HSCs) are supported by their local tissue microenvironment, or niche. During embryonic development, HSCs mainly form within the aorta-gonad-mesonephros region before migrating to the fetal liver. Around birth, HSCs move to the bone marrow, where they remain throughout life. Normal hematopoiesis requires a functional HSC-supporting niche in the bone marrow. The bone marrow niche is composed of many cell types, one of the most important of which is perivascular mesenchymal stromal cells (MSCs) (reviewed in Lee et al., 2017). MSCs, often identified by their expression of paired related homeobox 1 (*Prx1*) or leptin receptor (*Lepr*), have been shown to be adjacent to HSCs and

secrete key HSC-supporting cytokines stem cell factor (*Scf*) and CXCL12 (also known as stromal cell-derived factor 1 or *Sdf-1*) (reviewed in Lee et al., 2017). *Prx1* is expressed throughout mesenchymal cells of the developing limb bud from E9.5 (Logan et al., 2019). Lineage tracing of *Prx1*$^{+}$ cells revealed labeling of chondrocytes, osteoblasts, adipocytes, and stromal cells, demonstrating that *Prx1* expression occurs in early multipotent mesenchymal progenitors (Kawanami et al., 2009; Sanchez-Gurmaches et al., 2015). Transplantation of developing progenitor MSCs at E14.5 into recipient kidney capsules results in the formation of ectopic bone marrow with recipient HSCs, demonstrating that these cells are capable of generating all necessary mesenchymal components of the HSC niche (Chan et al., 2009). In contrast, *Lepr* is expressed in post-natal *Prx1*$^{+}$ MSCs in the bone marrow, suggesting they are derived from and downstream of *Prx1*$^{+}$ mesenchymal progenitors (Zhou et al., 2014). It is not understood how HSC-supporting MSCs are generated and maintained throughout life. Despite attempts to create *in vitro* HSC-supporting environments, current technology is limited and unable to replicate the full capacity of the bone marrow niche. Understanding how the niche is formed and regulated is important for developing such technologies and offers great potential medical benefit in advancing HSC-based therapies.

We have previously shown that the epitranscriptional modification N6-methyladenosine (m^6A) and its methyltransferase METTL3 play important roles in HSC-intrinsic regulation (Lee et al., 2019), but it was unknown whether m^6A and METTL3 also impact HSC-extrinsic regulation. We hypothesized that it also plays a role in the HSC niche *in vivo*.

RESULTS

Prx1-cre; Mettl3$^{fl/fl}$ mice have reduced survival and abnormal limb development

To assess if *Mettl3* plays a role in regulating mesenchymal stromal cells, the key component of the HSC niche in the bone marrow, we crossed *Prx1-cre* (Logan et al., 2002) with

Mettl3^{fl} (Lee et al., 2019; described in Chapter 2) to generate *Prx1-cre; Mettl3*$^{fl/fl}$ mice. As *Prx1-cre* starts to recombine in the limb at E9.5 (Logan et al., 2002), this allows us to delete *Mettl3* from limb bone marrow environment prior to the establishment of hematopoiesis around E17.5 (Christensen et al., 2004). *Prx1-cre; Mettl3*$^{fl/fl}$ mice were born in lower than expected numbers based on Mendelian ratios (**Figure 3.1a**) and displayed significantly decreased survival compared to littermate controls postnatally (**Figure 3.1b**). *Prx1-cre; Mettl3*$^{fl/fl}$ mice have similar body size to controls at birth, but are much smaller at later stages of development (**Figure 3.1c**), suggesting stunted growth. *Prx1-cre; Mettl3*$^{fl/fl}$ mice also have much shorter forelimb and hindlimbs and smaller and paler long bones (**Figure 3.1c**). Consistent with their paler appearance, hematoxylin and eosin staining of the bones revealed decreased hematopoietic cells and an abundance of eosin-stained mesenchymal tissue in *Mettl3*-depleted limbs (**Figure 3.1d**). By P14, *Prx1-cre; Mettl3*$^{fl/fl}$ femurs are almost completely filled with eosin-stained mesenchymal tissue and have no central bone marrow cavity (**Figure 3.1d**). These data suggest that *Mettl3* from *Prx1*$^{+}$ cells is required for the establishment of bone marrow within long bones.

Figure 3.1 *Prx1-cre; Mettl3*$^{fl/fl}$ mice have reduced survival and abnormal limb development.

(**a**) Observed numbers of *Prx1-cre; Mettl3*$^{fl/fl}$ and control mice out of 150 pups alive at P0 compared to expected numbers based on Mendelian ratios. P-valued based on two-tailed binomial test.

(**b**) Kaplan-Meyer survival analysis of control and *Prx1-cre; Mettl3*$^{fl/fl}$ mice. P value by log-rank test (n=99 for control, n=16 for *Prx1-cre; Mettl3*$^{fl/fl}$).

(**c**) Representative images of *Prx1-cre; Mettl3*$^{fl/fl}$ and control mice above corresponding images of femurs and tibias. Mice are aged P0, P5, P15, as indicated. Arrows point to visibly abnormal *Prx1-cre; Mettl3*$^{fl/fl}$ forelimbs.

(**d**) Representative images of hematoxylin and eosin staining from *Prx1-cre; Mettl3*$^{fl/fl}$ and control femurs at P0 or P14, as indicated. Black boxes indicate areas shown in higher magnification to the right.

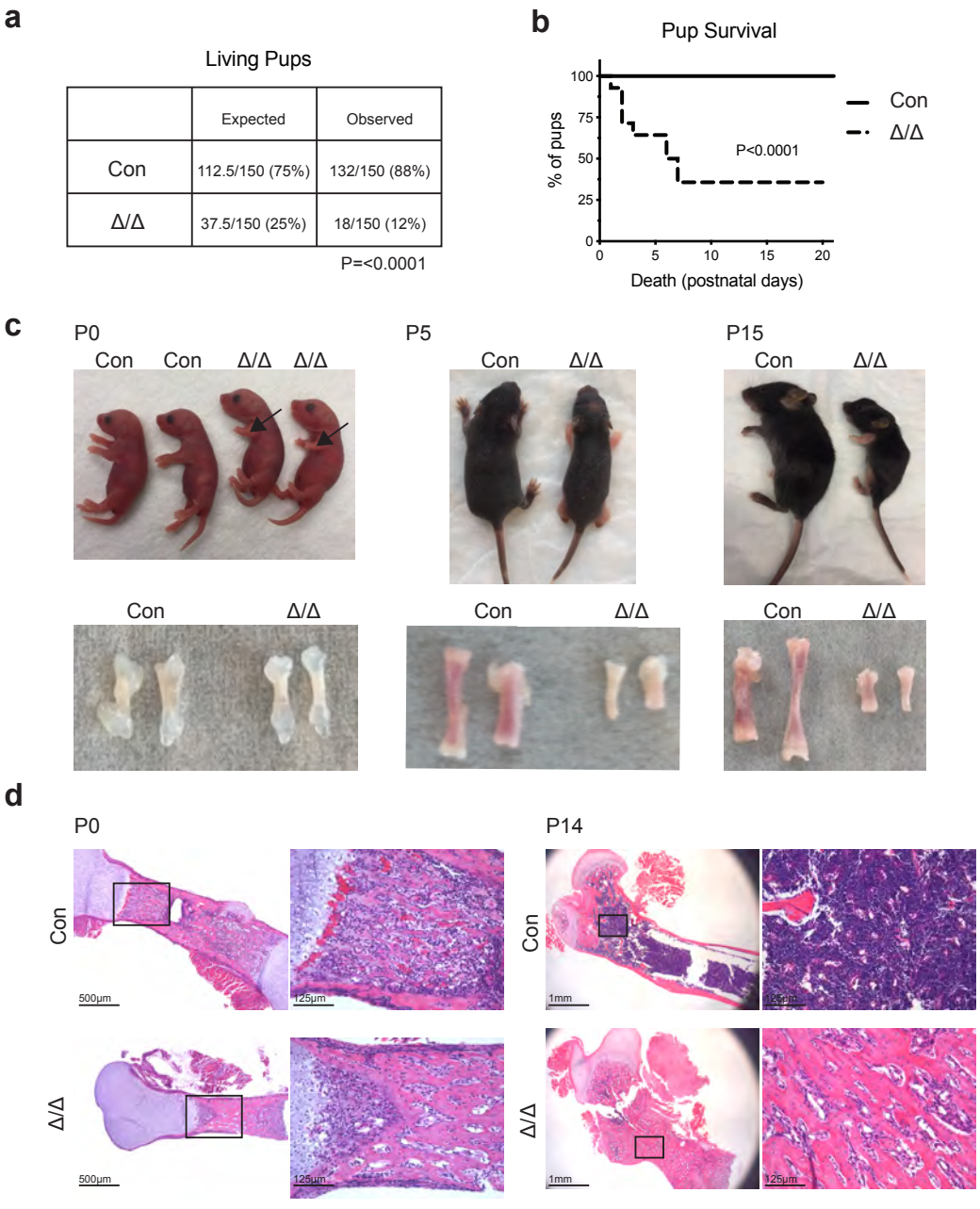
a
Living Pups
Expected
Observed
Con
112.5/150 (75%)
132/150 (88%)
Δ/Δ
37.5/150 (25%)
18/150 (12%)
P=<0.0001
b
Pup Survival
% of pups
100
75
50
25
0
0
5
10
15
20
Death (postnatal days)
P<0.0001
Con
Δ/Δ
c
P0
Con
Con
Δ/Δ
Δ/Δ
P5
Con
Δ/Δ
P15
Con
Δ/Δ
Con
Δ/Δ
Con
Δ/Δ
Con
Δ/Δ
d
P0
P14
Con
Δ/Δ
500μm
125μm
1mm
125μm

Figure 3.1

Prx1-cre; Mettl3$^{fl/fl}$ mice have perturbed hematopoiesis and a reduction in bone marrow HSCs

To specifically assess how their abnormal long bone development affected hematopoiesis, we analyzed the bone marrow from *Prx1-cre; Mettl3*$^{fl/fl}$ hindlimbs from birth to two weeks of age. *Mettl3*-deficient bones had reduced bone marrow cellularity at all stages examined (**Figure 3.2a**), consistent with histologic examination (**Figure 3.1d**). By flow cytometry, we found a reduction in the frequency of B220^{+} B cells, but no differences in the frequency of other types of mature blood cells analyzed, including CD41^{+} megakaryocytes, Mac1^{+}Gr1^{+} myeloid cells, Ter119^{+} red blood cells and CD3^{+} T cells. (**Figure 3.2b**). However, the frequency of Lin^{-}Sca1^{+}cKit^{+} (LSK) hematopoietic progenitors also trended towards a reduction at all stages (**Figure 3.2c-d**), with the most dramatic reduction observed in the CD150^{+}CD48^{-}LSK HSC compartment (**Figure 3.2e**). By two weeks of age, *Prx1-cre; Mettl3*$^{fl/fl}$ hindlimbs contained an average 160-fold fewer HSCs compared to littermate controls (**Figure 3.2f**), with nearly no HSCs. In contrast, *Prx1-cre; Mettl3*$^{fl/fl}$ vertebral marrow displayed normal HSC frequency (**Figure 3.2g**), consistent with the pattern of *Prx1-cre* expression in the limbs, but not the axial bones (Logan et al., 2002). These data suggest that a loss of *Mettl3* from MSCs prevents normal hematopoiesis with a profound impact on HSCs.

Figure 3.2 *Prx1-cre; Mettl3*$^{fl/fl}$ mice have perturbed hematopoiesis and a reduction in bone marrow HSCs.

(**a**) Bone marrow cellularity per hindlimb (n=3 for control (P0), n=3 for *Prx1-cre; Mettl3*$^{fl/fl}$ (P0), n=3 for control (P5), n=3 for *Prx1-cre; Mettl3*$^{fl/fl}$ (P5), n=3 for control (P10), n=3 for *Prx1-cre; Mettl3*$^{fl/fl}$ (P10), n=7 for control (P14-16), n=7 for *Prx1-cre; Mettl3*$^{fl/fl}$ (P14-16)).

(**b**) Frequencies of indicated bone marrow cell populations from P14-P16 hindlimbs (n=3 for control, n=3 for *Prx1-cre; Mettl3*$^{fl/fl}$).

(**c**) Representative flow cytometry gating strategy for HSCs in P14-P16 hindlimb bone marrow. Percentages reflect the frequency of the indicated population out of live bone marrow cells.

(**d**) Frequencies of bone marrow Lin^{-}Sca-1^{+}c-Kit^{+} (LSK) progenitors (n=3 for control (P0), n=3 for *Prx1-cre; Mettl3*$^{fl/fl}$ (P0), n=4 for control (P5), n=4 for *Prx1-cre; Mettl3*$^{fl/fl}$ (P5), n=3 for control (P10), n=3 for *Prx1-cre; Mettl3*$^{fl/fl}$ (P10), n=3 for control (P14-16), n=3 for *Prx1-cre; Mettl3*$^{fl/fl}$ (P14-16)).

(**e**) Frequency of bone marrow HSCs (n=3 for control (P0), n=3 for *Prx1-cre; Mettl3*$^{fl/fl}$ (P0), n=4 for control (P5), n=4 for *Prx1-cre; Mettl3*$^{fl/fl}$ (P5), n=3 for control (P10), n=3 for *Prx1-cre; Mettl3*$^{fl/fl}$ (P10), n=3 for control (P14-16), n=3 for *Prx1-cre; Mettl3*$^{fl/fl}$ (P14-16)).

(**f**) Bone marrow HSCs per hindlimb (n=3 for control (P0), n=3 for *Prx1-cre; Mettl3*$^{fl/fl}$ (P0), n=3 for control (P5), n=3 for *Prx1-cre; Mettl3*$^{fl/fl}$ (P5), n=3 for control (P10), n=3 for *Prx1-cre; Mettl3*$^{fl/fl}$ (P10), n=3 for control (P14-16), n=3 for *Prx1-cre; Mettl3*$^{fl/fl}$ (P14-16)).

(**g**) Frequency of HSCs in the vertebral bone marrow at P14-16 (n=2 for control, n=3 for *Prx1-cre; Mettl3*$^{fl/fl}$).

(**h**) Frequency of liver HSCs (n=3 for control (P0), n=3 for *Prx1-cre; Mettl3*$^{fl/fl}$ (P0), n=4 for control (P5), n=4 for *Prx1-cre; Mettl3*$^{fl/fl}$ (P5)).

(**i**) Frequency of spleen HSCs (n=3 for control (P0), n=3 for *Prx1-cre; Mettl3*$^{fl/fl}$ (P0), n=4 for control (P5), n=4 for *Prx1-cre; Mettl3*$^{fl/fl}$ (P5), n=3 for control (P10), n=3 for *Prx1-cre; Mettl3*$^{fl/fl}$ (P10), n=4 for control (P14-16), n=4 for *Prx1-cre; Mettl3*$^{fl/fl}$ (P14-16)).

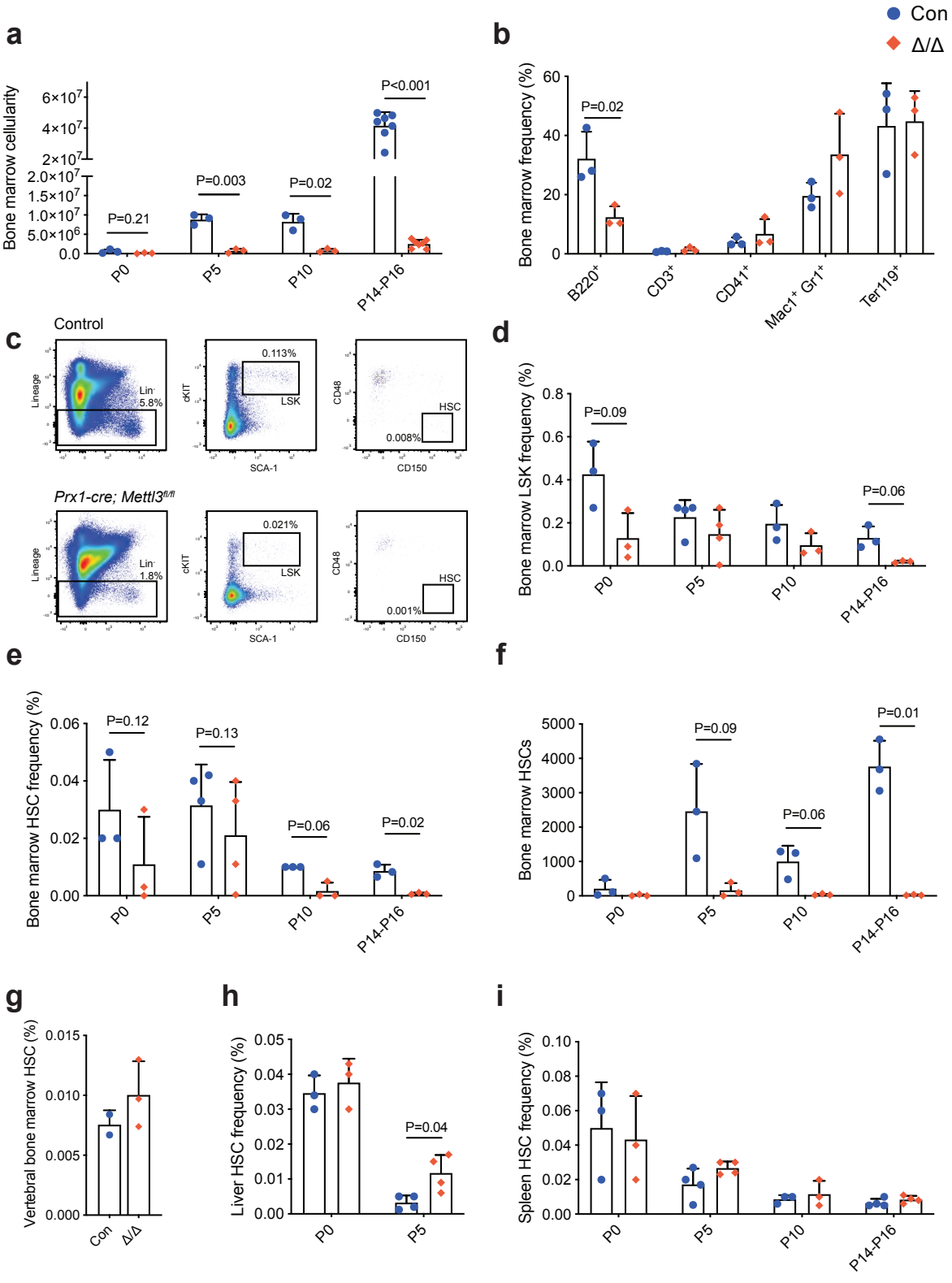
a
Bone marrow cellularity
6×10^7
4×10^7
2×10^7
2.0×10^7
1.5×10^7
1.0×10^7
5.0×10^6
0.0
P=0.21
P=0.003
P=0.02
P<0.001
P0
P5
P10
P14-P16
b
Con
Δ/Δ
Bone marrow frequency (%)
60
40
20
0
P=0.02
B220+
CD3+
CD41+
Mac1+ Gr1+
Ter119+
c
Control
Lineage
Lin-
5.8%
cKIT
0.113%
LSK
SCA-1
CD48
HSC
0.008%
CD150
Prx1-cre; Mettl3fl/fl
Lin-
1.8%
0.021%
0.001%
d
Bone marrow LSK frequency (%)
0.8
0.6
0.4
0.2
0.0
P=0.09
P=0.06
e
Bone marrow HSC frequency (%)
0.06
0.04
0.02
0.00
P=0.12
P=0.13
P=0.06
P=0.02
f
Bone marrow HSCs
5000
4000
3000
2000
1000
0
P=0.09
P=0.06
P=0.01
g
Vertebral bone marrow HSC (%)
0.015
0.010
0.005
0.000
Con
Δ/Δ
h
Liver HSC frequency (%)
0.05
0.04
0.03
0.02
0.01
0.00
P=0.04
i
Spleen HSC frequency (%)
0.10
0.08
0.06
0.04
0.02
0.00

Figure 3.2

HSCs predominantly reside in the fetal liver during embryonic development and migrate to the bone marrow around birth (Christensen et al., 2004). Newborn *Prx1-cre; Mettl3*$^{fl/fl}$ mice had normal HSC numbers in the livers compared with controls, suggesting the observed HSC depletion phenotype in the bone marrow was not due to HSC defects in the fetal liver stage (**Figure 3.2h**). Interestingly, *Prx1-cre; Mettl3*$^{fl/fl}$ mice had more HSCs in the liver at P5 compared to controls (**Figure 3.2h**). Fetal liver HSCs appeared to have a normal capacity to migrate into the bone marrow, as the vertebrae of *Prx1-cre; Mettl3*$^{fl/fl}$ mice had normal HSCs frequencies (**Figure 3.2g**). The frequency of splenic HSCs is also unaffected by loss of *Mettl3* in MSCs (**Figure 3.2i**), so the increase in liver HSCs is not likely to be explained by reactive extramedullary hematopoiesis. Thus, the loss of phenotypic HSCs observed in the bone marrow (**Figure 3.2e-f**) is likely due to a decreased migration of fetal liver HSCs into the *Mettl3*-depleted bone marrow environment.

Prx1-cre; Mettl3$^{fl/fl}$ hindlimb bone marrow has reduced reconstitution potential

To definitively determine if the number of functional HSCs in *Prx1-cre; Mettl3*$^{fl/fl}$ limbs is reduced, we performed limiting dilution transplantation assays. We transplanted differing doses of bone marrow cells (10,000, 30,000, or 80,000 cells) from control or *Mettl3*-depleted hindlimbs into irradiated recipient mice along with 300,000 recipient-type radioprotection bone marrow cells and measured the fraction of recipients that were successfully reconstituted in all major blood lineages (myeloid, B and T cells) at each dose, demonstrating HSC function. This allowed us to extrapolate the frequency of functional HSCs within the bone marrow and revealed a four-fold reduction in the frequency of functional HSCs within *Mettl3*-deficient bone marrow (**Figure 3.3c**). Thus, *Prx1-cre; Mettl3*$^{fl/fl}$ limb bone marrow has reduced long-term multi-lineage reconstitution potential, demonstrating that *Mettl3* in MSCs is required for normal HSC maintenance.

Figure 3.3 *Prx1-cre; Mettl3*$^{fl/fl}$ hindlimb bone marrow has reduced HSC frequency and function.

Limiting dilution transplantation of 10,000, 30,000, or 80,000 donor whole bone marrow cells as indicated from *Prx1-cre; Mettl3*$^{fl/fl}$ or *Mettl3*$^{fl/fl}$ controls with 300,000 competitor cells. Recipients were judged as responders if they showed donor-derived myeloid, B and T cells in the peripheral blood were assessed up to 16 weeks after transplantation. Samples were from independent recipients of two independent donor pairs from two experiments. Graph of results (left) and numbers of recipients and responders for the indicated conditions (right).

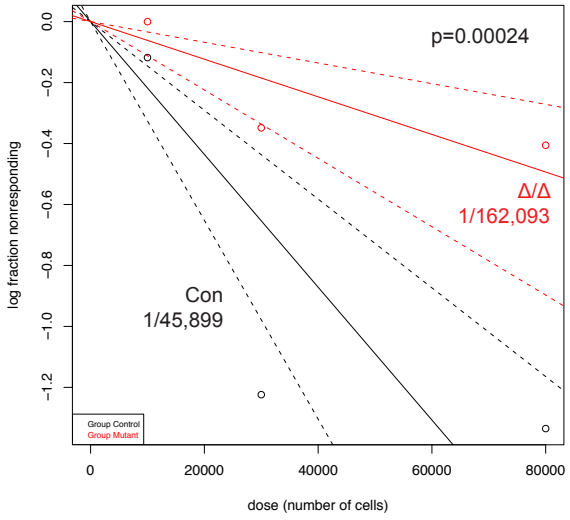

Cell Dose	Recipients	Responses
Con		
10,000	18	2
30,000	17	12
80,000	19	14
Δ/Δ		
10,000	17	0
30,000	17	5
80,000	18	6

Figure 3.3

CXCL12-expressing cells and CXCL12 expression is reduced in *Prx1-cre; Mettl3$^{fl/fl}$* hindlimbs

Our data (**Figure 3.2-3.3**) suggest that the HSC-supporting function of bone marrow MSCs is compromised after *Mettl3* deletion. *Cxcl12* is a chemokine known to be highly and specifically expressed by perivascular MSCs in adult bone marrow and has been shown to be required for HSC retention and maintenance and B cell development in the bone marrow (Greenbaum et al., 2013; Ding and Morrison, 2013; Tokoyoda et al., 2004). Previous genetic studies have shown that loss of *Cxcl12* or its receptor, *Cxcr4*, impairs the establishment of bone marrow hematopoiesis with a loss of bone marrow cellularity, HSCs, and B cells (Nagasawa et al., 1996; Ma et al.,1998; Tokoyoda et al., 2004), suggesting METTL3 may regulate the niche function of MSCs through regulating CXCL12 expression. To directly test whether there are defects of *Cxcl12* expression with bone marrow niche cells, we labeled HSC-supporting MSCs using the genetic transcriptional reporter *Cxcl12^{DsRed}* knock-in mice (Ding and Morrison, 2013). Histologic sections of *Prx1-cre; Mettl3$^{fl/fl}$* long bones showed that fewer *Cxcl12*-DsRed^{+} cells were in the bone marrow from P0 compared with controls (**Figure 3.4a**), around the time when HSCs would normally migrate from the fetal liver to the bone marrow (Christensen et al., 2004). By P14, control long bones contained abundant *Cxcl12*-DsRed^{+} stromal cells throughout the marrow cavity (**Figure 3.4b**). However, *Prx1-cre; Mettl3$^{fl/fl}$* long bones contained significantly fewer *Cxcl12*-DsRed^{+} cells that are restricted to small areas of the marrow, rather than evenly distributed as in *Cxcl12^{DsRed}* control mice (**Figure 3.4b**).

To understand how loss of *Mettl3* influences *Prx1*$^{+}$ MSCs, we crossed the *CAG-loxP-stop-loxP-ZsG* (*ZsG^{fl}*) Cre reporter allele (Madisen et al., 2010) into the *Prx1-cre; Mettl3$^{fl/fl}$* mice to trace the cell fate of *Prx1*$^{+}$ MSCs. Sections of *Prx1-cre; Mettl3$^{fl/fl}$;ZsG$^{fl/+}$*; *Cxcl12$^{DsRed/+}$* hindlimbs revealed Cre expression in cells throughout the *Mettl3*-depleted bones (**Figure 3.4b**). However, while *Prx1*$^{+}$-derived ZsG^{+} cells in the control marrow are largely *Cxcl12*-DsRed^{+} stromal cells, *Mettl3*-depleted mice have long bones filled with ZsG^{+} mesenchymal tissue that

does not express *Cxcl12*-DsRed (**Figure 3.4b**), suggesting a cell fate change of *Mettl3*-deficient MSCs.

By flow cytometry, there was a significant reduction in the frequency of $CD45^{-}Ter119^{-}$ *Cxcl12*-$DsRed^{+}$ cells in *Mettl3*-depleted long bones compared to littermate controls (**Figure 3.4c**). Using PDGFRα, an alternative marker for MSCs (Morikawa et al., 2009), similar results were obtained (**Figure 3.4d**). As our $Cxcl12^{DsRed}$ allele is a transcriptional reporter (Ding and Morrison, 2013), the levels of DsRed were not a direct readout of CXCL12 protein. To assess CXCL12 protein expression within the MSCs, we performed intracellular flow cytometry using an anti-CXCL12 antibody (R&D IC350F). This revealed a notable decrease in the expression of CXCL12 in $CD45^{-}Ter119^{-}PDGFR\alpha^{+}$ stromal cells (**Figure 3.4e**). Thus, *Prx1-cre;* $Mettl3^{fl/fl}$ limb bones have not only contain fewer HSC-supporting stromal cells, but also express less CXCL12 protein from those MSCs. Therefore, our data suggest that the hematopoietic defects observed in *Prx1-cre;* $Mettl3^{fl/fl}$ limbs are at least partially through the loss of CXCL12 from $Prx1^{+}$ MSCs.

Figure 3.4 CXCL12-expressing cells and CXCL12 expression is reduced in *Prx1-cre; Mettl3$^{fl/fl}$* hindlimbs.

(**a**) Representative confocal images of P0 *Cxcl12-DsRed* control and *Prx1-cre; Mettl3$^{fl/fl}$; Cxcl12$^{DsRed/+}$* femurs. Nuclei were stained with 4',6-diamidino-2-phenylindole (DAPI, blue).

(**b**) Representative confocal images of P14 *ZsG$^{fl/+}$; Cxcl12$^{DsRed/+}$* control and *Prx1-cre; Mettl3$^{fl/fl}$; ZsG$^{fl/+}$; Cxcl12$^{DsRed/+}$* femurs. Nuclei were stained with 4',6-diamidino-2-phenylindole (DAPI, blue).

(**c**) Representative flow cytometry plots (left) and quantification (right) of CD45$^-$Ter119$^-$*Cxcl12*-DsRed$^+$ cells in P14-P16 hindlimb bones. Percentages reflect the population frequency out of live bone marrow cells (n=3 for *Cxcl12$^{DsRed/+}$* control, n=2 for *Prx1-cre; Mettl3$^{fl/fl}$; Cxcl12$^{DsRed/+}$*).

(**d**) Frequency of CD45$^-$Ter119$^-$PDGFRα$^+$ stromal cells in P14-16 *Prx1-cre; Mettl3$^{fl/fl}$* or control hindlimb bones (n=4 for control, n=3 for *Prx1-cre; Mettl3$^{fl/fl}$*).

(**e**) Representative flow cytometry plot (left) and quantification (right) of CXCL12-FITC mean fluorescence intensity (MFI) in all bone marrow cells or CD45$^-$Ter119$^-$PDGFRα$^+$ cells in P14-P16 hindlimbs, as indicated (n=4 for control, n=3 for *Prx1-cre; Mettl3$^{fl/fl}$*). Values given are in arbitrary units (a.u.) normalized to IgG MFI.

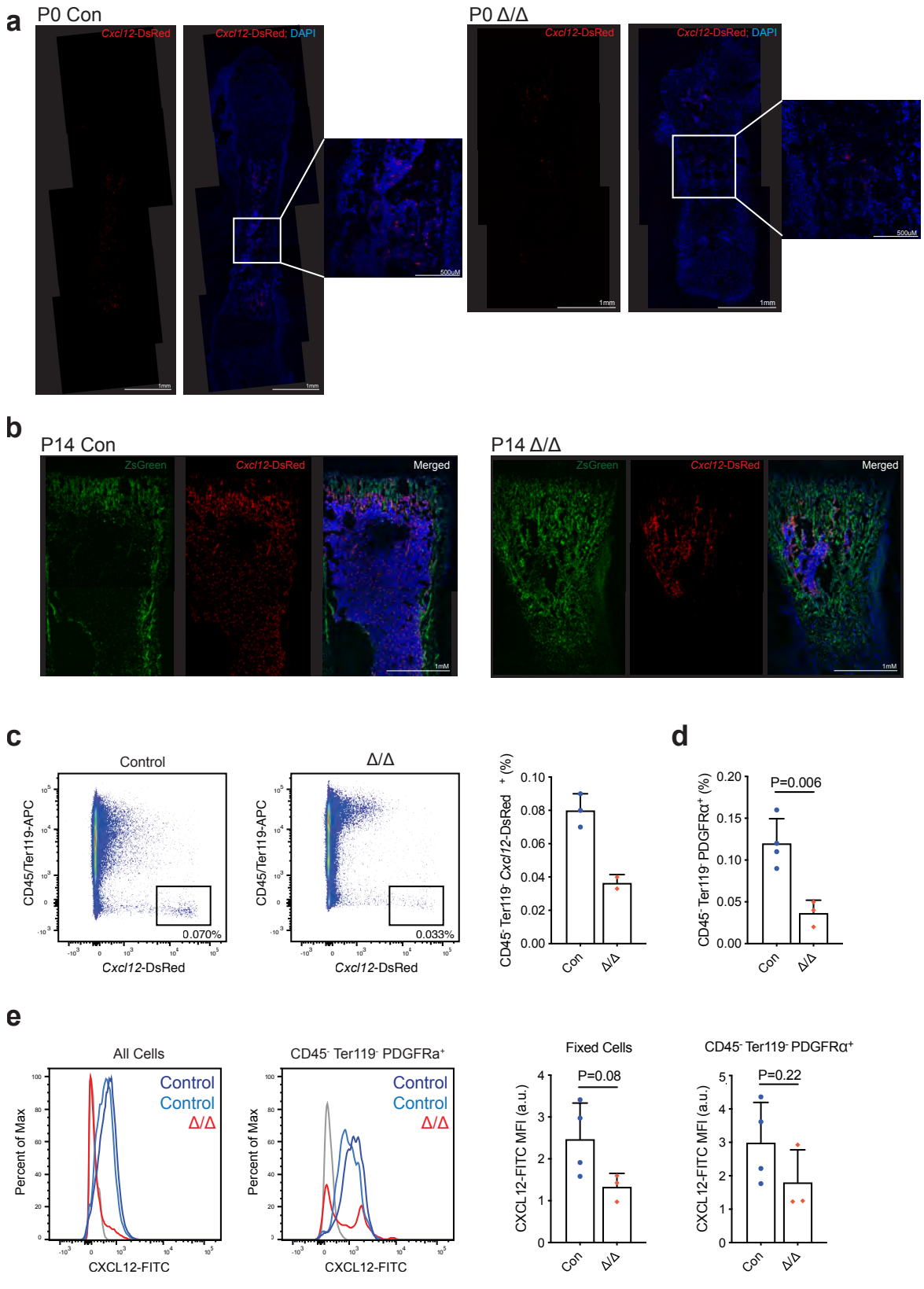
a
P0 Con
Cxcl12-DsRed
Cxcl12-DsRed; DAPI
P0 Δ/Δ
b
P14 Con
ZsGreen
Merged
P14 Δ/Δ
c
Control
Δ/Δ
CD45/Ter119-APC
Cxcl12-DsRed
0.070%
0.033%
CD45-Ter119-Cxcl12-DsRed+ (%)
Con
d
CD45-Ter119-PDGFRα+ (%)
P=0.006
e
All Cells
CD45- Ter119- PDGFRa+
Control
Δ/Δ
Percent of Max
CXCL12-FITC
Fixed Cells
CXCL12-FITC MFI (a.u.)
P=0.08
P=0.22

Figure 3.4

Lepr-cre; Mettl3$^{fl/fl}$ mice do not display hematopoietic defects

In adult bone marrow, HSC-supporting MSCs can be identified by their expression of Leptin receptor (*Lepr*) or *Prx1*. However, while *Prx1-cre* is expressed during embryogenesis (Logan et al., 2002), *Lepr-cre* is expressed only after birth (Zhou et al., 2014). To determine if *Mettl3* plays a role in regulating the post-natal bone marrow niche, we generated *Lepr-cre; Mettl3$^{fl/-}$* mice. Consistent with prior reports (Zhou et al., 2015; Ding et al., 2012; Ding and Morrison, 2013), *Lepr-cre* efficiently deleted *Mettl3* from CD45$^-$ Ter119$^-$ PDGFRα$^+$ stromal cells (**Figure 3.5a**). Interestingly, CD45$^-$ Ter119$^-$ PDGFRα$^+$ stromal cells express lower levels of *Mettl3* compared to whole bone marrow (**Figure 3.5a**). At 6 to 8 weeks of age, *Lepr-cre; Mettl3$^{fl/-}$* mice displayed normal white blood cell, red blood cell, or platelet counts compared to controls (**Figure 3.5b**). They also had normal bone marrow cellularity, HSC frequency, or CD45$^-$ Ter119$^-$ PDGFRα$^+$ stromal cell frequency (**Figure 3.5c-e**). While more work is needed to fully characterize the hematopoietic system of *Lepr-cre; Mettl3$^{fl/-}$* mice, our results thus far show that depletion of *Mettl3* from adult *Lepr*$^+$ MSCs does not result in the same severe HSC defects as loss of *Mettl3* from embryonic *Prx1*$^+$ MSCs. Thus, *Mettl3* may have a preferential role in the establishment of the HSC niche, as opposed to its maintenance.

Figure 3.5 *Lepr-cre; Mettl3$^{fl/-}$* mice do not display hematopoietic defects.

(**a**) qPCR analysis of *Mettl3* mRNA expression in control whole bone marrow and CD45$^-$Ter119$^-$ PDGFRα$^+$ stromal cells from *Lepr-cre; Mettl3$^{fl/-}$* or control mice (n=*** for control bone marrow, n=6 for control stromal cells, n=6 for *Lepr-cre; Mettl3$^{fl/-}$* stromal cells).

(**b**) White blood cell, red blood cell, and platelet counts as indicated in adult *Lepr-cre; Mettl3$^{fl/-}$* or control mice (n=3 for control, n=3 for *Lepr-cre; Mettl3$^{fl/-}$*).

(**c**) Bone marrow cellularity per hindlimb in adult *Lepr-cre; Mettl3$^{fl/-}$* or control mice (n=3 for control, n=3 for *Lepr-cre; Mettl3$^{fl/-}$*).

(**d**) Frequency of bone marrow HSCs in adult *Lepr-cre; Mettl3$^{fl/-}$* or control mice (n=3 for control, n=3 for *Lepr-cre; Mettl3$^{fl/-}$*).

(**e**) Frequency of CD45$^-$Ter119$^-$PDGFRa$^+$ stromal cells in adult *Lepr-cre; Mettl3$^{fl/-}$* or control mice (n=3 for control, n=3 for *Lepr-cre; Mettl3$^{fl/-}$*).

n.s. = not significant; p value > 0.02 by two-sided Student's t-test.

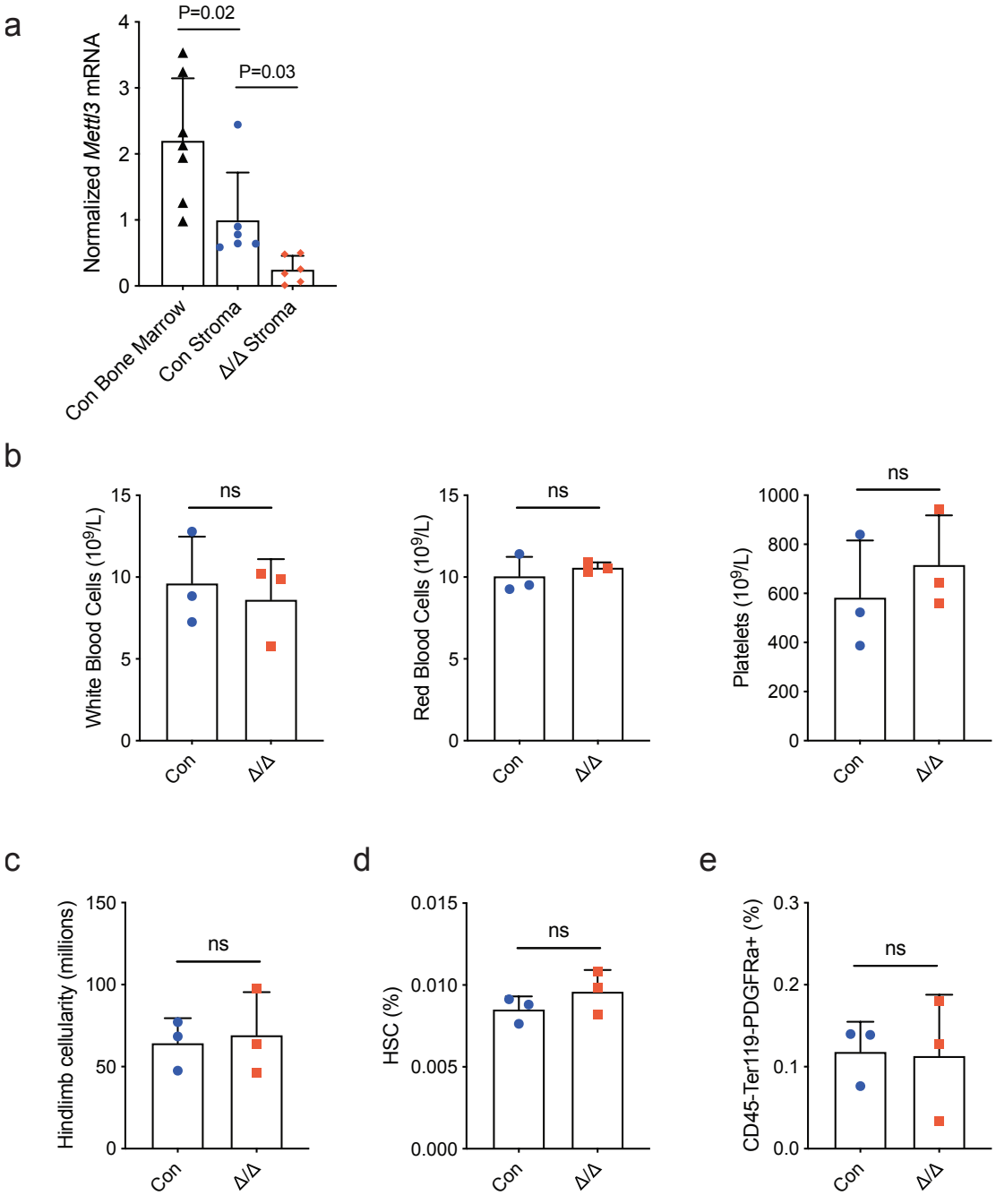
a
P=0.02
P=0.03
Normalized Mettl3 mRNA
Con Bone Marrow
Con Stroma
Δ/Δ Stroma
b
White Blood Cells (10^9/L)
Red Blood Cells (10^9/L)
Platelets (10^9/L)
ns
Con
Δ/Δ
c
Hindlimb cellularity (millions)
d
HSC (%)
e
CD45-Ter119-PDGFRa+ (%)

Figure 3.5

DISCUSSION

The results reported are preliminary and only broadly characterize the effects of loss of *Mettl3* from long bone MSCs, a key component of the HSC niche. We have demonstrated that *Mettl3* is required in developmental MSCs for the establishment of the bone marrow niche and normal hematopoiesis in the limbs. Loss of *Mettl3* from *Prx1*$^{+}$ cells results in decreased survival in utero and postnatally (**Figure 3.1a-b**). While we do not know the cause, we suspect their survival defect could be related to *Prx1*$^{+}$ expression and *Mettl3* deletion in embryonic cranial mesenchyme (Logan et al., 2002) and to their decreased size, which may confer a competitive disadvantage for maternal support. It is unlikely to be related to hematopoietic defects, as we found normal HSC frequencies in fetal livers and vertebral marrow (**Figure 3.2g-h**). In contrast, we saw a preferential loss of HSCs and B cells from *Mettl3*-deficient limb bone marrow (**Figure 3.2**), at least partially caused by the loss of CXCL12-expressing MSCs (**Figure 3.4**). As HSCs remain longer in *Prx1-cre; Mettl3*$^{fl/fl}$ livers (**Figure 3.2g**), we hypothesize that these mice have defects in HSC migration to the long bones from their loss of CXCL12-expressing MSCs. As it appears that fetal liver HSCs can be maintained in the vertebral marrow normally (**Figure 3.2g**), the impairment of HSC-supporting activity seems specific to the *Mettl3*-deficient bone marrow. Interestingly, Wu et al. demonstrated that the key HSC-regulating cytokines *Cxcl12* and *Scf* are m^{6}A targets in adult MSCs *in vitro* (Wu et al., 2018). While m^{6}A targets may be context and cell-type dependent, it is very possible that *Cxcl12* and *Scf* are also m^{6}A targets of developing MSCs *in vivo*. We are performing m^{6}A methylome sequencing to directly address whether *Cxcl12* and *Scf* are targets of m^{6}A in *Prx1*$^{+}$ MSCs in fetal long bones. Thus, we hypothesize that loss of *Mettl3* perturbs m^{6}A regulation of *Cxcl12* and *Scf*, causes loss of CXCL12 (and possibly SCF and other niche factors) expression and compromises HSC-supporting function. Further work is ongoing to explore this hypothesis.

A recent study found that *Mettl3* deletion in MSCs leads to osteoporosis in adult mice, shifting the balance of MSC fate towards adipogenesis, rather than bone formation (Wu et al., 2018). Our work is consistent with this notion of m^{6}A regulation of MSC fate, as we have found *Mettl3* to be critical for MSC development of normal limb mesenchymal tissue, including HSC-supporting stromal cells, to the detriment of hematopoiesis. Interestingly, *Lepr-cre; Mettl3*$^{fl/-}$ mice do not display the same hematopoietic defects as *Prx1-cre; Mettl3*$^{fl/fl}$ mice. One possible explanation for this is residual expression of *Mettl3* from *Lepr*$^+$ cells from incomplete deletion (**Figure 3.5e**). However, our experience using *Lepr-cre* has shown over 90% efficiency in other conditional mouse models and strong phenotypic effects when used to conditionally delete important niche factors like *Scf* and *Cxcl12* (Zhou et al., 2015; Ding et al., 2012; Ding and Morrison, 2013). It is possible that we are achieving lower deletion efficiencies due to contamination from other bone marrow cells, which express higher levels of *Mettl3* than stromal cells and may cause us to underestimate the deletion efficiency (**Figure 3.5a**). Thus, another possibility is that there is a functional difference in the role of *Mettl3* within MSCs at different developmental stages. This also raises the possibility of two distinct cell identities: developmental *Prx1*$^+$ MSCs and their downstream *Lepr*$^+$ MSCs progenies. Understanding the relationships between these different cell types offers great potential in furthering our understanding of how the HSC niche is formed and regulated.

Consistent with our findings on the role of *Mettl3* in HSCs and myeloid cells (Chapter 2), these results also suggest that *Mettl3* has specific roles in stem and progenitor cells and is more dispensable in downstream cells. With roles for m^{6}A also reported in embryonic stem cells and neural progenitors, it is possible that *Mettl3* and m^{6}A may be a distinguishing feature of stem cells in general.

ACKNOWLEDGMENTS

L.D. was supported by the Rita Allen Foundation, a Irma Hirschl Trust Research Award, the National Heart, Lung and Blood Institute (R01HL132074) and a Leukemia and Lymphoma Society Scholar Award. H.L. was supported by the Columbia Medical Scientist Training Program and the National Heart, Lung and Blood Institute (F30HL142196-01).

CHAPTER 4

CONCLUSIONS AND GENERAL DISCUSSION

Hematopoietic stem cells (HSCs) are a paradigm tissue stem cell, characterized by their ability for life-long self-renewal and multi-lineage differentiation. HSC function is regulated by complex cell-intrinsic and -extrinsic pathways, but the mechanisms that control balanced self-renewal and differentiation are poorly understood. I have shown that the epitranscriptional modification N^6-methyladenosine (m^6A) plays critical roles in regulating HSC function, both within the HSC itself (Chapter 2, **Figure 4.1a**) and through regulation of HSC-supporting mesenchymal stromal cells (MSCs) in the bone marrow (Chapter 3, **Figure 4.1b**). While the role of DNA modifications in HSC function has been characterized (Broske et al., 2009; Challen et al., 2012), this is one of the first works to demonstrate the role for RNA modification in adult stem cells.

HSCs seem to be preferentially affected by loss of *Mettl3*, while mature myeloid cells display no obvious defects (Chapter 2). This specific requirement for m^6A in HSCs, but not more mature cells, may be one explanation for why previous studies on broader populations of hematopoietic cells, such as $CD34^+$ HSPCs and lineage-negative cells, did not report significant effects from loss of *Mettl3* (Barbieri et al., 2017; Vu et al., 2017). In contrast, I have demonstrated that focusing specifically on the HSC compartment reveals an HSC-specific reliance on m^6A-regulation. To my knowledge, this is the first time that m^6A has been shown to have differential importance at the stem cell level, but little importance in more mature cells, thus giving us greater insight into the unique properties of stem cells and how they are distinct from their progeny.

Around the time that these results described in Chapter 2 were published, several other studies on the role for m^6A within HSCs were also released. They similarly found that loss of *Mettl3* from adult HSCs causes an expansion of the HSC pool and reduced reconstitution potential from a defect in differentiation (Yao et al., 2018; Cheng et al., 2019). Cheng *et al*. also found that *Myc* was a direct m^6A target and the HSC differentiation defect could be partially rescued by *Myc* overexpression, confirming our findings (Chapter 2). Thus, we and several other investigators have found that m^6A specifically regulates HSC differentiation over other aspects of HSC function. My preliminary work in MSCs also suggests a role for m^6A in MSC fate determination (Chapter 3). These observations are consistent with findings in the broader m^6A field, including studies on embryonic stem cell, neural progenitors, embryonic endothelium, naïve immune cells and leukemia stem cells, all suggesting that m^6A has specific roles for the transition from an undifferentiated to more differentiated state.

My work on m^6A is also consistent with prior studies on HSC differentiation and offers some additional insights into past findings. MYC is a master regulator of HSC differentiation that is known to be post-translationally regulated by ubiquitin-mediated degradation (Reavie et al., 2010; Wilson et al., 2004; Ehninger et al., 2014). My work and others demonstrates that expression of MYC protein, but not RNA, is also highly regulated by m^6A, making m^6A an additional post-transcriptional regulator of *Myc* and HSC differentiation (Chapter 2; Cheng et al., 2019).

This fits within the context of other proposed regulators of *Myc*, including RBM15. *Rbm15* knock-out mice expanded LSK, HSC, myeloid and megakaryocyte populations with defects in HSC reconstitution capacity and B cell and megakaryocyte differentiation (Niu et al., 2009; Raffel et al., 2007). Megakaryocyte differentiation defects could be partially rescued by *Myc* overexpression, so it was suggested that the hematopoietic abnormalities were related to regulation of *Myc* by RBM15 (Niu et al., 2009). However, the molecular mechanisms were never fully elucidated. At the time of these studies, RBM15 was not yet known to be involved in the

m^{6}A methyltransferase complex, so whether the effects of loss of *Rbm15* were due to impacts on the m^{6}A pathway or a different function of *Rbm15* was not clear. *Mx1-cre; Mettl3$^{fl/fl}$* mice show striking similarities to *Rbm15* knock-out mice in their expanded LSKs, HSCs, and megakaryocyte pools with abnormal differentiation (Chapter 2). Given the role of m^{6}A in the regulation of *Myc* that I have demonstrated and the similarities in the *Rbm15* knock-out phenotype, it seems probable that the effects of loss of *Rbm15* are caused by disruption of the m^{6}A pathway.

As m^{6}A has been shown to play important roles in leukemia cell fate, m^{6}A and METTL3 have been proposed to be promising therapeutic targets. However, my work and others' has shown that loss of m^{6}A also has dramatic effects on HSCs, and this will be an important consideration for development of these therapies (Yao et al., 2018; Cheng et al., 2019). Interestingly, the role of m^{6}A in HSCs seems to be opposite the proposed role of m^{6}A in leukemia cells. Several groups have found that loss of m^{6}A through depletion of *Mettl3* or *Mettl14* promotes differentiation of leukemia cells (Barbieri et al., 2017; Vu et al., 2017; Weng et al., 2017). However, despite having opposite effects on differentiation, m^{6}A regulates *Myc* in both myeloid leukemia cells and HSCs (Barbieri et al., 2017; Vu et al., 2017; Weng et al., 2017; Yao et al., 2018; Cheng et al., 2019). What causes this difference in cellular fate between the cell types is unclear. The observed effects in leukemia cells were seen using leukemia cell lines *in vitro* and cultured leukemia cells transplanted into recipient mice (Barbieri et al., 2017; Vu et al., 2017; Weng et al., 2017), so it is possible that different findings may result when depleting m^{6}A in other *in vivo* leukemia models, such as with genetic mouse models, which we are currently exploring. However, it is also possible that the observed effects differ from differing m^{6}A targets and m^{6}A reader proteins, which are known to be context dependent (Xiao et al., 2019). Though I show that *Myc* is a major m^{6}A target regulating HSC differentiation, we also identified 994 other *Mettl3*-dependent m^{6}A targets within HSCs. Some of those targets include known HSC regulators like *Tet2* and *Junb,* which have also been implicated in leukemogenesis

(Moran-Crusio et al., 2011; Li et al., 2011; Passague et al., 2001). How these targets are impacted after *Mettl3*-depletion and whether their dysregulation also impacts HSC function is still unknown. Furthermore, understanding how the full spectrum of m^6A targets and readers differ between leukemia cells and HSCs also needs further study. All of these unknowns will be important to investigate for the development of any METTL3- or m^6A-targeted therapies.

Characterizing epitranscriptional regulation requires appropriate tools, which have only begun to be developed. The first methods to profile m^6A targets have been heavily reliant on anti-m^6A antibodies for immunostaining, immunoblotting and immunoprecipitation experiments (Meyer et al., 2012; Dominissini et al., 2012). Unfortunately, these antibodies are not specific to m^6A; they also recognize another modified adenosine, N6,2'-O-dimethyladenosine (m^6Am) (Mauer et al., 2017). m^6Am is not methylated by METTL3 or recognized by m^6A reader proteins (Mauer et al., 2017). This antibody cross-reactivity has only recently been appreciated, complicating interpretation of previous studies, including my own. While were able to show that 48% of our high confidence m^6A mRNA targets in HSCs were *Mettl3*-dependent, it is possible that some of the other high confidence targets contain m^6Am, rather than m^6A (**Figure 2.9c-d**). However, recent technical advances in m^6A profiling have allowed for m^6A and m^6Am to be distinguished (Linder et al., 2015). Newer antibody-independent m^6A profiling methods have also allowed for m^6A-specific transcriptome characterization, and these results have suggested that antibody-based methods may be underestimating the true number of m^6A modifications within a transcriptome (Garcia-Campos et al., 2019; Meyer, 2019). Thus, it is likely that there are additional m^6A targets in HSCs that were not identified in my work, but may have important roles in m^6A-based regulation of HSC function.

The m^6A profiling methods in my work were limited to the identification of m^6A-containing transcripts within HSCs and MSCs, leaving valuable information unknown, such as the location and density of m^6A sites on a transcript and the stoichiometry of m^6A-modified targets within a transcriptome. However, recent advances in m^6A profiling could provide those additional

insights. Techniques such as "m^{6}A individual-nucleotide resolution crosslinking and immunoprecipitation" (miCLIP) can determine the exact location and number of methylation sites on a given transcript (Linder et al., 2015). In certain contexts, it is now also possible to determine the stoichiometry of a given methylation site among a transcript pool (Garcia-Campos et al., 2019). More complete characterization of the methylation profiles could offer further explanation for current unknowns, such as how HSCs are distinguished from downstream progenitors which also express high levels of *Mettl3* (**Figure 2.1a**).

There is also emerging evidence that METTL3 has functions independent of its role as a methyltransferase. METTL3 has been localized to both the nucleus and cytoplasm, with differing hypothesized functions in the different subcellular compartments. When METTL3 is localized to nuclear speckles, it is found in association with other members of the m^{6}A-methyltransferase complex and is thus assumed to function in the writing of m^{6}A on pre-mRNA targets (Meyer and Jaffrey, 2017). However, in human cancer cell lines, cytoplasmic METTL3 has been shown to associate with ribosomes and form "loops" that promote ribosome retention on transcripts and increase translation efficiency, independent of METTL3's catalytic activity (Lin et al., 2016). Determining which effects from loss of *Mettl3* in HSCs and MSCs are due to m^{6}A-perturbation versus m^{6}A-independent METTL3 functions are critical for the development of effective m^{6}A- or METTL3-based therapeutics.

While the functional importance of m^{6}A has only been recognized in the last decade, it is quickly emerging as a major subject of interest and has sparked the investigation of over 150 other RNA modifications (Boccaletto et al., 2018). With ongoing development of new tools to study RNA modifications, it is likely that further work will answer remaining questions about HSC regulation by m^{6}A and characterize the role of other RNA modifications in HSC function. From healthy stem cells to aberrant leukemia cells, it is becoming clear that epitranscriptional regulation is a powerful mechanism for influencing cell fate and a promising target for potential therapeutics.

Figure 4.1 METTL3 and m^{6}A regulates hematopoietic stem cells (HSCs) both cell-intrinsically and –extrinsically.

(**a**) m^{6}A on *Myc* mRNA promotes MYC translation and is required for HSC differentiation.

(**b**) m^{6}A in embryonic *Prx1*$^+$ mesenchymal stromal cells is required for development of CXCL12-expressing HSC-supporting stromal cells in the limb bone marrow niche.

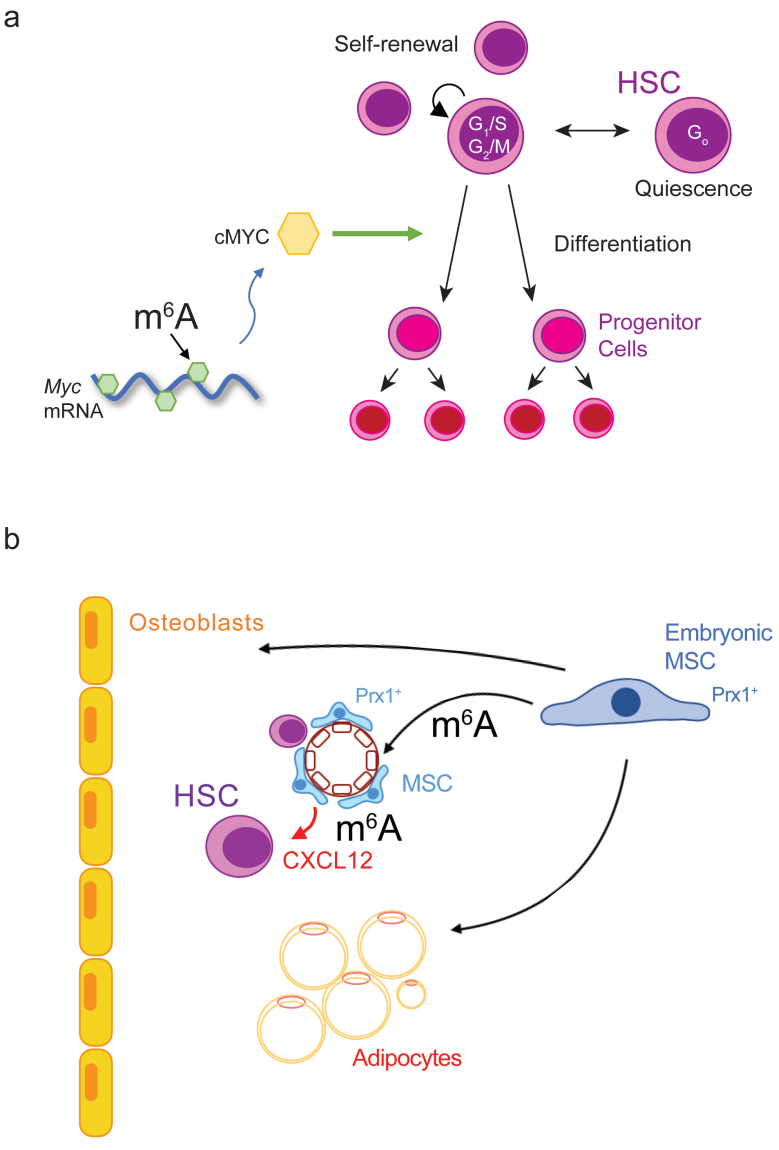

Figure 4.1

REFERENCES

Acar, M., Kocherlakota, K. S., Murphy, M. M., Peyer, J. G., Oguro, H., Inra, C. N., … Morrison, S. J. (2015). Deep imaging of bone marrow shows non-dividing stem cells are mainly perisinusoidal. *Nature*, *526*(7571), 126–130. https://doi.org/10.1038/nature15250

Agarwala, S. D., Blitzblau, H. G., Hochwagen, A., & Fink, G. R. (2012). RNA Methylation by the MIS Complex Regulates a Cell Fate Decision in Yeast. *PLoS Genetics*, *8*(6). https://doi.org/10.1371/journal.pgen.1002732

Aguilo, F., Avagyan, S., Labar, A., Sevilla, A., Lee, D.-F., Kumar, P., … Snoeck, H.-W. (2011). Prdm16 is a physiologic regulator of hematopoietic stem cells. *Blood*, *117*(19), 5057–5066. https://doi.org/10.1182/blood-2010-08-300145

Aguilo, F., Zhang, F., Sancho, A., Fidalgo, M., Di Cecilia, S., Vashisht, A., … Walsh, M. J. (2015). Coordination of m6A mRNA Methylation and Gene Transcription by ZFP217 Regulates Pluripotency and Reprogramming. *Cell Stem Cell*, *17*(6), 689–704. https://doi.org/10.1016/j.stem.2015.09.005

Akiyama‡, H., Kim‡, J.-E., Nakashima, K., Balmes, G., Iwai, N., Deng, J. M., … Crombrugghe, B. de. (2005). Osteo-chondroprogenitor cells are derived from Sox9 expressing precursors. *Proceedings of the National Academy of Sciences*, *102*(41), 14665–14670. https://doi.org/10.1073/pnas.0504750102

Ara, T., Tokoyoda, K., Sugiyama, T., Egawa, T., Kawabata, K., & Nagasawa, T. (2003). Long-Term Hematopoietic Stem Cells Require Stromal Cell-Derived Factor-1 for Colonizing Bone Marrow during Ontogeny. *Immunity*, *19*(2), 257–267. https://doi.org/10.1016/S1074-7613(03)00201-2

Barbieri, I., Tzelepis, K., Pandolfini, L., Shi, J., Millán-Zambrano, G., Robson, S. C., … Kouzarides, T. (2017). Promoter-bound METTL3 maintains myeloid leukaemia by m^6A-dependent translation control. *Nature*, *552*(7683), 126. https://doi.org/10.1038/nature24678

Batista, P. J., Molinie, B., Wang, J., Qu, K., Zhang, J., Li, L., … Chang, H. Y. (2014). M6A RNA Modification Controls Cell Fate Transition in Mammalian Embryonic Stem Cells. *Cell Stem Cell*, *15*(6), 707–719. https://doi.org/10.1016/j.stem.2014.09.019

Boccaletto, P., Machnicka, M. A., Purta, E., Piątkowski, P., Bagiński, B., Wirecki, T. K., … Bujnicki, J. M. (2018). MODOMICS: A database of RNA modification pathways. 2017 update. *Nucleic Acids Research*, *46*(Database issue), D303–D307. https://doi.org/10.1093/nar/gkx1030

Bröske, A.-M., Vockentanz, L., Kharazi, S., Huska, M. R., Mancini, E., Scheller, M., … Rosenbauer, F. (2009). DNA methylation protects hematopoietic stem cell multipotency from myeloerythroid restriction. *Nature Genetics*, *41*(11), 1207–1215. https://doi.org/10.1038/ng.463

Calado, D. P., Sasaki, Y., Godinho, S. A., Pellerin, A., Köchert, K., Sleckman, B. P., … Rajewsky, K. (2012). The cell-cycle regulator c-Myc is essential for the formation and

maintenance of germinal centers. *Nature Immunology*, *13*(11), 1092–1100. https://doi.org/10.1038/ni.2418

Carrelha, J., Meng, Y., Kettyle, L. M., Luis, T. C., Norfo, R., Alcolea, V., … Jacobsen, S. E. W. (2018). Hierarchically related lineage-restricted fates of multipotent haematopoietic stem cells. *Nature*, *554*(7690), 106–111. https://doi.org/10.1038/nature25455

Challen, G. A., Sun, D., Jeong, M., Luo, M., Jelinek, J., Berg, J. S., … Goodell, M. A. (2012). Dnmt3a is essential for hematopoietic stem cell differentiation. *Nature Genetics*, *44*(1), 23–31. https://doi.org/10.1038/ng.1009

Chan, C. K. F., Chen, C.-C., Luppen, C. A., Kim, J.-B., DeBoer, A. T., Wei, K., … Weissman, I. L. (2009). Endochondral ossification is required for haematopoietic stem-cell niche formation. *Nature*, *457*(7228), 490–494. https://doi.org/10.1038/nature07547

Chen, J. Y., Miyanishi, M., Wang, S. K., Yamazaki, S., Sinha, R., Kao, K. S., … Weissman, I. L. (2016). Hoxb5 marks long-term haematopoietic stem cells and reveals a homogenous perivascular niche. Nature, 530(7589), 223–227. https://doi.org/10.1038/nature16943

Chen, T., Hao, Y.-J., Zhang, Y., Li, M.-M., Wang, M., Han, W., … Zhou, Q. (2015). M6A RNA Methylation Is Regulated by MicroRNAs and Promotes Reprogramming to Pluripotency. *Cell Stem Cell*, *16*(3), 289–301. https://doi.org/10.1016/j.stem.2015.01.016

Cheng, Y., Luo, H., Izzo, F., Pickering, B. F., Nguyen, D., Myers, R., … Kharas, M. G. (2019). M6A RNA Methylation Maintains Hematopoietic Stem Cell Identity and Symmetric Commitment. *Cell Reports*, *28*(7), 1703-1716.e6. https://doi.org/10.1016/j.celrep.2019.07.032

Christensen, J. L., Wright, D. E., Wagers, A. J., & Weissman, I. L. (2004). Circulation and Chemotaxis of Fetal Hematopoietic Stem Cells. *PLOS Biology*, *2*(3), e75. https://doi.org/10.1371/journal.pbio.0020075

Clausen, B. E., Burkhardt, C., Reith, W., Renkawitz, R., & Förster, I. (1999). Conditional gene targeting in macrophages and granulocytes using LysMcre mice. *Transgenic Research*, *8*(4), 265–277. https://doi.org/10.1023/A:1008942828960

Decker, M., Leslie, J., Liu, Q., & Ding, L. (2018). Hepatic thrombopoietin is required for bone marrow hematopoietic stem cell maintenance. *Science*, *360*(6384), 106–110. https://doi.org/10.1126/science.aap8861

Desrosiers, R., Friderici, K., & Rottman, F. (1974). Identification of Methylated Nucleosides in Messenger RNA from Novikoff Hepatoma Cells. *Proceedings of the National Academy of Sciences of the United States of America*, *71*(10), 3971–3975.

Ding, L., & Morrison, S. J. (2013). Haematopoietic stem cells and early lymphoid progenitors occupy distinct bone marrow niches. *Nature*, *495*(7440), 231–235. https://doi.org/10.1038/nature11885

Ding, L., Saunders, T. L., Enikolopov, G., & Morrison, S. J. (2012). Endothelial and perivascular cells maintain haematopoietic stem cells. *Nature*, *481*(7382), 457–462. https://doi.org/10.1038/nature10783

Dominissini, D., Moshitch-Moshkovitz, S., Salmon-Divon, M., Amariglio, N., & Rechavi, G. (2013). Transcriptome-wide mapping of N6-methyladenosine by m6A-seq based on immunocapturing and massively parallel sequencing. *Nature Protocols*, *8*(1), 176–189. https://doi.org/10.1038/nprot.2012.148

Dominissini, D., Moshitch-Moshkovitz, S., Schwartz, S., Salmon-Divon, M., Ungar, L., Osenberg, S., … Rechavi, G. (2012). Topology of the human and mouse m6A RNA methylomes revealed by m6A-seq. *Nature*, *485*(7397), 201–206. https://doi.org/10.1038/nature11112

Eaves, C. J. (2015). Hematopoietic stem cells: Concepts, definitions, and the new reality. *Blood*, *125*(17), 2605–2613. https://doi.org/10.1182/blood-2014-12-570200

Ehninger, A., Boch, T., Uckelmann, H., Essers, M. A., Müdder, K., Sleckman, B. P., & Trumpp, A. (2014). Posttranscriptional regulation of c-Myc expression in adult murine HSCs during homeostasis and interferon-α-induced stress response. *Blood*, *123*(25), 3909–3913. https://doi.org/10.1182/blood-2013-10-531038

Farlik, M., Halbritter, F., Müller, F., Choudry, F. A., Ebert, P., Klughammer, J., … Bock, C. (2016). DNA Methylation Dynamics of Human Hematopoietic Stem Cell Differentiation. *Cell Stem Cell*, *19*(6), 808–822. https://doi.org/10.1016/j.stem.2016.10.019

Feng, C. G., Weksberg, D. C., Taylor, G. A., Sher, A., & Goodell, M. A. (2008). The p47 GTPase Lrg-47 (Irgm1) Links Host Defense and Hematopoietic Stem Cell Proliferation. *Cell Stem Cell*, *2*(1), 83–89. https://doi.org/10.1016/j.stem.2007.10.007

Ficara, F., Murphy, M. J., Lin, M., & Cleary, M. L. (2008). Pbx1 Regulates Self-Renewal of Long-Term Hematopoietic Stem Cells by Maintaining Their Quiescence. *Cell Stem Cell*, *2*(5), 484–496. https://doi.org/10.1016/j.stem.2008.03.004

Forsberg, E. C., Passegué, E., Prohaska, S. S., Wagers, A. J., Koeva, M., Stuart, J. M., & Weissman, I. L. (2010). Molecular Signatures of Quiescent, Mobilized and Leukemia-Initiating Hematopoietic Stem Cells. *PLOS ONE*, *5*(1), e8785. https://doi.org/10.1371/journal.pone.0008785

Fustin, J.-M., Doi, M., Yamaguchi, Y., Hida, H., Nishimura, S., Yoshida, M., … Okamura, H. (2013). RNA-Methylation-Dependent RNA Processing Controls the Speed of the Circadian Clock. *Cell*, *155*(4), 793–806. https://doi.org/10.1016/j.cell.2013.10.026

Garcia-Campos, M. A., Edelheit, S., Toth, U., Safra, M., Shachar, R., Viukov, S., … Schwartz, S. (2019). Deciphering the “m6A Code” via Antibody-Independent Quantitative Profiling. *Cell*. https://doi.org/10.1016/j.cell.2019.06.013

Geula, S., Moshitch-Moshkovitz, S., Dominissini, D., Mansour, A. A., Kol, N., Salmon-Divon, M., … Hanna, J. H. (2015). M6A mRNA methylation facilitates resolution of naïve pluripotency toward differentiation. *Science*, *347*(6225), 1002–1006. https://doi.org/10.1126/science.1261417

Greenbaum, A., Hsu, Y.-M. S., Day, R. B., Schuettpelz, L. G., Christopher, M. J., Borgerding, J. N., … Link, D. C. (2013). CXCL12 in early mesenchymal progenitors is required for

haematopoietic stem-cell maintenance. *Nature*, *495*(7440), 227–230. https://doi.org/10.1038/nature11926

He, S., Kim, I., Lim, M. S., & Morrison, S. J. (2011). Sox17 expression confers self-renewal potential and fetal stem cell characteristics upon adult hematopoietic progenitors. *Genes & Development*, *25*(15), 1613–1627. https://doi.org/10.1101/gad.2052911

Hock, H., Hamblen, M. J., Rooke, H. M., Schindler, J. W., Saleque, S., Fujiwara, Y., & Orkin, S. H. (2004). Gfi-1 restricts proliferation and preserves functional integrity of haematopoietic stem cells. *Nature*, *431*(7011), 1002–1007. https://doi.org/10.1038/nature02994

Hsu, P. J., Zhu, Y., Ma, H., Guo, Y., Shi, X., Liu, Y., … He, C. (2017). Ythdc2 is an N 6 -methyladenosine binding protein that regulates mammalian spermatogenesis. *Cell Research*, *27*(9), 1115–1127. https://doi.org/10.1038/cr.2017.99

Huang, C.-Y., Bredemeyer, A. L., Walker, L. M., Bassing, C. H., & Sleckman, B. P. (2008). Dynamic regulation of c-Myc proto-oncogene expression during lymphocyte development revealed by a GFP-c-Myc knock-in mouse. *European Journal of Immunology*, *38*(2), 342–349. https://doi.org/10.1002/eji.200737972

Huang, H., Weng, H., Sun, W., Qin, X., Shi, H., Wu, H., … Chen, J. (2018). Recognition of RNA N 6 -methyladenosine by IGF2BP proteins enhances mRNA stability and translation. *Nature Cell Biology*, *20*(3), 285–295. https://doi.org/10.1038/s41556-018-0045-z

Ivanova, N. B., Dimos, J. T., Schaniel, C., Hackney, J. A., Moore, K. A., & Lemischka, I. R. (2002). A Stem Cell Molecular Signature. *Science*, *298*(5593), 601–604. https://doi.org/10.1126/science.1073823

Iwama, A., Oguro, H., Negishi, M., Kato, Y., Morita, Y., Tsukui, H., … Nakauchi, H. (2004). Enhanced Self-Renewal of Hematopoietic Stem Cells Mediated by the Polycomb Gene Product Bmi-1. *Immunity*, *21*(6), 843–851. https://doi.org/10.1016/j.immuni.2004.11.004

Jaffrey, S. R., & Kharas, M. G. (2017). Emerging links between m6A and misregulated mRNA methylation in cancer. *Genome Medicine*, *9*. https://doi.org/10.1186/s13073-016-0395-8

Ji, H., Ehrlich, L. I. R., Seita, J., Murakami, P., Doi, A., Lindau, P., … Feinberg, A. P. (2010). Comprehensive methylome map of lineage commitment from haematopoietic progenitors. *Nature*, *467*(7313), 338–342. https://doi.org/10.1038/nature09367

Kawanami, A., Matsushita, T., Chan, Y. Y., & Murakami, S. (2009). Mice expressing GFP and CreER in osteochondro progenitor cells in the periosteum. *Biochemical and Biophysical Research Communications*, *386*(3), 477–482. https://doi.org/10.1016/j.bbrc.2009.06.059

Kiel, M. J., Yilmaz, Ö. H., Iwashita, T., Yilmaz, O. H., Terhorst, C., & Morrison, S. J. (2005). SLAM Family Receptors Distinguish Hematopoietic Stem and Progenitor Cells and Reveal Endothelial Niches for Stem Cells. Cell, 121(7), 1109–1121. https://doi.org/10.1016/j.cell.2005.05.026

Kuhn, R., Schwenk, F., Aguet, M., & Rajewsky, K. (1995). Inducible gene targeting in mice. *Science*, *269*(5229), 1427–1429. https://doi.org/10.1126/science.7660125

Laurenti, E., & Göttgens, B. (2018). From haematopoietic stem cells to complex differentiation landscapes. *Nature*, *553*(7689), 418–426. https://doi.org/10.1038/nature25022

Lee, H., Bao, S., Qian, Y., Geula, S., Leslie, J., Zhang, C., … Ding, L. (2019). Stage-specific requirement for Mettl3-dependent m6A mRNA methylation during haematopoietic stem cell differentiation. *Nature Cell Biology*, *21*(6), 700–709. https://doi.org/10.1038/s41556-019-0318-1

Lee, Y., Decker, M., Lee, H., & Ding, L. (2017). Extrinsic regulation of hematopoietic stem cells in development, homeostasis and diseases. *Wiley Interdisciplinary Reviews: Developmental Biology*, *6*(5), e279. https://doi.org/10.1002/wdev.279

Li, H.-B., Tong, J., Zhu, S., Batista, P. J., Duffy, E. E., Zhao, J., … Flavell, R. A. (2017). M6A mRNA methylation controls T cell homeostasis by targeting the IL-7/STAT5/SOCS pathways. *Nature*, *548*(7667), 338–342.

Li, Z., Cai, X., Cai, C.-L., Wang, J., Zhang, W., Petersen, B. E., … Xu, M. (2011). Deletion of Tet2 in mice leads to dysregulated hematopoietic stem cells and subsequent development of myeloid malignancies. *Blood*, *118*(17), 4509–4518. https://doi.org/10.1182/blood-2010-12-325241

Liberzon, A., Subramanian, A., Pinchback, R., Thorvaldsdóttir, H., Tamayo, P., & Mesirov, J. P. (2011). Molecular signatures database (MSigDB) 3.0. *Bioinformatics*, *27*(12), 1739–1740. https://doi.org/10.1093/bioinformatics/btr260

Lin, S., Choe, J., Du, P., Triboulet, R., & Gregory, R. I. (2016). The m6A Methyltransferase METTL3 Promotes Translation in Human Cancer Cells. *Molecular Cell*, *62*(3), 335–345. https://doi.org/10.1016/j.molcel.2016.03.021

Linder, B., Grozhik, A. V., Olarerin-George, A. O., Meydan, C., Mason, C. E., & Jaffrey, S. R. (2015). Single-nucleotide-resolution mapping of m6A and m6Am throughout the transcriptome. *Nature Methods*, *12*(8), 767–772. https://doi.org/10.1038/nmeth.3453

Liu, J., Yue, Y., Han, D., Wang, X., Fu, Y., Zhang, L., … He, C. (2014). A METTL3-METTL14 complex mediates mammalian nuclear RNA N6-adenosine methylation. *Nature Chemical Biology*, *10*(2), 93–95. https://doi.org/10.1038/nchembio.1432

Logan, M., Martin, J. F., Nagy, A., Lobe, C., Olson, E. N., & Tabin, C. J. (2002). Expression of Cre recombinase in the developing mouse limb bud driven by a Prxl enhancer. *Genesis*, *33*(2), 77–80. https://doi.org/10.1002/gene.10092

Luca, C. de, Kowalski, T. J., Zhang, Y., Elmquist, J. K., Lee, C., Kilimann, M. W., … Chua, S. C. (2005). Complete rescue of obesity, diabetes, and infertility in *db/db* mice by neuron-specific LEPR-B transgenes. *The Journal of Clinical Investigation*, *115*(12), 3484–3493. https://doi.org/10.1172/JCI24059

Lv, J., Zhang, Y., Gao, S., Zhang, C., Chen, Y., Li, W., … Liu, F. (2018). Endothelial-specific m^6A modulates mouse hematopoietic stem and progenitor cell development via Notch signaling. *Cell Research*, *28*(2), 249–252. https://doi.org/10.1038/cr.2017.143

Ma, H., Wang, X., Cai, J., Dai, Q., Natchiar, S. K., Lv, R., … He, C. (2019). N 6 - Methyladenosine methyltransferase ZCCHC4 mediates ribosomal RNA methylation. *Nature Chemical Biology*, *15*(1), 88–94. https://doi.org/10.1038/s41589-018-0184-3

Ma, Q., Jones, D., Borghesani, P. R., Segal, R. A., Nagasawa, T., Kishimoto, T., … Springer, T. A. (1998). Impaired B-lymphopoiesis, myelopoiesis, and derailed cerebellar neuron migration in CXCR4- and SDF-1-deficient mice. *Proceedings of the National Academy of Sciences*, *95*(16), 9448–9453. https://doi.org/10.1073/pnas.95.16.9448

Madisen, L., Zwingman, T. A., Sunkin, S. M., Oh, S. W., Zariwala, H. A., Gu, H., … Zeng, H. (2010). A robust and high-throughput Cre reporting and characterization system for the whole mouse brain. *Nature Neuroscience*, *13*(1), 133–140. https://doi.org/10.1038/nn.2467

Matsubara, A., Iwama, A., Yamazaki, S., Furuta, C., Hirasawa, R., Morita, Y., … Nakauchi, H. (2005). Endomucin, a CD34-like sialomucin, marks hematopoietic stem cells throughout development. *The Journal of Experimental Medicine*, *202*(11), 1483–1492. https://doi.org/10.1084/jem.20051325

Mauer, J., Luo, X., Blanjoie, A., Jiao, X., Grozhik, A. V., Patil, D. P., … Jaffrey, S. R. (2017). Reversible methylation of m6Am in the 5′ cap controls mRNA stability. *Nature*, *541*(7637), 371–375. https://doi.org/10.1038/nature21022

Meyer, K. D. (2019). DART-seq: An antibody-free method for global m 6 A detection. *Nature Methods*, 1–6. https://doi.org/10.1038/s41592-019-0570-0

Meyer, K. D., & Jaffrey, S. R. (2014). The dynamic epitranscriptome: N6-methyladenosine and gene expression control. *Nature Reviews Molecular Cell Biology*, *15*(5), 313–326. https://doi.org/10.1038/nrm3785

Meyer, K. D., & Jaffrey, S. R. (2017). Rethinking m6A Readers, Writers, and Erasers. *Annual Review of Cell and Developmental Biology*, *33*(1), 319–342. https://doi.org/10.1146/annurev-cellbio-100616-060758

Meyer, K. D., Saletore, Y., Zumbo, P., Elemento, O., Mason, C. E., & Jaffrey, S. R. (2012). Comprehensive Analysis of mRNA Methylation Reveals Enrichment in 3′ UTRs and near Stop Codons. *Cell*, *149*(7), 1635–1646. https://doi.org/10.1016/j.cell.2012.05.003

Miyamoto, K., Araki, K. Y., Naka, K., Arai, F., Takubo, K., Yamazaki, S., … Hirao, A. (2007). Foxo3a Is Essential for Maintenance of the Hematopoietic Stem Cell Pool. *Cell Stem Cell*, *1*(1), 101–112. https://doi.org/10.1016/j.stem.2007.02.001

Moran-Crusio, K., Reavie, L., Shih, A., Abdel-Wahab, O., Ndiaye-Lobry, D., Lobry, C., … Levine, R. L. (2011). Tet2 Loss Leads to Increased Hematopoietic Stem Cell Self-Renewal and Myeloid Transformation. *Cancer Cell*, *20*(1), 11–24. https://doi.org/10.1016/j.ccr.2011.06.001

Morikawa, S., Mabuchi, Y., Kubota, Y., Nagai, Y., Niibe, K., Hiratsu, E., … Matsuzaki, Y. (2009). Prospective identification, isolation, and systemic transplantation of multipotent mesenchymal stem cells in murine bone marrow. *Journal of Experimental Medicine*, *206*(11), 2483–2496. https://doi.org/10.1084/jem.20091046

Morrison, S. J., Hemmati, H. D., Wandycz, A. M., & Weissman, I. L. (1995). The purification and characterization of fetal liver hematopoietic stem cells. *Proceedings of the National Academy of Sciences*, *92*(22), 10302–10306. https://doi.org/10.1073/pnas.92.22.10302

Morrison, Sean J., & Scadden, D. T. (2014). The bone marrow niche for haematopoietic stem cells. *Nature*, *505*(7483), 327–334. https://doi.org/10.1038/nature12984

Nagasawa, T., Hirota, S., Tachibana, K., Takakura, N., Nishikawa, S., Kitamura, Y., … Kishimoto, T. (1996). Defects of B-cell lymphopoiesis and bone-marrow myelopoiesis in mice lacking the CXC chemokine PBSF/SDF-1. *Nature*, *382*(6592), 635–638. https://doi.org/10.1038/382635a0

Nakada, D., Oguro, H., Levi, B. P., Ryan, N., Kitano, A., Saitoh, Y., … Morrison, S. J. (2014). Oestrogen increases haematopoietic stem-cell self-renewal in females and during pregnancy. *Nature*, *505*(7484), 555–558. https://doi.org/10.1038/nature12932

Niu, C., Zhang, J., Breslin, P., Onciu, M., Ma, Z., & Morris, S. W. (2009). C-Myc is a target of RNA-binding motif protein 15 in the regulation of adult hematopoietic stem cell and megakaryocyte development. *Blood*, *114*(10), 2087–2096. https://doi.org/10.1182/blood-2009-01-197921

Nombela-Arrieta, C., Pivarnik, G., Winkel, B., Canty, K. J., Harley, B., Mahoney, J. E., … Silberstein, L. E. (2013). Quantitative imaging of haematopoietic stem and progenitor cell localization and hypoxic status in the bone marrow microenvironment. *Nature Cell Biology*, *15*(5), 533–543. https://doi.org/10.1038/ncb2730

Omatsu, Y., Seike, M., Sugiyama, T., Kume, T., & Nagasawa, T. (2014). Foxc1 is a critical regulator of haematopoietic stem/progenitor cell niche formation. *Nature*, *508*(7497), 536–540. https://doi.org/10.1038/nature13071

Osawa, M., Hanada, K., Hamada, H., & Nakauchi, H. (1996). Long-Term Lymphohematopoietic Reconstitution by a Single CD34-Low/Negative Hematopoietic Stem Cell. *Science*, *273*(5272), 242–245. https://doi.org/10.1126/science.273.5272.242

Passegué, E., Jochum, W., Schorpp-Kistner, M., Möhle-Steinlein, U., & Wagner, E. F. (2001). Chronic Myeloid Leukemia with Increased Granulocyte Progenitors in Mice Lacking JunB Expression in the Myeloid Lineage. *Cell*, *104*(1), 21–32. https://doi.org/10.1016/S0092-8674(01)00188-X

Patil, D. P., Chen, C.-K., Pickering, B. F., Chow, A., Jackson, C., Guttman, M., & Jaffrey, S. R. (2016). M6A RNA methylation promotes XIST-mediated transcriptional repression. *Nature*, *537*(7620), 369–373. https://doi.org/10.1038/nature19342

Pendleton, K. E., Chen, B., Liu, K., Hunter, O. V., Xie, Y., Tu, B. P., & Conrad, N. K. (2017). The U6 snRNA m6A Methyltransferase METTL16 Regulates SAM Synthetase Intron Retention. *Cell*, *169*(5), 824-835.e14. https://doi.org/10.1016/j.cell.2017.05.003

Perry, R. P., & Kelley, D. E. (1974). Existence of methylated messenger RNA in mouse L cells. *Cell*, *1*(1), 37–42. https://doi.org/10.1016/0092-8674(74)90153-6

Picelli, S., Faridani, O. R., Björklund, Å. K., Winberg, G., Sagasser, S., & Sandberg, R. (2014). Full-length RNA-seq from single cells using Smart-seq2. *Nature Protocols*, *9*(1), 171–181. https://doi.org/10.1038/nprot.2014.006

Ping, X.-L., Sun, B.-F., Wang, L., Xiao, W., Yang, X., Wang, W.-J., … Yang, Y.-G. (2014). Mammalian WTAP is a regulatory subunit of the RNA N6-methyladenosine methyltransferase. *Cell Research*, *24*(2), 177–189. https://doi.org/10.1038/cr.2014.3

Raffel, G. D., Mercher, T., Shigematsu, H., Williams, I. R., Cullen, D. E., Akashi, K., … Gilliland, D. G. (2007). Ott1(Rbm15) has pleiotropic roles in hematopoietic development. *Proceedings of the National Academy of Sciences*, *104*(14), 6001–6006. https://doi.org/10.1073/pnas.0609041104

Reavie, L., Gatta, G. D., Crusio, K., Aranda-Orgilles, B., Buckley, S. M., Thompson, B., … Aifantis, I. (2010). Regulation of hematopoietic stem cell differentiation by a single ubiquitin ligase–substrate complex. *Nature Immunology*, *11*(3), ni.1839. https://doi.org/10.1038/ni.1839

Rebel, V. I., Miller, C. L., Eaves, C. J., & Lansdorp, P. M. (1996). The repopulation potential of fetal liver hematopoietic stem cells in mice exceeds that of their liver adult bone marrow counterparts. *Blood*, *87*(8), 3500–3507.

Robinson, M. D., McCarthy, D. J., & Smyth, G. K. (2010). edgeR: A Bioconductor package for differential expression analysis of digital gene expression data. *Bioinformatics*, *26*(1), 139–140. https://doi.org/10.1093/bioinformatics/btp616

Rodríguez, C. I., Buchholz, F., Galloway, J., Sequerra, R., Kasper, J., Ayala, R., … Dymecki, S. M. (2000). High-efficiency deleter mice show that FLPe is an alternative to Cre- loxP. *Nature Genetics*, *25*(2), 139–140. https://doi.org/10.1038/75973

Rodriguez-Fraticelli, A. E., Wolock, S. L., Weinreb, C. S., Panero, R., Patel, S. H., Jankovic, M., … Camargo, F. D. (2018). Clonal analysis of lineage fate in native haematopoiesis. *Nature*, *553*(7687), 212–216. https://doi.org/10.1038/nature25168

Rossi, L., Lin, K. K., Boles, N. C., Yang, L., King, K. Y., Jeong, M., … Goodell, M. A. (2012). Less Is More: Unveiling the Functional Core of Hematopoietic Stem Cells through Knockout Mice. *Cell Stem Cell*, *11*(3), 302–317. https://doi.org/10.1016/j.stem.2012.08.006

Sanchez-Gurmaches, J., Hsiao, W.-Y., & Guertin, D. A. (2015). Highly Selective In Vivo Labeling of Subcutaneous White Adipocyte Precursors with Prx1-Cre. *Stem Cell Reports*, *4*(4), 541–550. https://doi.org/10.1016/j.stemcr.2015.02.008

Schwartz, S., Mumbach, M. R., Jovanovic, M., Wang, T., Maciag, K., Bushkin, G. G., … Regev, A. (2014). Perturbation of m6A Writers Reveals Two Distinct Classes of mRNA Methylation at Internal and 5′ Sites. *Cell Reports*, *8*(1), 284–296. https://doi.org/10.1016/j.celrep.2014.05.048

Seike, M., Omatsu, Y., Watanabe, H., Kondoh, G., & Nagasawa, T. (2018). Stem cell niche-specific Ebf3 maintains the bone marrow cavity. *Genes & Development*, *32*(5–6), 359–372. https://doi.org/10.1101/gad.311068.117

Shenghui, H., Nakada, D., & Morrison, S. J. (2009). Mechanisms of Stem Cell Self-Renewal. *Annual Review of Cell and Developmental Biology*, *25*(1), 377–406. https://doi.org/10.1146/annurev.cellbio.042308.113248

Shi, H., Wei, J., & He, C. (2019). Where, When, and How: Context-Dependent Functions of RNA Methylation Writers, Readers, and Erasers. *Molecular Cell*, *74*(4), 640–650. https://doi.org/10.1016/j.molcel.2019.04.025

Sibbritt, T., Patel, H. R., & Preiss, T. (2013). Mapping and significance of the mRNA methylome. *Wiley Interdisciplinary Reviews: RNA*, *4*(4), 397–422. https://doi.org/10.1002/wrna.1166

Śledź, P., & Jinek, M. (2016). Structural insights into the molecular mechanism of the m6A writer complex. *ELife*, *5*, e18434. https://doi.org/10.7554/eLife.18434

Subramanian, A., Tamayo, P., Mootha, V. K., Mukherjee, S., Ebert, B. L., Gillette, M. A., … Mesirov, J. P. (2005). Gene set enrichment analysis: A knowledge-based approach for interpreting genome-wide expression profiles. *Proceedings of the National Academy of Sciences of the United States of America*, *102*(43), 15545–15550. https://doi.org/10.1073/pnas.0506580102

Sugiyama, T., Kohara, H., Noda, M., & Nagasawa, T. (2006). Maintenance of the Hematopoietic Stem Cell Pool by CXCL12-CXCR4 Chemokine Signaling in Bone Marrow Stromal Cell Niches. *Immunity*, *25*(6), 977–988. https://doi.org/10.1016/j.immuni.2006.10.016

Tokoyoda, K., Egawa, T., Sugiyama, T., Choi, B.-I., & Nagasawa, T. (2004). Cellular Niches Controlling B Lymphocyte Behavior within Bone Marrow during Development. *Immunity*, *20*(6), 707–718. https://doi.org/10.1016/j.immuni.2004.05.001

Vu, L. P., Pickering, B. F., Cheng, Y., Zaccara, S., Nguyen, D., Minuesa, G., … Kharas, M. G. (2017). The N6-methyladenosine (m6A)-forming enzyme METTL3 controls myeloid differentiation of normal hematopoietic and leukemia cells. *Nature Medicine*, *advance online publication*. https://doi.org/10.1038/nm.4416

Wang, Xiang, Feng, J., Xue, Y., Guan, Z., Zhang, D., Liu, Z., … Yin, P. (2016). Structural basis of N^6-adenosine methylation by the METTL3–METTL14 complex. *Nature*, *534*(7608), 575–578. https://doi.org/10.1038/nature18298

Wang, Xiao, Lu, Z., Gomez, A., Hon, G. C., Yue, Y., Han, D., … He, C. (2014). N^6-methyladenosine-dependent regulation of messenger RNA stability. *Nature*, *505*(7481), 117–120. https://doi.org/10.1038/nature12730

Wang, Xiao, Zhao, B. S., Roundtree, I. A., Lu, Z., Han, D., Ma, H., … He, C. (2015). N6-methyladenosine Modulates Messenger RNA Translation Efficiency. *Cell*, *161*(6), 1388–1399. https://doi.org/10.1016/j.cell.2015.05.014

Wang, Y., Li, Y., Yue, M., Wang, J., Kumar, S., Wechsler-Reya, R. J., … Zhao, J. C. (2018). N 6 -methyladenosine RNA modification regulates embryonic neural stem cell self-renewal through histone modifications. *Nature Neuroscience*, *21*(2), 195–206. https://doi.org/10.1038/s41593-017-0057-1

Weissman, I. L., & Shizuru, J. A. (2008). The origins of the identification and isolation of hematopoietic stem cells, and their capability to induce donor-specific transplantation tolerance and treat autoimmune diseases. *Blood*, *112*(9), 3543–3553. https://doi.org/10.1182/blood-2008-08-078220

Weng, H., Huang, H., Wu, H., Qin, X., Zhao, B. S., Dong, L., … Chen, J. (2017). METTL14 Inhibits Hematopoietic Stem/Progenitor Differentiation and Promotes Leukemogenesis via mRNA m6A Modification. *Cell Stem Cell*, *0*(0). https://doi.org/10.1016/j.stem.2017.11.016

Wilson, A., Murphy, M. J., Oskarsson, T., Kaloulis, K., Bettess, M. D., Oser, G. M., … Trumpp, A. (2004). C-Myc controls the balance between hematopoietic stem cell self-renewal and differentiation. *Genes & Development*, *18*(22), 2747–2763. https://doi.org/10.1101/gad.313104

Wu, J., Anczuków, O., Krainer, A. R., Zhang, M. Q., & Zhang, C. (2013). OLego: Fast and sensitive mapping of spliced mRNA-Seq reads using small seeds. *Nucleic Acids Research*, *41*(10), 5149–5163. https://doi.org/10.1093/nar/gkt216

Wu, Y., Xie, L., Wang, M., Xiong, Q., Guo, Y., Liang, Y., … Yuan, Q. (2018). Mettl3-mediated m 6 A RNA methylation regulates the fate of bone marrow mesenchymal stem cells and osteoporosis. *Nature Communications*, *9*(1), 4772. https://doi.org/10.1038/s41467-018-06898-4

Xiang, Y., Laurent, B., Hsu, C.-H., Nachtergaele, S., Lu, Z., Sheng, W., … Shi, Y. (2017). RNA m6A methylation regulates the ultraviolet-induced DNA damage response. *Nature*, *advance online publication*. https://doi.org/10.1038/nature21671

Xiao, S., Cao, S., Huang, Q., Xia, L., Deng, M., Yang, M., … Xia, L. (2019). The RNA N 6 - methyladenosine modification landscape of human fetal tissues. *Nature Cell Biology*, *21*(5), 651–661. https://doi.org/10.1038/s41556-019-0315-4

Yan, Q., Weyn-Vanhentenryck, S. M., Wu, J., Sloan, S. A., Zhang, Y., Chen, K., … Zhang, C. (2015). Systematic discovery of regulated and conserved alternative exons in the mammalian brain reveals NMD modulating chromatin regulators. *Proceedings of the National Academy of Sciences*, *112*(11), 3445–3450. https://doi.org/10.1073/pnas.1502849112

Yao, Q. J., Sang, L., Lin, M., Yin, X., Dong, W., Gong, Y., & Zhou, B. O. (2018). Mettl3–Mettl14 methyltransferase complex regulates the quiescence of adult hematopoietic stem cells. *Cell Research*, 1. https://doi.org/10.1038/s41422-018-0062-2

Yoon, K.-J., Ringeling, F. R., Vissers, C., Jacob, F., Pokrass, M., Jimenez-Cyrus, D., … Song, H. (2017). Temporal Control of Mammalian Cortical Neurogenesis by m6A Methylation. *Cell*, *171*(4), 877-889.e17. https://doi.org/10.1016/j.cell.2017.09.003

Yue, Y., Liu, J., & He, C. (2015). RNA N6-methyladenosine methylation in post-transcriptional gene expression regulation. *Genes & Development*, *29*(13), 1343–1355. https://doi.org/10.1101/gad.262766.115

Zeller, K. I., Jegga, A. G., Aronow, B. J., O'Donnell, K. A., & Dang, C. V. (2003). An integrated database of genes responsive to the Myc oncogenic transcription factor: Identification of

direct genomic targets. *Genome Biology*, *4*(10), R69. https://doi.org/10.1186/gb-2003-4-10-r69

Zhang, C., Chen, Y., Sun, B., Wang, L., Yang, Y., Ma, D., … Liu, F. (2017). M^6A modulates haematopoietic stem and progenitor cell specification. *Nature*, *549*(7671), 273–276. https://doi.org/10.1038/nature23883

Zhou, B. O., Ding, L., & Morrison, S. J. (2015). Hematopoietic stem and progenitor cells regulate the regeneration of their niche by secreting Angiopoietin-1. *ELife*, *4*, e05521. https://doi.org/10.7554/eLife.05521

Zhou, B. O., Yue, R., Murphy, M. M., Peyer, J. G., & Morrison, S. J. (2014). Leptin-Receptor-Expressing Mesenchymal Stromal Cells Represent the Main Source of Bone Formed by Adult Bone Marrow. *Cell Stem Cell*, *15*(2), 154–168. https://doi.org/10.1016/j.stem.2014.06.008

Zou, P., Yoshihara, H., Hosokawa, K., Tai, I., Shinmyozu, K., Tsukahara, F., … Suda, T. (2011). P57Kip2 and p27Kip1 Cooperate to Maintain Hematopoietic Stem Cell Quiescence through Interactions with Hsc70. *Cell Stem Cell*, *9*(3), 247–261. https://doi.org/10.1016/j.stem.2011.07.003

APPENDIX A: EXPERIMENTAL METHODS

Mice

Mx1-cre (Kuhn et al., 1995), *Lysm-cre* (Clausen et al., 1999), *Myc-GFP* (Huang et al., 2008), and *Rosa-loxpMyc* (Calado et al., 2012) mice were obtained from the Jackson Laboratory and maintained on C57BL/B6 background. *Rosa26-creER* mice (de Luca et al., 2005) were generated and provided by Dr. T. Ludwig at Columbia University. *Prx1-cre* (Logan et al., 2002) and *CAG-loxP-stop-loxP-ZsG* (Madisen et al., 2010) were obtained from the Jackson Laboratory and maintained on C57BL/B6 background. Other mice used in this study included $Cxcl12^{DsRed}$ (Ding and Morrison, 2013). $Mettl3^{fl}$ mice were generated by electroporation of a targeting vector (obtained from the Knockout Mouse Project Repository, KOMP) into V6.5 embryonic stem (ES) cells. Correctly targeted ES cell clone, validated by PCR and southern blot analysis, was identified and injected into BDF1 blastocysts and chimeric mice were generated. Chimeric mice were bred with C57BL/6 mice to obtain germline transmission. The resulting mice were crossed with Flpe mice (Rodriguez et al., 2000) to remove the Neo cassette. These mice were backcrossed at least 6 times onto C57BL/6 background before analysis. To induce Cre expression in *Mx1-cre;* $Mettl3^{fl/fl}$ or *Mx1-cre;* $Mettl3^{fl/fl}$; $Rosa\text{-}loxPMyc^{fl/fl}$ mice, 6-8wk old animals were intraperitoneally injected with 10ug polyinosinic-polycytidylic acid (pIpC, GE or InvivoGen) in PBS every other day for 5 injections. Mice were analyzed either 10-14 days, 2-3 months, or 4 months after the final injection, as indicated in each experiment. To induce Cre expression in *Rosa26-CreERT2;* $Mettl3^{fl/fl}$ mice, recipients were given 1ug tamoxifen in 50uL corn oil by gavage every other day for 5 doses. All mice were housed in specific pathogen-free, Association for the Assessment and Accreditation of Laboratory Animal Care (AAALAC)-approved facilities at the Columbia University Medical Center. All protocols were approved by the Institute Animal Care and Use Committee of Columbia University. The study is compliant with all relevant ethical regulations regarding animal research.

Genotyping PCR Primers

The following primers were used for genotyping:

Mettl3^{fl} allele: GTTGATGAAATTATCAGTACAATGGTTCTGA;

GTAAAGAACAACTCTGGTTATCGTCATCG.

Mettl3 deletion allele: GGATGATTTCTTCTACCATTACCTCTACCC;

CAGAAAGCCCATCCTCAGCGTG.

5FU administration

For 5-fluorouracil (5-FU; Sigma-Aldrich) treatment, *Mx1-cre; Mettl3*$^{fl/fl}$ and littermate control mice were treated with pIpC as previously described. 10 days after the last pIpC injection, mice were injected intraperitoneally with 150 mg/kg 5-FU weekly until death or experimental conclusion.

Complete Blood Counts

Peripheral blood was collected by tail vein or cardiac puncture into EDTA-coated capillary tubes. Blood samples were analyzed by Genesis (Oxford Science Inc).

Flow cytometry

Bone marrow cells were isolated by flushing the long bones or by crushing the long bones, pelvis, and vertebrae with mortar and pestle in Ca^{2+} free and Mg^{2+} free HBSS with 2% heat-inactivated bovine serum. Splenic cells were obtained by crushing the spleens between two glass slides. The splenic and bone marrow cells were passed through a 25G needle several times and filtered through 70μm nylon mesh. The following antibodies were used to perform HSC staining: lineage markers (anti-CD2 (RM2-5), anti-CD3 (17A2), anti-CD5 (53-7.3), anti-CD8a (53-6.7), anti-B220 (6B2), anti-Gr-1 (8C5), anti-Ter119(TER-119), anti-Sca-1 (E13-161.7), anti-c-kit (2B8), anti-CD48 (HM48-1), anti-CD150 (TC15-12F12.2). Additionally, the following antibodies were used to perform hematopoietic progenitor staining as previously described

(Ding and Morrison, 2013): lineage markers (anti-CD2 (RM2-5), anti-CD3 (17A2), anti-CD5 (53-7.3), anti-CD8a (53-6.7), anti-B220 (6B2), anti-Gr-1 (8C5), anti-Ter119(TER-119), anti-Sca-1 (E13-161.7), anti-c-kit (2B8), anti-CD34 (RAM34), anti-FLT3 (A2F10), anti-CD16/32 (93), anti-IL7Rα (A7R34).

For flow cytometric analysis of bone marrow stromal cells, bone marrow was flushed or crushed from the hindlimbs using HBSS with 2% bovine serum. Whole bone marrow was then digested with Collagenase IV (200U/ml) and DNase I (200U/ml) at 37^{o}C for 20 minutes. Samples were then stained with antibodies and analyzed by flow cytometry. Anti-CD140a (APA5), anti-CD45 (30F-11) and anti-TER119 (TER-119) antibodies were used to isolate perivascular stromal cells. For intracellular staining, cells were fixed and permeabilized using the eBioscience Transcription Factor Staining kit per manufacturer's instructions. Cells were then stained with antibodies anti-CXCL12-FITC (R&D, ICF350F) and mouse IgG1k-FITC (MOPC-21) in eBioscience permeabilization buffer and analyzed by flow cytometry.

Cell cycle, DNA damage, cell death, reactive oxygen species analysis.

For BrdU incorporation analysis, mice intraperitoneally injected with 0.1mg/kg BrdU and maintained on 0.5mg/ml BrdU water for 5 days before the analysis. The frequency of BrdU^{+} cells was determined by flow cytometry using an APC BrdU Flow Kit (BD Biosciences) per manufacturer's instructions. To measure γH2AX levels, cells were stained for SLAM markers, fixed and permeabilized (BD Biosciences BrdU Flow Kit) and stained with anti-γH2AX (Biolegend, clone 2F3), followed by flow cytometry. Annexin V staining was performed using Annexin V Apoptosis Detection Kit APC (eBioscience) per manufacturer's instructions. ROS levels were measured by DCFDA staining (29-79-dichlorofluorescein diacetate, ThermoFisher Scientific). After antibody staining, cells were incubated with 10uM DCFDA for 15 minutes at 37^{o}C, followed by flow-cytometry.

Long-term competitive reconstitution assay

Adult recipient mice were lethally irradiated by a Cesium 137 Irradiator (JL Shepherd and Associates) at 300 rad/min with two doses of 540 rad (total 1080 rad) delivered at least two hours apart. Cells were transplanted by retro-orbital venous sinus injection of anesthetized mice. Mice were transplanted with either 5 x 10^5 donor and 5 x 10^5 competitor bone marrow cells or 50 sorted donor HSCs and 3 x 10^5 competitor bone marrow cells, as indicated. Donor mice were either untreated or sacrificed10 days after pIpC treatment, as indicated. For limiting dilution assays, mice were transplanted with 3 x 10^5 competitor bone marrow cells and either 10,000, 30,000, or 80,000 bone marrow cells as indicated. Recipient mice were temporarily maintained on antibiotic water (Baytril 0.17g/L) for 14 days after transplantation. Peripheral blood from recipient mice was analyzed by flow cytometry at indicated timepoints for at least 16 weeks after transplantation to assess the level of donor-derived blood lineages (donor chimerism), including myeloid, B, and T cells. For post-transplantation Cre-induction experiments, recipients' peripheral blood was analyzed over at least two time points at least 6-8 weeks after transplantation to ensure stable engraftment before treatment with pIpC (10ug per mouse per dose for 5 doses) or tamoxifen (1ug per mouse per dose for 5 doses). For limiting dilution assays, recipient mice were considered reconstituted if they contained donor myeloid, B and T cells in their peripheral blood cell above background levels at both 8 weeks and 16 weeks post-transplantation. Blood was subjected to ammonium chloride potassium red cell lysis before antibody staining. Antibodies including anti-CD45.2 (104), anti-CD45.1 (A20), anti-CD3 (17A2), anti-B220 (6B2), anti-Gr1 (8C5), and anti-Mac1 (M1/70) were used to stain cells.

Colony-forming unit assay

10,000 bone marrow cells, 100,000 spleen cells, 200 LSK cells, single MPP, single HSCs or other hematopoietic progenitors were plated in methylcellulose culture medium (3434,

STEMCELL Technologies) and incubated at 37°C. Colonies were counted 9-12 days after plating on an Olympus CKX41 microscope (Olympus) and scored as derived from erythroid progenitor cells (BFU-E and CFU-E), granulocyte-macrophage progenitor cells (CFU-GM, CFU-G and CFU-M), megakaryocyte progenitor cells (CFU-MK) and multipotent granulocyte, erythroid, macrophage and megakaryocyte progenitor cells (CFU-GEMM).

Viral transduction and colony-forming assay

Retroviruses were produced by transfecting 293T cells with pMIG-Myc (Addgene plasmid #18119) or pMIG vectors along with pCL-Eco and collecting media after 48-72hrs. Virus titers were determined by transduction of NIH-3T3 fibroblasts with serial dilutions of viral media. 200 HSCs were sorted from *Mx1-cre; Mettl3*$^{fl/fl}$ mice 10 days after pIpC treatment and plated into DMEM with 15% heat-inactivated fetal bovine serum, 100ng/ml SCF, 10ng/ml IL-3, 10ng/ml IL-6 and 50μM b-mercaptoethanol. Cells were transduced with >120 MOI retrovirus particles in the presence of 8ug/mL polybrene and spun at 1400g for 1.5hrs at 20°C. Cells were then collected and plated in 1.5mL of methylcellulose culture medium and incubated at 37°C for 9-12 days. Colonies were collected in bulk and resuspended in $Ca2^{+}$- and $Mg2^{+}$-free HBSS with 2% heat-inactivated bovine serum before staining with antibodies. Cells were then analyzed by flow cytometry.

Macrophage Culture and phagocytosis assay

One million whole bone marrow cells were plated in 12-well plates and cultured at 37°C in Dulbecco's Modified Eagle Medium (DMEM; Thermo Fisher) supplemented with 10% Fetal Bovine Serum (LifeTech) and 30% L929 supernatant. After 6 days, non-adherent cells were removed and macrophages were re-plated in fresh medium. Stimulation and phagocytosis assays were carried out on the 7th day.

For stimulation assays, 1ug/mL lipopolysaccharides (LPS; Sigma) were added to cells for 3 hours. Stimulated and unstimulated control cells were harvested into Trizol (Invitrogen) and RNA was isolated according to manufacturer's instructions. Samples were reverse transcribed and subject to qPCR, as previously described.

For phagocytosis assays, cells were incubated for 1 hours at 37°C or 4°C at a multiplicity of infection (MOI) of 1:50 with Fluoresbrite® carboxylate microspheres (Polyscience), washed in PBS with 1% FBS. Non-adherent cells and excess microspheres were removed by washing with DMEM before macrophages were collected and analyzed by flow cytometry.

Histopathology and immunostaining

For histopathology analyses, freshly dissected long bones were fixed in 4% paraformaldehyde at 4°C for 24 hours. They were stored in 70% ethanol before being decalcified, paraffin embedded, sectioned and stained with hematoxylin and eosin. For immunostaining, long bones were fixed in a formalin-based fixative at 4°C for 2 hours. Bones were then embedded in 8% (w/v) gelatin in PBS. Samples were snap-frozen with liquid nitrogen and sectioned by cryostat. Sections were dried overnight at room temperature and stored at -80°C. Sections were rehydrated in PBS for 5 minutes before immunostaining. Slides were mounted with HardSet Antifade Mounting Medium (Vector Laboratories) and imaged on a Nikon Eclipse Ti inverted microscope.

qRT-PCR

Cells were sorted directly into Trizol. Total RNA was extracted according to manufacturer's instructions. Total RNA was subjected to reverse transcription using SuperScript III (Invitrogen). Quantitative real-time PCR was run using SYBR green on a CFX Connect (Biorad) system. β-

actin was used to normalize the RNA content of samples. Primer sequences: *β-actin*: GCTCTTTTCCAGCCTTCCTT*;* CTTCTGCATCCTGTCAGCAA. *Mettl3*: AAGGAGCCGGCTAAGAAGTC; TCACTGGCTTTCATGCACTC. *Myc*: TCTCCCCAAGGGAAGACGAT; TTGCTCTTCTTCAGAGTCGCT *Tnfa*: GGAACTGGCAGAAGAGGCACTC; GCAGGAATGAGAAGAGGCTGAGAC. *Il6*: CCTCTGGTCTTCTGGAGTACC; ACTCCTTCTGTGACTCCAGC. *Il1b*: GCACTACAGGCTCCGAGATGAAC; TTGTCGTTGCTTGGTTCTCCTTGT.

MeRIP-qPCR

poly(A)+RNA was isolated from whole bone marrow cells or sorted HSCs using Dynabeads Oligo-(dT)25 magnetic beads (ThermoFisher Scientific) according to manufacturer's instructions. 1.25 µg of anti-m^{6}A antibody (Synaptic Systems) was pre-bound to Protein A/G magnetic beads (Millipore) in IP buffer (20-mM Tris pH 7.5, 140-mM NaCl, 1% NP-40, 2-mM EDTA) for 1 h. Sample RNA was incubated with antibody-bound Protein A/G beads for 2 hours at 4 ºC. Samples were washed twice in low-salt-wash buffer (10-mM Tris pH 7.5, 5 mM EDTA), twice with high-salt-wash buffer (20-mM Tris pH 7.5, 1-M NaCl, 1% NP-40, 0.5% sodium deoxycholate, 0.1% SDS, 1-mM EDTA) and twice with RIPA buffer (20-mM Tris pH 7.5, 150-mM NaCl, 1% NP-40, 0.5% sodium deoxycholate, 0.1% SDS, 1-mM EDTA). All wash solutions for each sample were collected as the "unbound" fraction. RNA was eluted from the beads by incubating with 50µl 20mM N6-methyladenosine 5-monophosphate sodium salt (Sigma- Aldrich) for 1hr at 4 ºC. Following ethanol precipitation, input, unbound, and m^{6}A-bound fraction RNA was reverse-transcribed using Superscript III (Invitrogen) with random hexamers. Enrichment of m^{6}A-containing transcripts was determined by quantitative PCR relative to *Rplp0* expression. The primer sequences for *Rplp0*: GATGGGCAACTGTACCTGACTG and CTGGGCTCCTCTTGGAATG.

RNA-seq and meRIP-seq

For RNA-seq, libraries were prepared according to the Smart-seq2 protocol as described (Picelli et al., 2014) from 150 sorted HSCs from *Mx-1cre; Mettl3*$^{fl/fl}$ or control mice 10 days after pIpC treatment. Three control and four *Mx-1cre; Mettl3*$^{fl/fl}$ biological replicate samples were sequenced by Illumina HiSeq 2500 with paired-end 100-bp read length.

For meRIP-seq, poly(A)+RNA was isolated from 3,000 sorted HSCs from C57BL/6J mice or *Mx-1cre; Mettl3*$^{fl/fl}$ mice 10 days after pIpC injection using Dynabeads Oligo-(dT)25 magnetic beads (ThermoFisher Scientific) according to manufacturer's instructions. 1.25 µg of anti-m^{6}A antibody (Synaptic Systems) or rabbit IgG (Jackson ImmunoResearch) was pre-bound to Protein A/G magnetic beads (Millipore) in IP buffer (20-mM Tris pH 7.5, 140-mM NaCl, 1% NP-40, 2-mM EDTA) for 1 h. Sample RNA was incubated with antibody-bound Protein A/G beads for 2 hours at 4 ºC. Samples were washed twice in low-salt-wash buffer (10-mM Tris pH 7.5, 5 mM EDTA), twice with high-salt-wash buffer (20-mM Tris pH 7.5, 1-M NaCl, 1% NP-40, 0.5% sodium deoxycholate, 0.1% SDS, 1-mM EDTA) and twice with RIPA buffer (20-mM Tris pH 7.5, 150-mM NaCl, 1% NP-40, 0.5% sodium deoxycholate, 0.1% SDS, 1-mM EDTA). All wash solutions for each sample were collected as the "unbound" fraction. RNA was eluted from the beads by incubating with 50µl 20mM N6-methyladenosine 5-monophosphate sodium salt (Sigma) for 1hr at 4 ºC. Following ethanol precipitation, RNA from input, m^{6}A-antibody unbound, and m^{6}A-antibody eluted, and IgG eluted fractions was reverse transcribed, amplified, tagmented and index according to the Smart-seq2 protocol (Picelli et al., 2014). Three biological replicate samples were sequenced by Illumina HiSeq 2500 or NextSeq 500 with paired-end 100-bp or 150-bp read length.

Analysis of RNA-seq and meRIP-seq data was performed using the Quantas pipeline (https://zhanglab.c2b2.columbia.edu/index.php/Quantas) (Yan et al., 2015) with minor

modifications. In brief, raw reads were mapped to the mouse genome and an exon-junction database using OLego (Wu et al., 2013). Due to the low input during library preparation, potential PCR duplicates were removed using Picard (http://broadinstitute.github.io/picard). Exonic and junction reads were then counted to estimate transcript abundance (read per kilobase per million reads, or RPKM) and perform differential expression analysis using edgeR (Robinson et al., 2010).

Cumulative distribution analysis of RNA-seq $\log_2$ fold changes in expression between *Mettl3*-depleted and control HSCs was performed in R using the ecdf function. Groups were defined as m^6A (meRIP-seq FDR<0.05, FC>2) or non-m^6A (the rest of the genes), excluding genes with RNA-seq RPKM <1 for both *Mettl3*-depleted and control HSCs. Significance of difference between the cumulative distribution curves was determined using Kolmogorov–Smirnov test.

Statistics and Reproducibility

All experiments were repeated on biological replicates independently with similar results. The exact sample sizes for each experiment were indicated in figure legends. All statistics comparing two groups used two-sided Student t-test. The Kaplan-Meier estimation and two-sided log-rank test were used to compare survival difference between mouse groups. Statistical analyses were performed with Microsoft Excel or GraphPad Prism7.

Data Availability

Sequencing data that support the findings of this study have been deposited in the Gene Expression Omnibus (GEO) under accession code GSE123527. All other data supporting the findings of this study are available from the corresponding authors on reasonable request.

APPENDIX B: m^{6}A TARGETS

995 transcripts found to be methylated in wild-type HSCs (log2(FC)>1 and FDR<0.05) with significantly decreased m^{6}A enrichment in Mettl3$^{\Delta/\Delta}$ compared to wild-type HSCs (p<0.05). Gene names are listed along with their m^{6}A enrichment in wild-type HSCs (expressed as log2(FC)).

Gene Name	log_2 (FC)	Gene Name	log_2 (FC)	Gene Name	log_2 (FC)
Nup62	8.338	Lgals3bp	3.461	Ifnar1	6.996
Csgalnact1	7.598	Sash3	3.648	Nup50	5.464
Fam32a	5.159	BC017643	4.399	Morc2a	7.434
Il16	4.825	Spop	3.700	Atxn7l3b	4.761
Myc	4.899	Dnajb1	4.614	2700089E24Rik	4.456
Rhof	4.897	Fbxw2	4.031	Slc44a2	3.236
Ccpg1	4.977	Mob3c	6.374	Adipor2	3.107
Cited2	4.660	Kcnk5	5.057	D230037D09Rik	7.287
Nceh1	6.939	Tnfaip8	3.689	Tspyl1	5.197
Mki67	7.110	Phax	5.680	Il21r	3.911
Grwd1	6.676	Poglut1	4.639	Paqr7	4.147
Gemin4	8.262	Taf5l	6.602	AI467606	3.861
Fut8	4.784	Map3k4	9.291	Yars	3.370
Minpp1	4.844	Klhl6	3.673	Slfn2	4.871
Tsc22d1	3.837	Usp1	5.157	A830007P12Rik	4.815
Nfe2l2	4.482	Lrrc33	5.573	Cdc42ep3	4.454
Il17ra	5.759	Evi2b	4.685	Sephs2	5.519
Art4	5.131	Itga5	4.504	Icam1	4.711
Gcnt2	5.527	Gpatch4	4.050	Crkl	9.388
Baz2b	6.752	Gimap6	3.418	Zfp956	7.280
Galnt1	4.920	Chst12	4.930	Fen1	3.569
Zfp36l2	4.070	Abcc1	4.456	Chtf8	3.407
Hspa5	3.473	Gypc	5.822	Lpar6	6.890
C87436	5.364	Mfsd5	4.355	Thap7	3.756
Msh6	5.292	Pcyt2	3.136	Sertad1	6.830
Nol9	7.138	Arf6	4.151	Sfxn1	3.035
Tuba4a	3.946	Zscan12	9.535	Mtap	3.553
Rnmtl1	9.710	Bid	4.209	Stim2	6.989
8430406I07Rik	6.789	Btbd6	10.358	Keap1	6.084
Tagap1	5.357	Rgs1	4.828	Mgat1	5.978
Ythdf2	4.374	Ltbr	3.948	Znrf1	4.184
Zfp12	8.993	Cand1	4.024	Gna15	5.849
Tpst2	3.633	Jun	6.655	Ifi47	3.649
Mesdc2	5.167	Dapp1	3.340	H2-Q6	3.968

Mycn	3.783	Krba1	8.752	Rpp38	7.589
Rrp36	4.636	Nxt1	3.523	Nkx2-3	5.315
Gemin7	3.972	Eif1a	3.401	Gimap1	3.382
Rcsd1	4.078	Imp3	3.040	Fbxl4	6.989
D19Ertd386e	7.943	Antxr2	8.079	Psen1	3.609
6230427J02Rik	3.454	Fem1c	8.080	Rap2b	6.148
Zfp202	8.842	Mettl13	6.722	Naa40	3.181
Fam105b	5.006	Zfp869	6.248	Rnf19a	7.985
2510039O18Rik	4.638	Emilin2	8.784	C1rl	4.594
Usp10	5.220	Erp29	2.838	Tbc1d10c	2.270
Cog8	3.993	5930416I19Rik	3.986	Elf2	4.612
Sdpr	4.666	Ip6k1	3.697	Cd27	2.344
Cops8	2.983	Arhgap29	8.791	Junb	3.434
Nfe2	2.769	Gm962	12.947	Isg20l2	3.468
Neurl3	3.923	Hmg20a	3.767	F2rl3	3.782
G3bp2	3.040	Ninj1	2.646	Agpat6	4.298
Fam57a	4.861	Klf13	4.638	Kti12	3.143
1110054O05Rik	4.215	Peo1	3.255	Zbtb24	6.843
Dgcr14	3.163	Fbxo5	4.732	Tfam	2.951
Adprhl2	3.443	Nck1	4.989	Ints5	6.169
Galnt2	3.725	Ifngr1	2.882	Pcyox1	4.985
Snord88a	3.924	Rrp15	3.239	Prkab1	3.534
Csrp2bp	6.244	Pglyrp2	2.958	2010321M09Rik	2.722
Afg3l2	3.538	Wdr73	3.241	Ccdc69	3.806
Rnpepl1	4.163	Pde4b	5.872	Zfp777	8.356
B9d2	3.493	Cmpk2	4.844	Lrrc14	3.872
Bag4	7.446	Cep68	4.317	Ppp2r2a	2.823
Slc22a3	3.651	Nif3l1	3.034	Ldlrap1	2.890
Slx4	10.521	H1f0	2.725	B4galt4	5.670
Sec24b	5.734	Slc15a4	7.258	Parg	6.723
Klf10	3.688	Toe1	4.918	Poli	5.748
Ndst2	4.019	Vps4a	2.901	Tlr2	8.157
Vamp5	2.895	Igtp	3.258	2810408M09Rik	6.651
Selplg	2.822	Twistnb	3.189	Cant1	3.517
Pdia4	2.903	Setd2	6.461	Gpr125	9.285
St6galnac4	6.021	Rbmxl1	3.551	Zfp422	3.036
Cdca4	3.742	Ppp2r1b	2.807	Flcn	3.208
Zc3h11a	5.131	Slc35a4	2.619	Qrich1	3.641
Txnl4a	2.488	Plk4	6.316	Srxn1	7.836
Rhoh	4.071	Irgm1	4.584	Umps	2.844
Fli1	3.327	Polr2m	2.513	Krcc1	3.432
St3gal2	7.514	Ccm2	2.545	Mesdc1	6.144
Smad2	3.172	Trappc5	2.827	Gimap5	2.714

Arid1a	5.736	Rilpl1	5.657	Klhl9	4.064
Akap1	7.605	Atg13	4.048	Adpgk	3.507
Ier2	2.920	Fam110a	4.773	Mrps7	2.579
Ppm1g	2.131	Slco4a1	4.061	Tmem186	5.098
Fbxo46	8.397	Zcchc17	2.615	Zfp961	7.042
Ccdc66	7.129	Tor1aip2	4.004	Golph3l	3.535
Slfn9	7.258	1110034A24Rik	3.296	Prosc	3.777
Slc16a9	7.901	Zfp58	7.956	Zfp955b	9.417
Mppe1	2.751	Hpse	8.933	Pard6b	9.676
Zbtb2	8.378	9030418K01Rik	7.517	Gm4951	9.391
Zmym1	8.123	Rrs1	4.541	Slc43a3	2.234
Socs6	8.525	Mtpap	3.743	Bag5	5.225
Rb1cc1	6.781	Brip1	6.624	AI480653	5.021
Tmem177	5.814	Ywhah	2.122	Mettl6	4.790
Fkrp	8.249	Rragc	4.665	Gmppb	3.219
1110057K04Rik	3.625	Cebpz	2.755	Fam69b	2.477
Cbx2	9.534	Ttpal	5.077	Rab35	3.654
Slc1a5	2.137	Pank2	2.751	Sdccag3	3.282
Tesk2	5.746	Sp3	3.006	Tagap	7.442
Xylt2	9.094	Tbxa2r	3.489	Tmem140	3.105
A230050P20Rik	2.747	Fbxo34	8.222	BC003965	4.277
Mak16	2.678	Ppp4r1	4.871	Abhd15	4.892
Mgat2	3.301	Men1	2.729	Mif4gd	2.763
Pdf	2.915	Dusp6	4.123	Adnp2	7.231
Usf1	4.443	Rhog	2.526	Ccdc21	3.604
Crk	5.136	Tnfsf14	7.447	Dem1	5.402
Rabif	4.095	Atp5sl	2.800	Sema4b	4.234
Ctso	3.934	1700040I03Rik	3.801	Ccdc86	2.857
B3gnt2	5.603	Gspt2	8.720	Mier3	6.754
Dhx33	8.925	Ehd4	3.018	Ctdp1	4.894
Zfp324	9.776	Pnrc1	2.536	Rit1	2.891
Zfp46	9.908	Zfand5	2.060	Tradd	3.696
Pias1	3.686	Trmt5	8.728	4930453N24Rik	4.766
Ccdc32	4.836	Chpf2	4.174	Fut10	5.780
Rcl1	2.425	Arsa	2.868	Rnf26	4.479
Gata2	2.289	Lphn2	7.756	Sap30bp	3.582
P2ry2	8.004	Gmeb2	7.431	Gab2	9.803
3110056O03Rik	2.766	Wtap	2.670	Orc2	2.480
Elovl1	2.240	Tmem246	3.969	Fam179b	9.214
Zfp386	4.493	Pias4	3.463	Gcnt1	6.720
Csk	2.188	Limd1	5.427	1110002N22Rik	5.612
E130304F04Rik	12.460	Rtp4	4.967	Ammecr1l	4.436
Ado	3.867	Dedd2	6.132	Lcmt2	6.260

4930444A02Rik	6.059	Fgd5	8.106	Tspyl3	4.826
Fam134b	3.906	Nlgn2	6.499	Mtrf1l	6.277
Palb2	7.282	Dcun1d1	3.333	Mrpl43	2.285
Pms2	3.498	Tmem104	5.868	BC006779	9.189
Ftsj2	9.546	2310003H01Rik	3.736	Zfp282	6.024
Pdcl	4.008	Mcm9	3.116	Thsd1	7.577
Dynll1	2.274	1810048J11Rik	5.519	Gnaz	8.894
Inpp1	3.576	Gm16517	3.365	2310003C23Rik	2.945
Orai3	2.656	Wdr55	2.348	0610011L14Rik	3.218
2410016O06Rik	3.790	Mlycd	3.313	Aqp9	3.596
Rnf145	3.687	1700017B05Rik	5.855	Rft1	2.710
4831426I19Rik	9.104	Tssc4	2.293	Tab2	7.474
Tmem11	3.675	Mrpl41	3.171	Trex1	3.473
Zfp870	8.578	Wdr85	2.862	A730011L01Rik	3.708
Rlf	7.447	Aldh1b1	9.020	Mrpl12	1.785
Ptpn22	3.237	Smcr7l	4.448	Cables1	5.258
Asb8	5.191	B3gnt5	8.286	Cdc25a	3.433
Sesn1	2.201	Rinl	3.946	Spata2	5.788
Cd79b	3.180	Inpp5e	2.460	Arl4a	4.525
Yipf5	3.529	Hs3st1	9.343	Panx1	3.511
Rnf8	2.735	Sppl3	3.265	Adora2a	4.062
Zfp472	6.959	Prpf4	3.232	6330503K22Rik	6.076
S1pr4	2.582	Tnrc6c	6.387	Dnajb9	3.724
Chmp1b	5.039	Zfp64	3.823	Adam17	2.309
Tk2	2.747	Tmem41a	2.375	Hps6	8.386
Slc19a1	2.292	Ptgs1	2.082	Zfp809	5.258
Cdv3	3.146	Dsn1	3.554	Litaf	2.477
Nrbf2	8.052	Ptrh2	3.489	Gcc2	5.699
Gp5	3.594	Zfp771	2.703	Gpr157	12.104
BC147527	11.979	Pter	6.355	2400003C14Rik	2.040
Tut1	4.116	Lhfpl2	7.661	Tmem185b	5.434
Tysnd1	2.950	Plekhg5	9.514	Brms1	1.940
Rora	9.693	Ubap1	2.975	Fam174b	3.160
Taf3	6.972	H2afx	2.067	Bet1l	3.988
Mcl1	3.118	Fam58b	4.798	Plekhg2	8.018
Clp1	4.788	Dos	5.035	Kctd20	2.444
Zdhhc7	3.409	Zmym2	4.595	Dctn5	1.923
Nipbl	5.140	Fam136a	3.087	Klf9	6.548
Sac3d1	3.642	Mettl11a	2.476	Tifa	3.810
Fignl1	4.598	Ubl3	3.366	Gpn2	3.004
Tmem115	4.477	Gadd45g	4.176	Gpr171	4.000
Rg9mtd1	4.059	Gtdc2	4.972	Fzd7	8.712
Nol12	2.620	Extl2	5.173	Snx20	5.216

Abcb9	8.340	Fiz1	2.680	Bivm	4.255
9130023H24Rik	6.639	Ctdspl	7.545	1700123O20Rik	2.529
Nudt1	2.589	Mrps26	1.960	Scamp4	1.977
Slc39a7	1.771	Gm12250	5.473	Myct1	2.021
Socs2	3.885	Pofut2	2.174	Six5	6.121
Gsg2	7.312	Zfp11	11.476	Gata3	4.026
Zscan22	6.635	A630001G21Rik	4.709	Cops2	2.152
Fut7	4.847	Mmaa	3.284	Zfp191	6.149
Btbd7	8.003	Slc35c2	1.792	Cinp	2.761
Egln2	1.996	2310008H09Rik	3.072	Mcart1	2.696
Endod1	8.377	Mrps2	2.876	Cpt2	3.988
Kcnn4	1.677	Cpd	9.023	Pi4kb	4.848
Gatc	2.963	Cnpy3	2.222	Glrp1	8.991
Foxo1	9.095	Txndc11	2.528	Icam2	1.905
Il15ra	3.480	2310011J03Rik	2.257	Slc16a6	4.434
Pla2g15	4.083	Rab38	1.740	Zfp87	2.959
D4Wsu53e	1.977	Shoc2	3.196	Itpk1	2.488
Slc25a46	3.236	4931414P19Rik	8.092	Hyal2	3.869
Zdhhc3	1.968	4833420G17Rik	2.258	Dicer1	5.446
Klhl25	10.102	Nat6	2.786	Zfp280b	7.779
3110062M04Rik	2.506	Rara	7.101	Slc43a2	4.421
Tnfaip8l1	9.278	Psmd5	1.768	Utp3	2.842
Metrnl	8.945	Rbak	9.402	Tsen54	2.271
E330016A19Rik	6.903	Tmem121	8.880	Hmox2	1.702
AA987161	7.989	Elk3	3.047	2900026A02Rik	7.891
Zfp773	8.011	Dars2	2.449	Slc35e4	4.395
4632434I11Rik	7.538	Rab31	2.413	Zbtb45	3.828
Ccdc85b	3.568	Elmod3	3.059	Asnsd1	1.882
Fam116a	2.635	Klhl26	5.161	Zkscan6	3.433
Gins3	6.704	Slc35b3	2.648	Sphk2	2.763
Ywhag	2.426	Eme2	2.091	Abt1	4.008
Ttl	7.413	Mdm2	3.370	Dph2	2.891
Zkscan5	5.891	Pik3ca	7.266	Slc36a4	7.846
Flywch1	2.729	Lsm10	3.370	2210020M01Rik	2.581
Yeats4	1.957	Ffar2	6.203	2410002F23Rik	3.715
Mfap3	4.576	4933403G14Rik	11.325	Snrk	5.122
Tusc2	2.782	Cbll1	3.829	Mad2l1bp	4.119
P2ry14	7.872	B3gntl1	3.656	Jmjd4	5.740
Ndnl2	5.390	Lass4	2.040	Chmp1a	1.711
Sec22a	3.566	Mrps27	2.402	Chd9	4.563
Sash1	9.919	Sdhaf2	3.765	Ehbp1	7.723
Cdk9	3.577	2810432D09Rik	3.368	Zfp142	7.397
Gusb	1.742	Zfp639	4.508	Cln5	3.256

Ccdc71	4.435	Orai1	2.409	Znrd1as	9.149
Rhob	3.940	Gdf3	2.757	Terf2ip	4.317
Dclre1b	3.772	Spsb4	8.293	Vps37b	3.570
Stx5a	1.964	Mudeng	3.561	Ikbip	5.472
Zfp456	7.932	Slc16a13	4.755	Rps19bp1	2.560
BC055004	5.444	Xbp1	1.611	Hyls1	7.758
Pck2	1.789	Zbtb25	5.286	Trim13	5.465
Fem1a	6.528	Slc37a3	7.865	Thtpa	2.630
Arglu1	3.054	Acpl2	2.697	Ccdc59	2.832
Ccdc88c	8.328	Zmat1	6.018	Gpr107	3.541
Neu1	3.555	Tuba8	1.788	Rnf185	4.866
Gpn1	1.994	Fuca2	2.326	Nat2	7.574
Susd3	2.556	Mfhas1	8.489	Sigmar1	1.895
Lig3	3.701	Snapc2	2.530	Acot11	5.327
Ddit3	2.728	AI837181	5.426	Ppp1r15b	3.524
Fam55c	5.486	Pi4k2a	4.452	Homez	5.375
Dph5	2.386	Haus6	5.936	9430023L20Rik	2.207
Jtb	1.978	Phf23	3.661	Dolk	4.915
Tet2	6.190	Tgif1	3.751	Rad51ap1	2.621
Med18	6.675	Fancm	9.137	H2-Q7	1.707
Rffl	2.723	Fam109a	5.402	Htr2a	8.186
2010015L04Rik	9.330	Cxxc5	2.497	Fbxo22	1.874
S1pr2	4.800	1810055G02Rik	7.929	Psmd7	1.509
1810058I24Rik	1.829	Zfp780b	7.646	Lrrc8a	5.138
Map1lc3b	1.637	Sco2	2.141	Alg11	4.797
Rdh11	2.538	Tnfsf4	7.999	St3gal1	3.270
Zfp784	7.770	Rnf122	3.730	Ndufaf1	2.504
2810008M24Rik	2.807	Zscan29	6.975	Zswim1	5.562
Mn1	8.510	Arfgap1	4.420	Thap11	2.801
Irf2bp2	5.191	Zfp85-rs1	7.660	2310022A10Rik	2.622
Kpna6	4.394	Spsb2	3.851	Bcl11a	1.699
Tmub2	1.927	Ube2d1	2.871	Pcyox1l	3.722
Mdfic	6.910	Ptp4a3	1.468	Msl3l2	4.649
Snip1	3.613	Ythdf3	5.322	2010111I01Rik	2.671
Batf	2.266	D16Ertd472e	2.971	Cwc25	4.613
2610035D17Rik	3.956	Rrp7a	1.771	Kbtbd2	4.711
Cd3eap	2.906	Rspry1	3.164	Spry1	7.928
Eri2	6.766	Wdr81	8.757	Slc30a5	1.606
Zfp161	5.995	Lipt1	6.751	Gimap9	3.404
Gng11	1.845	Dscr3	2.562	Fdxr	2.060
Dexi	3.958	Slc7a6	1.926	Spred1	3.840
2700078E11Rik	4.343	Lias	2.169	8030462N17Rik	10.417
Zfp810	9.142	Cdadc1	2.751	Dedd	2.605

Btbd8	10.410	Glb1	1.534	Pde4c	11.488
Paqr8	7.188	Bnip1	2.502	Rnf25	2.070
Kctd1	2.745	Txndc15	1.847	Zfp677	8.378
Il17re	3.060	Ccdc127	3.527	1810063B07Rik	2.691
Tmem17	7.521	Zfp429	7.000	AI462493	1.983
Tmem44	6.262	Ercc4	3.791	Rint1	3.021
Arl11	8.257	Gm20604	3.547	Nup62-il4i1	6.578
Pop7	2.582	2610002I17Rik	2.688	Dnajc14	1.543
Zfp260	3.201	D630039A03Rik	4.451	1810026J23Rik	1.949
Ppp2r5e	2.834	Armc10	1.950	Havcr2	8.854
Triap1	3.343	Trappc3	1.707	Rnf139	2.729
Ngrn	2.463	Rab43	3.070	Mul1	3.394
Ttll4	5.735	3230401D17Rik	3.641	5530601H04Rik	2.247
Zkscan14	3.737	Grpel2	4.032	Zfp184	10.775
Slc10a3	2.089	Slc25a11	1.357	Armcx6	3.958
Ephb4	9.667	Leprotl1	1.587	2310014F07Rik	9.461
Zfp189	8.810	Med7	2.423	Glyctk	8.266
Tor1a	1.733	Rpp14	1.765	Kctd21	10.824
Rpusd4	2.484	Nupl2	4.337	Zfp951	5.649
1810008A18Rik	2.132	Patz1	3.718	Cnnm2	9.072
Irf3	1.568	Naip5	3.755	Taf11	2.170
Spsb3	1.936	Zfp609	7.218	Tmub1	2.652
Ptprcap	1.375	Nudt7	2.418	Dyrk3	4.287
Angptl4	2.932	Fbxo28	6.315	Alg9	1.723
Maml3	8.727	Tmem173	1.742	H2-Q9	1.931
2700007P21Rik	3.764	Fitm2	7.227	Sertad3	4.373
Zfp770	9.987	Traf1	4.318	Dnajc30	3.592
2010002N04Rik	3.364	Xkr5	4.567	Pars2	5.284
Pigm	4.448	Zfp646	6.841	Zc3h6	5.215
0610007P22Rik	2.300	Eepd1	5.997	Mrpl50	2.647
LOC330599	8.995	Sumo1	1.758	Fam118a	4.259
Zfp958	4.266	Ubiad1	4.097	Fam108b	3.137
Zfp710	4.066	Kbtbd4	2.390	Cstf1	2.297
Pcbp1	1.346	Grin2d	10.517	Agpat2	1.627
Cdc26	1.710	Gemin8	4.184	2010002M12Rik	7.088
Adck2	1.905	Map3k14	7.839	Nob1	1.570
Zbed6	8.074	Mrpl19	1.694	Cox19	2.408
Commd5	4.418	Fadd	3.771	Fam69a	1.961
Cd276	9.023	Map3k8	6.389	Slc10a7	3.164
B4galnt1	1.814	Tef	3.684	Gp9	1.637
Mterfd2	2.546	Gpr132	3.745	2810422O20Rik	4.973
Mrgpre	7.924	Mapk7	4.262	Gmpr	1.499
Usp44	8.360	Fam110b	5.489	Ctla2b	1.814

Cd200r1	3.020	Gabpb2	3.293	Ggn	9.263
Bspry	10.797	Epb4.1l1	11.328	Cno	3.875
Tmem168	5.302	Harbi1	4.996	4930547N16Rik	6.178
Tm2d2	1.488	Gm9776	7.632	Fut4	7.338
Tk1	1.588	Slc25a29	8.544	2610029G23Rik	1.545
Mbd3	1.399	Msrb2	1.517	Dbr1	3.127
6430527G18Rik	6.261	Rp9	1.348	Fam173b	3.442
Notch4	7.688	Pelo	4.324	Caml	2.652
Tigd2	4.397	Fam192a	1.684	Cxx1c	2.520
Kctd14	3.336	AW209491	4.980	Zfp874b	5.822
Asb6	2.572	Tor2a	1.591	Ppapdc3	4.886
Zswim6	8.246	Herpud2	2.139	Hsd3b7	1.250
Coasy	1.641	Loh12cr1	4.056	Il1r1	8.030
BC024479	6.493	Ptger4	5.597	D17H6S53E	5.626
Ankrd10	1.354	Sephs1	1.946	Nsd1	2.565
2610002D18Rik	5.250	Tardbp	1.379	Ddx59	2.967
Clip2	7.730	Cdk13	5.465	Zfp707	4.705
Utp15	2.536	5830416P10Rik	8.149	Narfl	2.082
B3galt6	3.069	Rab19	11.171	Tob1	4.890
Zfp61	4.810	BC017158	1.776	D330012F22Rik	4.782
Mob2	1.857	Amigo3	10.219	Ydjc	1.750
Abtb1	2.182	Mir1901	7.645	Zfp865	4.078
Sh2d4a	8.406	Lrfn4	6.796	Btg1	2.940
C230052I12Rik	4.604	Rnf113a2	3.027	Tgif2	2.912
Sf3b5	1.506	Dnase2a	2.350	Ebag9	2.470
Ptcd2	1.399	Gm5512	3.000		